Effect of membrane potential on action of antimicrobial peptides lactoferricin B and its fragment

THESIS

Effect of membrane potential on action of antimicrobial peptides lactoferricin B and its fragment

June 2020

Shizuoka University

Graduate School of Science and Technology,

Department of Bioscience

FARZANA HOSSAIN

Abstract

Antimicrobial peptides (AMPs) can kill or inhibit growth of bacteria. Several studies suggested the membrane potential affects the activity of AMPs against bacterial cells. However, recent experimental results indicate that membrane potential greatly affects the plasma membrane of bacterial cells such as localization of many proteins and lipids. Thus, the role of membrane potential in the AMP actions becomes unclear. In this thesis, I investigated the role of membrane potential on AMP actions using giant unilamellar vesicles (GUVs) of lipid bilayers. For this purpose, first I developed the method of application of membrane potential to GUVs. Then, I investigated the effect of membrane potential on action of two AMPs using the single GUV method; one AMP is lactoferricin B (LfcinB) derived from bovine lactoferrin and the other is its fragment, LfB4-9 (RRWQWR). These AMPs have different mode of actions; LfcinB induces damage of the plasma membrane which causes rapid permeabilization whereas LfB4-9 can translocate across lipid bilayer without damaging the membrane. I also examined the effect of membrane potential on the interaction of these AMPs with single live *Escherichia coli* cells and single *E. coli* spheroplasts. Based on the obtained results, I discuss the role of membrane potential on the activity of AMPs with lipid bilayers and plasma membranes of bacterial cells.

(Chapter 2) In this chapter, I examined the effect of membrane potential on the action of LfcinB. First, I investigated the interaction of LfcinB with single live *E. coli* cells using confocal laser scanning microscopy (CLSM). *E. coli* cells was loaded with a fluorescent probe, calcein. I found that LfcinB induced rapid leakage of calcein from single *E. coli* cells. To examine the direct interaction of LfcinB with the plasma membrane, I investigated the interaction of LfcinB with single *E. coli* spheroplasts loaded with calcein. This experiment showed that LfcinB induced rapid leakage of calcein from single spheroplasts. These results indicate that LfcinB induced rapid permeabilization due to damage or pore formation to the plasma membrane of *E. coli* cells. To understand the role of membrane potential, I examined the effect of a proton ionophore, carbonyl cyanide *m*-chlorophenylhydrazone (CCCP) on LfcinB-induced leakage from single *E. coli* cells and spheroplasts. I found that presence of CCCP suppressed this leakage. Next, I examined the interaction of Lfcin B with single GUVs of *E. coli*-lipids (i.e., phosphatidylethanolamine/phosphatidylglycerol/cardiolipin (67/23/10 (weight % ratio)) containing a fluorescent probe, AlexaFluor 647 hydrazide (AF647) using the single GUV method with CLSM. LfcinB stochastically induced local rupture in *E. coli*-lipid GUVs, causing rapid leakage of AF647; however higher LfcinB concentrations were required to induce a significant rate of local rupture in *E. coli*-lipid GUVs in comparison with *E. coli* cells and spheroplasts. To identify this reason, I examined the effect of membrane potential on LfcinB-induced local rupture of GUVs. To apply membrane potential to

GUVs, I prepared *E. coli*-lipid GUVs whose membrane contains a monovalent cation channel, gramicidin A, and created K^+ concentration difference between the inside and the outside of the GUVs. I found that the rate constant of LfcinB-induced local rupture in GUVs increased greatly with increasing negative membrane potential. These results indicate that membrane potential plays a vital role in the LfcinB-induced local rupture of lipid bilayers and rapid permeabilization in *E. coli* plasma membrane. Based on these obtained results, I discussed the mode of action of LfcinB's antimicrobial activity and the effect of membrane potential.

(Chapter 3) In this chapter, I examined the effect of membrane potential on the action of LfB4-9. To reveal the location of LfB4-9 in cells and GUVs, I used a fluorescent probe lissamine rhodamine B (Rh)-labeled LfB4-9 (Rh-LfB4-9). First, I investigated the interaction of Rh-LfB4-9 with single *E. coli*-lipid GUVs containing AF647 and small GUVs comprising dioleoylphosphatidylglycerol (DOPG) and dioleoylphosphatidylcholine (DOPC) using the single GUV method with CLSM. I found that Rh-LfB4-9 entered the GUV lumen and bound to the membrane of the small GUVs without leakage of AF647, i.e., no pore formation or local rupture in the mother GUV. Using the same method of application of membrane potential to GUVs described in Chap. 2, I investigated the effect of membrane potential on the entry of Rh-LfB4-9 into single *E. coli*-lipid GUVs. I found that membrane potential greatly increased the rate of translocation of Rh-LfB4-9 into the GUV lumen and the rate of its entry increased with an increase in negative membrane potential. Next, I examined the interaction of Rh-LfB4-9 with single live *E. coli* cells and spheroplasts containing calcein using CLSM. I observed that in low peptide concentrations Rh-LfB4-9 entered the single *E. coli* cells and spheroplasts without leakage of calcein. A protonophore CCCP suppressed the entry of Rh-LfB4-9 into *E. coli* cells and spheroplasts. Based on these results, I discussed the effect of membrane potential on the action of Rh-LfB4-9.

Table of Contents

List of Figures

List of Abbreviations and Symbols

Abbreviation		Full form
AMP	:	Antimicrobial Peptide
LF	:	Lactoferrin
LfcinB	:	Lactoferricin B
LfB4-9	:	Lactoferricin B 4-9
GUV	:	Giant Unilamellar Vesicle
LUV	:	Large Unilamellar Vesicle
CLSM	:	Confocal Laser Scanning Microscopy
CPP	:	Cell-Penetrating Peptide
E. coli	:	*Escherichia coli*
E. coli-lipid	:	*E. coli* Polar Lipid Extract
DOPC	:	Dioleoylphosphatidylcholine
DOPG	:	Dioleoylphosphatidylglycerol
RH	:	Rhodamine
$DiOC_6(3)$	:	3,3′-Dihexyloxacarbocyanine Iiodine
AF647	:	Alexa Fluor 647 Hydrazide
Calcein-AM	:	Calcein-acetoxymethyl
BSA	:	Bovine Serum Albumin
CCCP	:	Carbonyl Cyanide m-Chlorophenylhydrazone
TEAC	:	Tetraethylammonium Chloride
DIC	:	Differential Interference Contrast
FI	:	Fluorescence Intensity
MIC	:	Minimum Inhibitory Concentration
φ_m	:	Membrane Potential
$P_{leak}(t)$	:	The fraction of leaked cells among all examined cells over time t
$P_{intact}(t)$	:	fraction of intact GUVs among the examined GUVs over time t
k_P	:	rate constant of the LfcinB-induced local rupture
$P_{entry}(t)$	:	Fraction of GUVs which peptides entered before a specific time t

Chapter 1

General Introduction

Chapter-1

General Introduction

1.1 Antimicrobial peptides (AMPs)

Antimicrobial peptides (AMPs) are a part of the innate immune response which are also named host defense peptides (HDPs) found amongst all classes of life. The first AMP was discovered in the early 1980 s, and subsequently AMPs have been found in almost every organism for example Magainin is an AMP which was first isolated from the African clawed frog Xenopus laevis (Zasloff et al., 1987). AMPs are effective, broad spectrum antibiotics and exhibit as potential novel therapeutic agents. These peptides are capable of killing bacteria of both gram negative and positive, fungi, viruses and also cancer cells (Amsterdam et al., 1996). This cationic, amphipathic AMPs have been demonstrated to provide attractive models where they target the negatively charged membranes of bacteria and permeabilize and inflict very low disturbance in eukaryotic cells (Sochacki et al., 2011).

AMPs are small, positively charged, amphipathic molecules and have variable amino acid composition with length approximately 6 to 100 amino acids. These peptides vary both in primary and secondary structure. According to its secondary structure, AMPs can be classified into four major groups, including β-sheet structures stabilized by two to three disulfide bridges, α-helices, loop structures containing only one disulfide bridge and extended structures (Boman et al., 1987). Most AMPs adopt amphipathic structures after binding to membranes, whose one side is aligned with hydrophilic amino acid residues and the other side have hydrophobic residues (Campos et al., 2004). This amphipathic structural might be one of reason for the bactericidal action of AMPs. This positively charged peptides are able to make interaction with the bacterial surface (negative charge) and with phospholipids headgroups of lipid membrane (negative charged). AMPs hydrophobic property enables it to enter the membrane interior (Wu et al., 1999).

There are various modes of action by which AMPs kill microbes. The most frequent target is cytoplasmic membrane, but this peptide has also the ability to inhibit the synthesis of DNA and protein, cell wall synthesis and protein folding (Hancock et al., 2002). The characteristics of these peptides like size, amphipathicity, positive charge would permit it to interact and thus create pores in the lipid membrane. They can cause damage or rupture of membrane by various mechanism like 'barrel stave', 'carpet' or 'toroidal pore'. Once the peptide concentrations exceed certain threshold values many water-soluble AMPs spontaneously bind to membranes and form transmembrane pores.

AMPs can bind to the negatively charged membranes of bacteria due to electrostatic interaction and cause damage of outer membrane, then permeabilize the inner membrane and then cause damage of both which leaking the internal contents (Li et al, 2007). The inner membrane of bacteria performs many vital functions such as transport, respiration processes, etc. and these functions are necessary for membrane integrity, and if the damage of the inner membrane occurs it can cause cell death.

There are several models to explain the possible effects of these peptides on the cytoplasmic membrane. Generally, AMPs may destabilize and permeabilize the membrane, or it can form distinct pores/channels in the membrane (Ulvatne et al., 2004). In the first case, the most popular models where it can form a peptide carpet (Gazit et al., 1995) or thinning of the membrane (Berneche et al., 1998; Heller et al, 2000; Ludtke et al., S., 1995). For the peptides which form pores, the models may include the barrel stave model (Bechinger et al., 1999; Shai et al., 1999), and the two-state model (Huang et al., 2000). The pore formation can causes leaking the internal contents from the inside of the cells.

Several AMPs are shown to have additional intracellular targets regardless of cytoplasmic membranes like it has the ability to hamper the DNA, RNA or protein synthesis (Kragol et al., 2001; Otvos et al., 2000; Park et al., 1998), the inhibition of macromolecular biosynthesis (Castle et al., M., 1999; Patrzykat et al., 2002; Subbalakshmi et al., 1998) and the bacterial enzymes inhibition (Andreu et al., 1998; Couto et al., 1993; Nishikata et al, 1991). Some AMPs work by interfering with synthesis of DNA and protein such as indolicidin and PR-39 (Subbalakshmi et al., 1998; Boman et al., 1993), and some prohibits cellular actions by attaching to DNA and RNA such as buforin (Park et al., 1998).

1.2   Interaction of AMPs with bacterial cells and spheroplasts

Gram-negative bacterial cell wall is composed of an outer membrane (OM) decorated with lipopolysaccharides (LPSs), peptidoglycan layer and cell membrane (CM). *Escherichia coli* (*E. coli*) has a cell membrane whose lipid composition is phosphatidylethanolamine (PE), phosphatidylglycerol (PG), and cardiolipin (CA) (Soblosky et al., 2016). Various biophysical studies have been performed using lipid composition which mimic the bacterial cells outer leaflet, such as purified LPS or lipid mixtures. By these mechanisms it was proposed that, these peptides can interact with outer membranes of bacterial cells and causes disgregation of the membrane by perturbing their integrity. Gram negative bacteria have asymmetric bilayer composed of three leaflets. The inner membrane contains PE, PG and cardiolipin followed by a peptidoglycan layer and the main component of outer membrane is LPS, it also has proteins like lipoproteins and beta barrel proteins (porins) (Silhavy et al., 2010; Duong et al., 1997). The outer membrane of this bacteria such as *E. coli* membrane also contain some enzymes, a phospholipase (PldA), a protease (OmpT) and a LPS modifying enzyme (PagP). Different types of experiments of these active peptides has been investigated against gram negative bacterial cells and proposed that peptides create aggregates on the outer membrane and then pass through the membrane, insert into the inner one and then attach with DNA and RNA finally (Hancock et al., 1999; Brogden et al., 2005).

Some studies of molecular mechanisms of these AMP's in bacterial cytoplasmic membranes have been studied using live bacteria (Steiner et al, 1988; Sochacki et al., 2011; Rangarajan et al., 2013; Barns et al., 2013; Fantner et al., 2010). However, there are some limitations in bacterial studies, such as it contains the outer membranes (Sochacki et al., 2011) and also the fact that the peptide can induce secondary effects, such as it can activate autodigestive enzymes which may lead to damage of cell membrane (Birnbaum et al., 1987; Elsbach et al., 1993). Recently, some studies of AMPs on *E. coli* and *Bacillus subtilis* have been performed using time-lapse fluorescence microscopy (Sochacki et al., 2011; Barns et al, 2013) and found that the action of AMPs on bacteria revealed two key steps. At first it directly interferes with cell wall synthesis and halt the growth and secondly it permeabilize the cytoplasmic membrane. By using fluorescence microscopy, the series of action of LL-37 (human AMP) can be carried out, as it attacks *E. coli* (K-12) and halts growth. Its antimicrobial activity mainly due to its attachment to the LPS of OM and O-antigen layers and then halting

of growth. The interaction of two cationic amphiphilic AMPs gramicidin S and PGLa with bacterial membranes have been investigated using electron microscopy (Hartmann et al., 2010). Various types of bubbles and blisters are found on *E. coli* cells surface revealed by SEM. It showed open holes and deep craters *Staphylococcus aureus* envelope and bursting of cells may occur after expose to AMP. Even at low AMP concentrations, the bacteria are able to permeabilize the membrane.

The cytoplasmic membranes of bacteria are normally shielded by outer membranes, for this they are much less accessible to experimental study. There may be several targets of AMP for gram negative bacteria like *E. coli* since it composed of an outer membrane, a inner membrane and in between a peptidoglycan layer. The spheroplast of gram-negative bacteria, the cells from which outer membranes have been removed by the action of enzymes, have been and are being used in a variety of different investigations for example patch clamp, fusion and also antibiotic studies (Sun et al., 2014). Spheroplasts are prepared from bacteria which cultured in medium containing an antibiotic (for example cephalexin) which inhibits cell division but still allow the cell growth. It produced long bacterial filaments, then digestion of the outer cell wall was done by the action of lysozyme, which produces spherical spheroplasts. Spheroplasts are typically 2 to 5 µm in diameter. It is even more important than larger size of it that, consistent slices of spherical spheroplast can be obtained during imaging (Lei et al., 2016). Sun et al., examined interaction of AMPs, LL37 and melittin with spheroplast made from *E. coli* cells by removing the outer membrane which made it feasible to act on cell membranes (Sun et a.l, 2016) and found that both peptides disintegrate the cell membranes.

1.3 Interaction of AMPs with lipid vesicles

AMPs can cause damage of bacterial membrane using various mechanisms. Even though many studies have been done on the action of AMPs, but its mechanisms of membrane damage are still unclear. Therefore, AMPs and lipid membrane (model membrane) interactions, have been the subjects of intense investigation. To investigate the interaction of AMPs with lipid bilayer, many researchers have used the suspension of many small vesicles such as large unilamellar vesicles (LUVs). For example, interaction of AMP lactoferricin B (LfB) with LUVs causes leaking of calcein (fluorescent dye), which indicate that damage of membrane occurred by LfcinB (Moniruzzaman et al., 2015). However, there are some limitations in this method. Here

5

during the investigation period, the structural changes of individual LUV and the different steps of the elementary processes of AMPs action cannot be monitored directly. On the other hand, giant unilamellar vesicles (GUVs) of lipid bilayers greater than 10 μm of diameters were used to examine the physical and biological properties of lipid membrane such as elasticity and shape change. (Saitoh et al., 1998., Tanaka et al., 2002, Yamashita et al., 2002., Baumgart et al., 2003). Recently, a suspension of many GUVs named GUVs suspension method was used to investigate interaction of AMPs with lipid bilayers. But the initial time course of binding of peptides with GUV membrane, pore formation and the kinetics of binding or unbinding of peptide with GUV membrane cannot be determined by GUV suspension method.

Yamazaki and his colleagues established a novel method, the single GUV method to investigate the interactions of substances with lipid bilayer (Tamba and Yamazaki., 2005; Yamazaki., 2008). In the single GUV method, a change in the GUV's structures and physical properties induced by their interaction with substances are measured as a function of time and spatial coordinates by using various types of microscopes and analyzed the physical parameters of a single GUV statistically over many single GUVs. In the single GUV method, the detailed information of elementary processes of interaction of peptides or proteins (such as rate constant of pore formation, membrane permeation, kinetics constants) with lipid bilayers have been determined (Islam et al., 2014b). This single GUV method has been successfully applied to AMP, magainin 2 (Tamba et al., 2005; 2009; Tamba et al., 2010; Karal et al., 2015); pore forming toxin, lysenin (Alam et al., 2012), LfcinB (Moniruzzaman et al., 2015). These AMPs induce damage in the GUVs such as pore formation and local rupture and causes membrane permeation of internal contents through the damage (Fig. 1.1) (Tamba and Yamazaki 2005, 2009; Tamba et al. 2010).

Many researchers have investigated the interaction of AMPs with lipid membrane using the single GUV method. Tamba et al., demonstrated that magainin 2 induces a thermal fluctuation in the lipid bilayers and forms a pore which followed a toroidal pore mechanism (Tamba et al., 2010). It was demonstrated that, pore formed by magainin 2 was elevated by tension caused by an external force and this pore is formed as a stretch-activated pore. The main cause of magainin 2-induced pore formation is the stretching of the inner leaflet of the lipid bilayer, and with the increases of stretch of the inner monolayer, the rate of this pore formation greatly increases. (Karal et al., 2015; Hasan et al., 2018). As I mentioned earlier, interaction of a

6

pore forming toxin, lysenin with lipid membrane was examined using single GUV method (Alam et al., 2012). In the interaction of this peptide with the lipid bilayer, many monomers of lysenin can bind to the membrane and form an oligomer, which causes a pore in lipid membranes (Alam et al., 2012). The single GUV method is also useful for examining the fundamental procedures for the entry of cell penetrating peptides (CPPs) into lipid membrane using CLSM (Islam et al., 2018; Islam et al., 2017; Islam et al., 2014; Sharmin et al., 2016; Moniruzzaman et al., 2017). Various data regarding the entrance of peptides inside the single vesicle before pore formation can be obtained using single GUV method. This method, provides the information regarding the rate of entry, the link between the entry and formation of pore, and time course for peptide amount increment in the GUV membrane and lumen (Islam et al., 2017; Islam et al., 2014; Sharmin et al., 2016; Moniruzzaman et al., 2017).

AMPs can also target the DNA or other proteins inside the cells besides the cell membrane, where it enters the cytoplasm by translocating across the cell membrane and bind with DNA or other proteins in the cytoplasm, which indicate that these AMPs have CPP like activity. Recently, Islam et al. developed a new single GUV method for CPPs (Islam et al., 2014a). In this method, single GUVs containing small GUVs and water-soluble fluorescent dye inside the mother GUV lumen was used. When a small amount of fluorescence dye-labeled CPPs enter the GUV lumen, they rapidly bind with the membrane of the small GUVs and thus fluorescence emits from the membrane of the small GUVs. This indicates that CPPs enter the GUV lumen of mother GUVs. In this method, simultaneously the FI of water-soluble dye in GUV lumen can be followed, which gives the information of leakage of the dye from the GUV. Therefore, the relationship between pore formation and entry of peptides can be obtained.

The peptide bilayer interaction is very complex aspects to understand. Hence, mostly the studies of these peptides have been carried out with model lipid membranes. Thus, it is not able to understand that whether the mechanism of AMPs on artificial membranes can be reproduced on live bacterial membranes or not, and whether the results of model membranes can be extended to bacterial membranes (Last et al., 2013). However, a bacterial membrane mimic lipid like *E. coli* lipid which has a similar lipid composition as *E. coli* can be a good candidate for study (Soblosky et al., 2016).
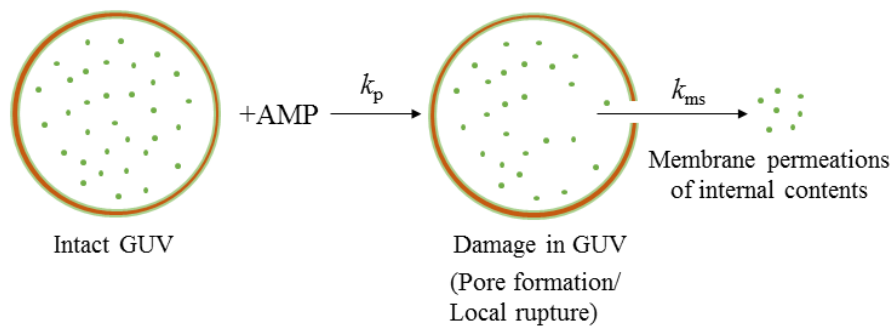
Figure 1.1: A scheme to represent the elementary steps of AMPs action. This figure is cited from the ref.

(Moghal et al., 2020B) with the permission from Springer.

1.4 Lactoferricin B (LfB) and its derivative (as examples of AMPs)

Lactoferrin (formerly known as lactotransferrin) is a multifunctional glycoprotein, which shows high affinity for iron. Its molecular weight is about 80 kDa. It is under the group of transferrin family and are able to bind and transfer Fe^{3+} ions (Metz-Boutique et al., 1984). In 1939 Sorensen and Sorensen first isolated lactoferrin (LF) from bovine milk. In 1960, researchers have proposed that in human milk it is the core iron binding protein (Groves, 1960; Johanson, 1960; Montreuil et al., 1960). LF is primarily found in mucosal secretions, particularly present in saliva, tears, vaginal fluids, semen (Van et al., 2001), bronchial and nasal secretions, gastrointestinal fluids, bile, and urine (Öztas et al., 2005). Lactoferrin have several protective activities such as (i) antimicrobial activity, due to iron deprivation, (ii) immunomodulatory activity, together with a specific antinflammatory effects, (iii) recently discovered anticancer activity (Francesco et al., 2016).

The location of Lfcin in bovine LF is at N-terminal. It has been produced by the gastric pepsin mediated hydrolysis of protein (Bellamy et al., 1992; Arnold et al., 1980; Brouwer et al., 2011; Strøm et al., 2003). It was isolated from mammals, such as bovines which named LfB and from humans called LfcinH (Farnaud et al., 2003; Sinha et al., 2013). LfB and the synthetic peptides derived from it exhibited antiviral (Andersen et al., 2001; Andersen et al., 2003), antifungal, antiparasitic anticarcinogenic and antibacterial activity (Farnaud et al., 2003; Bellamy et al., 1992; Strøm et al., 2003; Aguilera et al., 1999; Chan et al., 2006; Haukland et al., 2001; Liu et al., 2011; Tu et al., 2011; Ulvatne et al., 2004; Vorland et al., 1998).

LfB is derived from bovine Lf containing 17-41 residues, which have a disulfide (S-S) bond between cystein 19 and 36. LfB is more easily obtained compared with LfcinH, and it is more effective as an AMP (Marjolaine et ai., 2010). The net charge of bovine lactoferricin (LfB) is +8 (Rekdal et al., 1999), resulting from bovine lactoferrin's N-terminus (Bellamy et al., 1992). LfB is composed of 25 amino acid residue and the amino acid sequence is FKCRRWQWRMKKLGAPSITCVRRAF. It is a highly positively charged peptide due to five Arg and three Lys residues (Yamauchi et al., 1993). It is effective against Gram negative and Gram-positive bacteria (Vorland et al., 1999). The mechanism of action of LfB-induced antimicrobial activity is not yet elucidated, but it might be act on the cytoplasmic membrane due to its positive charge and amphipatic structure (Bellamy et al., 1992). The existence of phospholipid in the bacterial membrane may act as the criteria for selectivity of this cationic peptide. In susceptible bacteria it may causes inner membrane

depolarization, but the membrane integrity remains intact. The mechanism by which LfB works are not well understood, but Haukland et al. (Haukland et al., 2001) indicates that cell membrane might be a possible target.

Previously, Moniruzzaman et al. examined the interaction of LfcinB with dioleoylphosphatidylglycerol (DOPG) and dioleoylphosphatidylcholine (DOPC) GUVs labelled with calcein and found that a rapid leakage of calcein occurred from single GUVs induced by LfcinB (Moniruzzaman et al., 2015). It was also observed that the FI of a membrane impermeant fluorescent dye, SYTOX green in the *E. coli* cell suspension increased gradually with time, in the interaction of LfcinB with *E. coli* cell suspension containing SYTOX green, which suggested that influx of SYTOX green occurred from the outside of *E.coli* into the cytoplasm (Moniruzzaman et al., 2015). Therefore, it is necessary to examine the direct interaction of LfB with single live bacterial cells.

There are several fragments of peptide derived from LfB which have biological activities such as antibacterial, antiviral, antioxidant, and immunomodulatory activities. Huang et al. worked on three types of LfB-related peptides and found that pigmentation in B16F10 melanoma cells have been demonstrated to enhanced by these peptides. Among them, LfB17-34 can actively increase synthesis of melanin (Huang et al., 2017). LfB4-9 is a fragment of LfB, which has the highest antimicrobial activity among the shorter versions of LfB. It is composed of six amino acid residues (RRWQWR), this sequence is considered to be the antimicrobial active center of LfB (Maria et al., 2015). It has three positively-charged arginine residues which is considered to promote selective interaction with bacterial cell membrane (David et al., 2006). Using fluorescence spectroscopy, interaction of LfB4-9 with lipid membranes has been investigated which based on characteristics of Trp fluorescence and its quenching (Schibili et al., 2002).

LfB4-9 entered inside the *E. coli* cells and single GUVs but did not induce damages in these membranes, which indicate that LfB4-9 has cell penetrating activity (Moniruzzaman et al., 2017). However, they examined the interaction of Rh-LfB4-9with single *E. coli* cells in buffer, where the cells are not active or in sleeping state (Moniruzzaman et al., 2017). Moreover, the elementary processes and mechanism of the interactions of Rh-LfB4-9with lipid membranes and bacteria are still not clear.

1.5 Membrane potential and its role in AMP's action

Membrane potential is defined as the electric potential difference between the aqueous solution inside and outside a cell, which is generated by the difference in concentrations of ions (which can permeate through cell membrane via ion channel proteins) between the inside and the outside of the cell. For example, when the concentration of positively charged K^+ is high inside the cell than the outside, it can diffuse down by the concentration gradient to the outside of the cell through the ion channel, leaving behind uncompensated negative charges (Fig. 1.2). This separation of charges causes the membrane potential. Membrane potential not only plays an important role in excitable cells but it also plays important role in non-excitable cells (Cone et al., 1969). Usually all eukaryotic cells maintain a negative (resting) membrane potential across their cell membrane, which varies from −55 ~ −90 mV depending on cell types (Sperelakis, 2012; Hille, 1992; Sakmann and Neher, 1995; Zhou et al., 2015).

The proton motive force (pmf), which is a major energy source for cells is vital for the typical localization of a variety of morphogenetic proteins in various species of bacteria. The pmf is composed of the transmembrane pH difference (ΔpH) and the transmembrane electrochemical potential ($\Delta\varphi$) (Strahl et al., 2010). Membrane potential serves a vital role in different process of cell physiology as it is part of pmf generation and associated with generation of adenosine triphosphate (ATP), bacterial chemotaxis and existence at small pH (Novo et al., 1999). The activity of substance transport is increased with increase in membrane potential. Since bacteria do not contain mitochondria, membrane potential also acts like membrane integrity as well as energy source and cell viability (Muller et al., 2000). Bacterial pathogens in logarithmic phase growth commonly exhibit membrane potential of −130 mV to −150 mV (Yeaman et al., 2003). In early exponential phase *E. coli* membrane potential might hyperpolarizes to −220 mV and in late exponential phase it depolarizes to −140 mV (Bot et al., 2009). *E. coli* cells exhibit approximately −85 mV at pH 5.0 and −142 mV at pH 8.0 (Felle et al., 1980).

Change in membrane potential induces a change in the gradient of electric potential in the membrane, and thus, membrane potential directly or indirectly controls cell cycle, proliferation, migration, control of cell volume, development, regeneration, differentiation and wound healing (Kadir et al., 2018; Blackiston et al., 2009; Yang et al., 2013). For example, Ras protein is a signaling protein that can bind with membrane
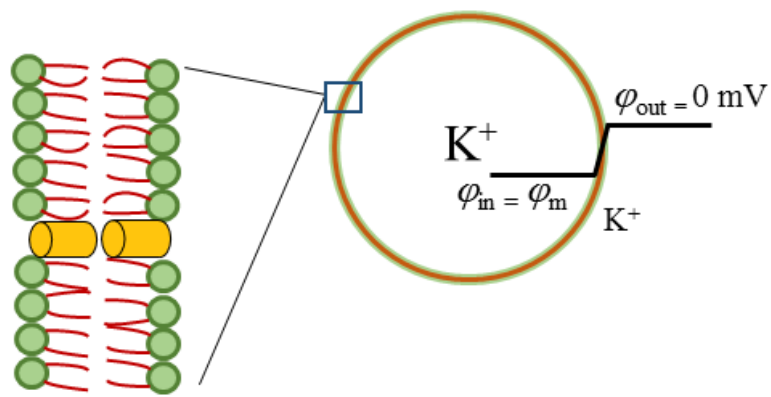
Figure 1.2: A scheme to represent the membrane potential across the cell membrane. This figure was cited from ref. (Moghal et al., 2020B) with a permission from Springer.

and play important role in cellular differentiation and proliferation. Zhou et al. reported that when depolarization of cell membrane occurs, it causes nanoscale reorganization of anionic phospholipids, such as phosphatidylserine and phosphatidylinositol 4, 5-bisphosphate, and accelerate nanoclustering of K-Ras and finally enhance MAPK signaling in nonexcitable or excitable cells (Zhou et al., 2015).

The cytoplasm of bacterial cell is well organized and it is essential for bacteria to function actively, the correct localization of their proteins, particularly those proteins that are involved in morphogenetic processes (Strahl et al., 2010). In most bacterial strain's membrane potential is vital for the typical orientation of various morphogenetic proteins. There are lot of substances with antimicrobial property in natural environment and microorganisms encounter a large number of these substances. Many of these antibiotics dissipate the membrane potential by targeting the cell membrane. For example, elongated cells of *B. subtilis* formed when incubated with the natural antibiotic nisin, which indicate a malfunctioning of Min system. Some antibiotics causes modification in structure of cell in *Spirocell*, it is supposed to be caused by the dissipation of the membrane potential induced by the delocalization of morphogenetic proteins (Strahl et al., 2010).

The effect of membrane potential in the AMPs and bacterial cells interaction have been suggested by some researchers (Yeaman et al., 1998; Wu et al., 1999). The action of platelet microbicidal protein-2 (PMP-2) for *Staphylococcus aureus* strain (6850) with a membrane potential of -150 mV to induce greater permeabilization than of another strain of *S. aureus* (JB-1) with membrane potential of -100 mV which indicate that, in this study membrane potential has a vital role (Yeaman et al., 1998). Hancock and colleague observed that large membrane voltage of usually -180 mV was essential to activate conductance in the planar bilayer's interaction with AMPs. In case of gramicidin S, indolicidin and Gram 4112 the antimicrobial property was decreased by decrease in membrane potential by increasing the concentration of K^+ from the outer side of *E. coli* cells whereas it did not cause any difference in the antimicrobial property of many peptides of α and β structured (Wu et al., 1999), suggesting that membrane potential is important for the antimicrobial property of some AMPs. Many researchers also examined the internalization process of CPPs across the cell membrane and obtained that membrane potential plays significant role in cellular uptake of CPPs (Rothbard et al., 2004; Rothbard et al., 2005; Zhang et al., 2009).

The interaction of CPPs with various lipid bilayers have also been investigated, and reported the effect of membrane potential on uptake process across the lipid bilayer (Henriques et al., 2005; Terrone et al., 2003).

1.6 Purpose of the thesis

As described in section 1.5, some experimental results using bacterial cells have suggested the effects of membrane potential on AMP activities (Yeaman et al., 1998; Wu et al., 1999). However, recent studies indicate that membrane potential greatly disturb the localization of many proteins in bacterial cells (Strahl et al., 2010). Therefore, the interpretation of the results of the effects of membrane potential on activities of AMPs obtained in bacterial cells becomes questionable. On the other hand, there have been no studies on the effect of membrane potential on the interactions of AMPs with lipid vesicles. In this thesis, I investigated the interaction of membrane potential, $\Delta\varphi$, on activities of AMPs using the single GUV method. As AMPs, I selected LfB and LfB4-9 because the interaction mode with lipid bilayers and the main cause of antimicrobial activity of these AMPs are different; LfB induces membrane damage and rapid permeabilization whereas LfB4-9 can translocate across lipid bilayer without damaging the membrane. I also examined the effect of $\Delta\varphi$ on the activities of these AMPs using single live *E. coli* cells and single spheroplasts obtained from *E. coli* cells. On the basis of the results of two AMPs, I discuss the role of $\Delta\varphi$ on the interaction of AMPs with lipid bilayers and cell membranes of bacterial cells and on the activity of AMPs.

In chapter 2, to reveal the mechanistic action of LfB's antimicrobial property, I investigated its interaction with single live *E. coli* cells and spheroplast of *E. coli* cells. Here, I prepared *E. coli* cells and also prepared the spheroplast from filamentous *E. coli* cells and labeled them with fluorescent dye, calcein. I found that LfB rapidly leaking the calcein from *E. coli* as well as from spheroplasts, which indicate that LfB causes rapid permeabilization by interacted directly with the cell membrane. To elucidate the elementary processes and its mechanism of membrane damage, I examined the interaction of this peptide with single *E. coli* lipid GUVs labelling with fluorescent dye, AF647. Here, I observed that this peptide induced local rupture in GUVs stochastically, rapidly lead to leakage of AF647. But very high concentrations of LfB were necessary to cause a significant rate of damage in GUVs when compared with the *E. coli* as well as with spheroplasts. I considered that this discrepancy is mainly by the cause of $\Delta\varphi$, which exist in the live cells and spheroplasts.

To clarify this reason, I investigate effect of $\Delta\varphi$, on membrane damage or pore formation in single GUVs induced by LfB. To identify the role of $\Delta\varphi$ on live cells I also study the effect of carbonyl cyanide m-chlorophenylhydrazone which is a proton-ionophore that are able to diminish the $\Delta\varphi$ across the membrane, on the LfB-caused leakage of internal contents from single *E. coli* cells and spheroplasts. On the basis of experimental data, I discussed the mechanisms of membrane damage or antimicrobial activity of LfB.

In chapter 3, to elucidate the elementary processes and mechanism of entry of LfB4-9 across the cytoplasmic membrane of cells, I inspected the interaction of rhodamine labeled LfB4-9 (Rh- LfB4-9) with single GUVs composed of *E. coli* lipid which has a similar lipid composition to the *E. coli* cell membrane, containing AF647 and small vesicles of DOPG/DOPC (molar ratio: 1/1), using the single GUV method. Here, I also study the interaction of Rh-LfB4-9 with live single *E. coli* cells in EZ rich medium (where the cells are active and can grow) and with spheroplast labelled with fluorescent dye calcein into its cytoplasm, using CLSM. I found that Rh-LfB4-9 entered the single GUVs without pore formation and also entered the *E. coli* cells and spheroplasts. Then I investigated the effect of membrane potential on the entry of this peptide into single GUVs, *E. coli* cells and spheroplasts. Various negative membrane potentials were induced across the lipid bilayer and the effect of membrane potential was investigated. Based on the obtained results, the effect of membrane potential on translocations of LfB4-9 across the lipid membranes and its mechanism of antimicrobial activity was discussed.

Chapter 2

Membrane Potential is Vital for Rapid Permeabilization of Plasma Membranes and Lipid Bilayers by the Antimicrobial Peptide Lactoferricin B

Chapter 2

Membrane Potential is Vital for Rapid Permeabilization of Plasma Membranes and Lipid Bilayers by the Antimicrobial Peptide Lactoferricin B

2.1 INTRODUCTION

Lactoferricin B (LfB) is a cationic AMPs, which is made by the hydrolysis of transferrin-like bovine lactoferrin in milk (e.g., pepsin digestion in the human stomach) (Bellamy et al., 1992; Kuwata et al., 1998). This peptide has antimicrobial activities against Gram-negative and -positive bacteria, yeast, and filamentous fungi (Kuwata et al., 1998; Yamauchi et al., 1993; Tomita et al., 1994). LfB is composed of 25-residue (FKCRRWQWRMKKLGAPSITCVRRAF) with five R residues and three K residues (Yamauchi et al., 1993). LfB has three-dimensional structure which exhibits an amphipathic character because one surface of the peptide is hydrophobic while its opposite surface is hydrophilic (Hwang et ai., 1998). There are shorter fragments of LfB which also have antimicrobial activity (Tomita et al., 1994, Kang et al., 1996; Schibli et al., 2002; Strom et al., 2002; Nguyen et al., 2005; Gifford et al., 2005). A shorter version of LfB composed entirely of D amino acid residues had the same antibacterial activity as that composed of natural L amino acid residues (Wakabayashi et al., 1999; Wakabayashi et al., 2003), indicating that proteins are not involved in the antibacterial activity of this peptide.

Moniruzzaman et al. investigated the interaction of LfB with single GUVs composed of negatively-charged DOPG and electrically neutral DOPC mixtures containing a water-soluble fluorescent dye, calcein, in their lumen using the single GUV method (Moniruzzaman et al., 2015). A process of AMP-induced damage of a membrane such as pore formation from a process of leakage (membrane permeation) of fluorescent dye through the damage can be separated using the single GUV method (Islam et al., 2014). The calcein concentration in the GUV lumen remained constant during the initial interaction of LfB with a single GUV, but leakage of calcein occurred suddenly from the GUV and after starting the leakage within 5 sec the leakage completed, with a concomitant decrease in GUV size. The same experiments using many "single GUVs" were carried out, and found that in all GUVs the leakage started at different time but it required only

less than 5 sec in all GUVs for complete leakage after starting. LfcinB-induced membrane damage inducing this rapid leakage was expressed by the term "local rupture" instead of "large pore". The FI of SYTOX green increased gradually with time in the interaction of LfcinB with *E. coli* cell suspension in the presence of a membrane impermeant fluorescent dye, SYTOX green, which suggested that LfcinB-induced influx of SYTOX green from the outside of *E. coli* into the cytoplasm (Moniruzzaman et al., 2015). All these investigations proposed that LfB-induced cell membrane damage is a main factor in its antimicrobial activity. However, experimental data demonstrating the direct interaction of LfB with single live bacterial cells is needed.

In this chapter, to reveal the mechanism of LfB's antimicrobial activity, its interaction with single *E. coli* cells were examined. Here, the interaction of LfB with live single *E. coli* cells containing water-soluble fluorescent dye, calcein in the cytoplasm were carried out using confocal laser scanning microscope (CLSM). A rapid leakage of calcein was induced by LfB from single *E. coli* cells, indicating that LfB induced rapid permeabilization due to damage or pore formation to the cell membrane. *E. coli* is a gram-negative, facultatively anaerobic bacterium composed of an outer membrane decorated with lipoplysaccharide, a peptidoglycan layer, and a cell membrane (inner membrane); hence, the targets of LfB may be several. I investigated the interaction of LfB with single spheroplasts derived from *E. coli* cells to find out whether direct interaction of LfB with the cell membrane plays a role in LfB-induced leakage. I prepared spheroplasts from filamentous *E. coli* cells and loaded calcein in the cytoplasm. Spheroplasts do not have an outer membrane and peptidoglycan and only the cell membrane and cytoplasm remain (Ruthe et al., 1985; Martinac et al., 1987; Wei et al., 2016; Sun et al., 2016). In this experiment I observed that LfB induced rapid leakage of calcein from single spheroplasts. To clarify the elementary processes and the mechanism of LfB-induced damage of the cell membrane,   the interactions of LfB with bacterial membrane mimic lipid bilayer i.e. GUVs of *E. coli* polar lipid extract (*E. coli*-lipid) were investigated using the single GUV method (Islam et al., 2014a; Tamba et al., 2005; Islam et al., 2014b; Hasan et al., 2018). Here I found LfB induced stochastic local rupture in *E. coli*-lipid- GUVs, but it required higher concentrations of LfB to induce a significant rate of local rupture compared with that observed in *E. coli* cells and spheroplasts. A hypothesis was proposed that this difference is mainly due to the membrane potential, which exist in the cells and spheroplasts. *E. coli* cells has a membrane potential of -100 ~ -130 mV at pH 6.0 ~ 7.0 (Felle et al., 1980) and it is expected that

the negative membrane potential could affect the interaction of highly positively charged LfB with the cell membrane due to strong electrostatic interactions. To verify this hypothesis, the effect of membrane potential on LfB-induced local rupture or pore formation in single GUVs and also the effect of proton-ionophore, carbonyl cyanide   m-chlorophenylhydrazone on the LfB-induced leakage of calcein from single *E. coli* cells and   spheroplasts were examined. On the basis of these results, I discussed the mode of action of LfB's antimicrobial activity.

2.2 MATERIALS AND METHODS

2.2.1 Materials

E. coli polar lipid extract was purchased from Avanti Polar Lipids, Inc. (Alabaster, AL). Bovine serum albumin (BSA) was purchased from Fuji Film Wako Pure Chemical Co. (Osaka, Japan). Alexa Fluor 647 hydrazide (AF647), calcein-acetoxymethyl (calcein-AM) and 3,3'- dihexyloxacarbocyanine iodide (DiOC6 (3)) were purchased from Thermo Fisher Scientific (Waltham, MA). Fmoc-amide resin was procured from Applied Biosystems (USA). Fmoc-amino acids, HBTU/HOBt were obtained from Peptide Institution Inc. Piperidine, 1-Methyl-2-Pyrrolidinone (NMP), N, N- Diisopropylethylamine (DIEA) were purchased from Sigma-Aldrich (USA). Phenol, Dimethylformamide (DMF), Methanol, Dichloromethane (DCM), t-butyl methyl ether (MTBE), Trifluoroacetic acid (TFA), Thianosole, NH_4OH, hydrogen per oxide (H_2O_2) were purchased from Fuji Film Wako Pure Chemical Co. (Osaka, Japan). 1, 2-ethanedithiol (EDT) was purchased from Nacalai Tesque, Inc., (Kyoto, Japan). Cephalexin, poly-L-lysine, deoxyribonuclease I (DNAase I), lysozyme, and carbonyl cyanide m-chlorophenylhydrazone (CCCP) were purchased from Sigma-Aldrich Co. (St. Louis, MO). Tetraethyl-ammonium chloride (TEAC) was purchased from Tokyo Chemical Industry Co., Ltd., Tokyo, Japan. EZ Rich Defined Medium (EZ rich medium) was purchased from TEKnova (Hollister, CA).

2.2.2 Peptide synthesis and identification

2.2.2.1 Peptide synthesis

LfB with an amide-blocked C terminus was synthesized by the FastMoc method using a 433A peptide synthesizer (PE Applied Biosystems, Foster City, CA) (Moniruzzaman et al., 2015). LfB composed of 25 amino acids and the sequence is FKCRRWQWRMKKLGAPSTICVRRAF.

Procedure of peptide synthesis:

Checked the chemicals (Piperidine, DCM, NMP, DIEA, HBTU/HOBt) and amino acids according to amount/cycle for LfB. Pressure of nitrogen was checked which should be > 5 pa. 1 mmol of F-moc amino acids with protection group were transferred into their respective cartridge. Prepared the reaction vessel with filter as per manual and took resin into it. Opened the exhaust vent and turned ON the fume hood. Reaction vessel was inserted into the machine and arranged the amino acids cartridges in the machine. Then the synthesis was started as per the program. After finished the synthesis cycle the reaction vessel was removed from the machine and kept 1h under hood and then dried overnight in desiccator.

```
      ┌─────────────┐                      ┌──────────────────────┐
      │ Fmoc-Resin  │                      │ Fmoc-Amino Acid (AA) │
      └─────────────┘                      └──────────────────────┘
               ↘            ┌──────────────────┐        ↙
                            │  Fmoc-AA-Resin   │
                            └──────────────────┘
                                     │
                            ┌──────────────────────┐
                            │ Deprotection Fmoc group │
                            └──────────────────────┘
                                     │
                      ┌────────────────────────────────┐
                      │ Coupling of new Fmoc Amino      │
                      │ Acid with deprotected AA-Resin  │
                      └────────────────────────────────┘
                                     │
                      ┌────────────────────────────────┐
                      │ In second cycle Deprotection and │
                      │ coupling again                  │
                      └────────────────────────────────┘
                                     │
                      ┌────────────────────────────────┐
                      │ Deprotection and coupling       │
                      │ continuously untill finished the full │
                      │ sequence of peptide synthesis   │
                      └────────────────────────────────┘
```
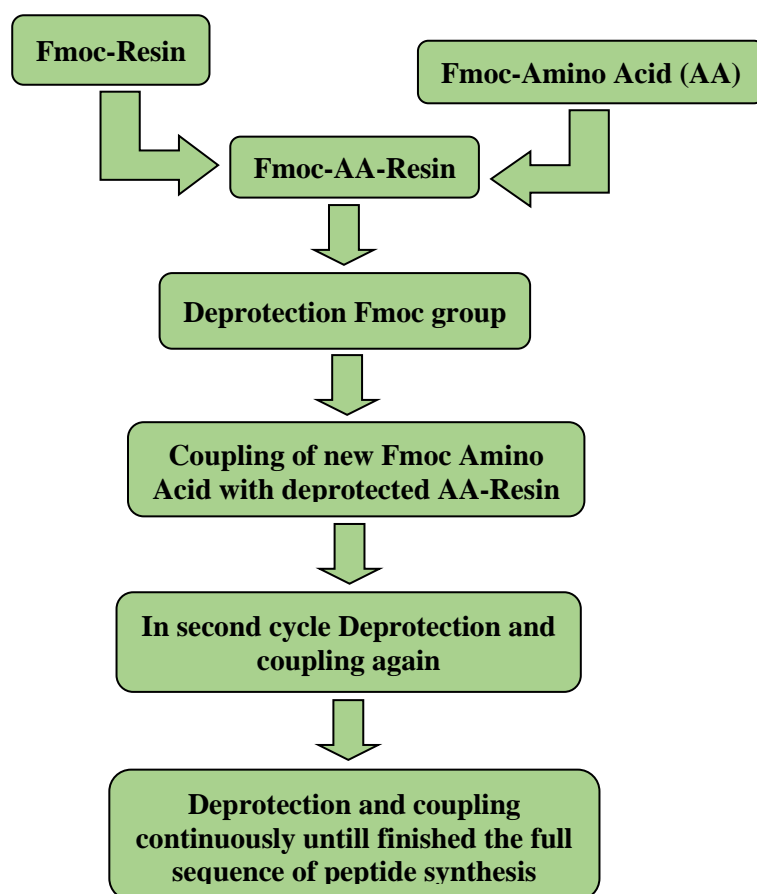
Schematic flow diagram of peptide synthesis

2.2.2.2 Cleavage and purification of LfB

Cleavage procedure of LfB

Trifluoroacetic acid (TFA), 1, 2-ethanedithiol (EDT), and MilliQ water was used to cleave the peptide from the resin. 150 mg of phenol, 50 µl of EDT, 100 µl of thianosole, 100 µl of MilliQ and 2 ml of TFA were taken in a falcon tube, which was kept it in ice for 600 sec. 50 mg of peptide resin were added into it and kept in ice for 600 sec. Then, the mixture was stirred for 2 h, after it was cooled in ice for 300 sec, this solution was filtered through glass wools and collected in a falcon tube containing ~40 ml of t-butyl methyl ether (MTBE). Then the solution was washed by centrifugation at 6000 rpm for 1800 sec at 4° C for 3 times using a centrifuge (himac CF 15R high-speed micro centrifuge, Hitachi, Japan). The supernatant were discarded and dissolved the pellet by adding 10 ml of MilliQ into it. Kept it in ice for 600 sec and then kept in liquid N_2 for 1800 sec for solidification. After that lyophilized the peptide using lyophilizer (VD-800R freeze dryer, TAITEC).

Purification and analysis of LfB

Purification and analysis of the LfB were done using reversed phase HPLC (LC-20AT and SPD-20A, Shimadzu, Kyoto, Japan) with 5 C18-AR-300 semipreparative column (10 x 250 mm, 10 µm) and a 5 C18-AR-II analytical column (4.6 x 250 mm, 5 µm; Cosmosil, Nacalai Tesque, Inc., Kyoto, Japan) by using the method described previously (Moniruzzaman et al., 2015). The HPLC data was analyzed using the Smart Chrom software (KYA technologies, Tokyo, Japan). The crude peptides main peak of a HPLC chromatogram was the reduced LfB (with two sulfhydryl groups). The fraction of main peak were collected and then lyophilized it. I used the lyophilized powder as the purified peptide. When analyzed the purified peptide only one peak was observed in a HPLC chromatogram, which was the oxidized LfB (with a disulfide bond).

Methods of purification of crude LfB:

The gradient program for purification of LfB was 30%-40% solvent B for 2400 sec (i,e, 0.25%/min). In the HPLC machine, solvent A (MilliQ + 0.1% TFA) and solvent B (Acetonitrile 90%+10% MilliQ + 0.1% TFA) were used as mobile phase. The sample were injected into injector after the mobile phase reached at equilibrium point. Took ~10 mg of crude LfB and dissolved in 1 ml milliQ. The parameter for purification

of crude LfB was set as, flow rate: 3 ml/min and run time: 3600 sec. Then the sample were loaded into injector and then injector knob was moved downward to start the program.

Methods of analysis of purified LfB:

The gradient program for analysis of purified LfB was (30%-40%) solvent B/40 min. Here in the same way took ~0.5 mg of purified LfB and dissolved in 100 µl milliQ. The parameter for analysis of purified LfB was set as, flow rate: 1 ml/min and run time: 3600 sec. Then the sample were loaded into injector and then injector knob was moved downward to start the program.

2.2.2.3 Determination of LfB concentration:

A small amount of LfB were dissolved in pipes buffer or media. Took absorbance at 278 nm. Calculated the concentration using the molar extinction coefficient of Trp ($5500\ M^{-1}cm^{-1}$). LfB has two Trp residues, so the molar extinction coefficient was $11000\ M^{-1}\ cm^{-1}$.

2.2.3 CLSM investigation of the interaction of LfB with single *E. coli* cells containing calcein

An *E. coli* (JM-109) suspension was subcultured on nutrient agar plates and incubated at 37 °C overnight to obtain single colonies. After incubation single bacterial colony was dispersed (by vortexing) in 2 ml sterile nutrient broth media and grown at 37 °C for 6 to 7 h to get exponential phase cells (Moniruzzaman et al., 2015). Then centrifuged this culture suspension at $620 \times g$ for 600 sec. After centrifugation the supernatant were discarded, washed the cell pellet and resuspended the pellet in EZ rich medium (containing 50 mM NaCl and 1.3 mM K_2HPO_4 as main ion sources (Neidhardt e al., 1974)). Then the bacterial suspension was diluted to obtain a final bacterial concentration of 1×10^6 CFU/mL. *E. coli* cells were loaded with calcein according to the method of Dubey et al. (Dubey et al., 2011). Calcein AM is the acetomethoxy (AM) derivate of calcein which is widely used for labeling live cells. In live cells the acetomethoxy (AM) ester hydrolysis by intracellular esterases which converted the nonfluorescent calcein-AM to green-fluorescent calcein. When the calcein-AM transported into live cells cellular esterases cut off the AM groups, the molecule binds to calcium within cell resulting in acquiring strong green fluorescence, and gets trapped inside. Calcein-AM easily permeates intact live cells because of its hydrophobic nature. Here only the live cells were marked as

dead cells lack esterases. This feature made it very useful for testing of cell viability. In brief, I added a 50 µL aliquot of calcein-AM (1.0 µg/µL in DMSO solution) into 1.0 mL of the bacteria suspension, and was shaken for 2 h at room temperature under darkness using a rotary shaker. Then, centrifuged the suspension at $620 \times$ g for 600 sec, and resuspended the pellet in fresh EZ medium. I repeated this procedure twice. Then *transferred* the *E. coli* suspension into a hand-made chamber which was prepared on a glass slide by putting a U-shaped silicone-rubber spacer between the glass slide and a cover slip (Moniruzzaman et al., 2015). *E. coli* cells had settled onto the cover slip surface after 900 sec and were adsorbed thereafter. For fixing the live *E. coli* cells on the glass surface of cover slips, cover slips were coated with poly-L-lysine using the standard method. In brief, 20 ml of NH_4OH and 20 ml of H_2O_2 were added in 100 ml of milliQ and mixed well. This solution was heated upto 70-80° C. Then some cover slips were taken in a holder and soaked them into the hot solution for 600 sec. The cover slips were cooled to room temperature and washed by milliQ for 3 times and then washed it by ethanol. Then I dried the cover slips by N_2 gas. I took 10 µl of 0.01% poly-L-lysine and put cover slip into it and dried it well.

Interactions of LfB with single *E. coli* cells containing calcein were observed under a CLSM (FV-1000, Olympus, Tokyo, Japan) at 25 ± 1 °C with a stage thermocontrol system (Thermoplate, Tokai Hit, Shizuoka, Japan), in reference to a previously reported method (Moniruzzaman et al., 2017). For CLSM measurements, fluorescence images of calcein (excited by a laser at $\lambda = 473$ nm: 0.4%, HV: 582v, Gain: 4.125x, offset: 6%) and differential interference contrast (DIC) images were obtained using a 60×objective (UPLSAPO060X0, Olympus) (NA = 1.35) (Islam et al., 2014b; Moniruzzaman et al., 2017). During interaction of the peptide with single *E. coli* cells, various concentrations of LfB in the medium were added continuously to the vicinity of the single *E. coli* cells through a 20-µm-diameter glass micropipette positioned by a micromanipulator (Moniruzzaman et al., 2015; Karal et al., 2015). In brief, a GUV was selected under the microscope, and tip of the micropipette was approached near the GUV using the micromanipulator. I applied a small pressure inside the micropipette for adding the peptide solution in the vicinity of the GUV. Micropipette aspiration method was used and controlled the injection pressure by changing the height of water in a U-shaped glass tube. The distance between the tip of the micropipette and the single cells was 50 µm, and the applied pressure, ΔP (= $P_{in} - P_{out}$, where P_{in} are the pressure of the inside and P_{out} are the outside of a micropipette) was 30 Pa.

ΔP was measured by a differential pressure transducer (DP15, Validyne, CA), pressure amplifier (PA501, Validyne, CA), and a digital multimeter. Glass micropipettes were prepared by pulling 1.0 mm glass capillaries composed of borosilicate glass (G-1, Narishige, Tokyo, Japan) to a needlepoint using a puller (PC-10, Narishige) and then made it to a desired tip diameter by breaking it by quick fracture. Then, various concentrations of LfB solution were filled into the micropipette by aspiration using a vacuum pump. Details of these methods have been described previously (Karal et al., 2015; Yamazaki et al., 2008).

In the presence of CCCP the experiments for the interaction of LfB with single *E. coli* cells in the EZ rich medium, CCCP solution in DMSO in EZ media were mixed with the of *E. coli* cells suspension loaded with calcein (final concentrations of CCCP was 100 μM, DMSO was 0.5 %, and *E. coli* cells was 1×10^6 CFU/mL). I transferred this mixture into a hand-made microchamber and incubate for more than 600 sec, then I investigated LfBs interaction with single *E. coli* cells.

2.2.4 Preparation methods of spheroplasts of *E. coli* cells

An *E. coli* suspension was subcultured on nutrient agar plates and incubated at 37 °C for overnight to get single colonies. A single colony of bacteria was dispersed (by vortexing) in sterile nutrient broth media and grown for 10 to 12 h at 37 °C in an incubator shaker (MBR-032P. TAITEC, Koshigaya, Japan) at 200 rpm. After diluting this culture 10 times (final volume: 5 mL), 60 μL of 5 mg/mL cephalexin was added to this culture (final cephalexin concentration; 60 μg/mL). Then, the culture was shaken at 42 °C for 10−12 h, producing single-cell filaments with 50−150 μm length, which were confirmed using CLSM (Fig 2.1A (2)). I obtained these filaments as a pellet by centrifugation of the above suspension at 1500×g for 300 sec, then rinsed the pellet (without resuspension) by gentle addition of 1 mL of 0.8 M sucrose, and incubated it at room temperature for 60 sec. The supernatant was removed using a Pasteur pipette and resuspended in 2.5 mL of 0.8 M sucrose. Then the following reagents were added to this suspension in order; 150 μL of 1 M Tris-HCl (pH 7.8), 120 μL of 5 mg/mL lysozyme, 30 μL of 5 mg/mL DNase I, and 120 μL of 0.125 M EDTA-Na (pH 8.0), and then incubated it at room temperature for 480−600 sec. To stop the reaction, I added

Figure 2.1

(A)

(1) 2 μm

(2) 80 μm

Cephalexin

E coli cell

Long filament

Lysozyme

EDTA

(3) 5.5 μm

Spheroplast

(B)

(1) (2)

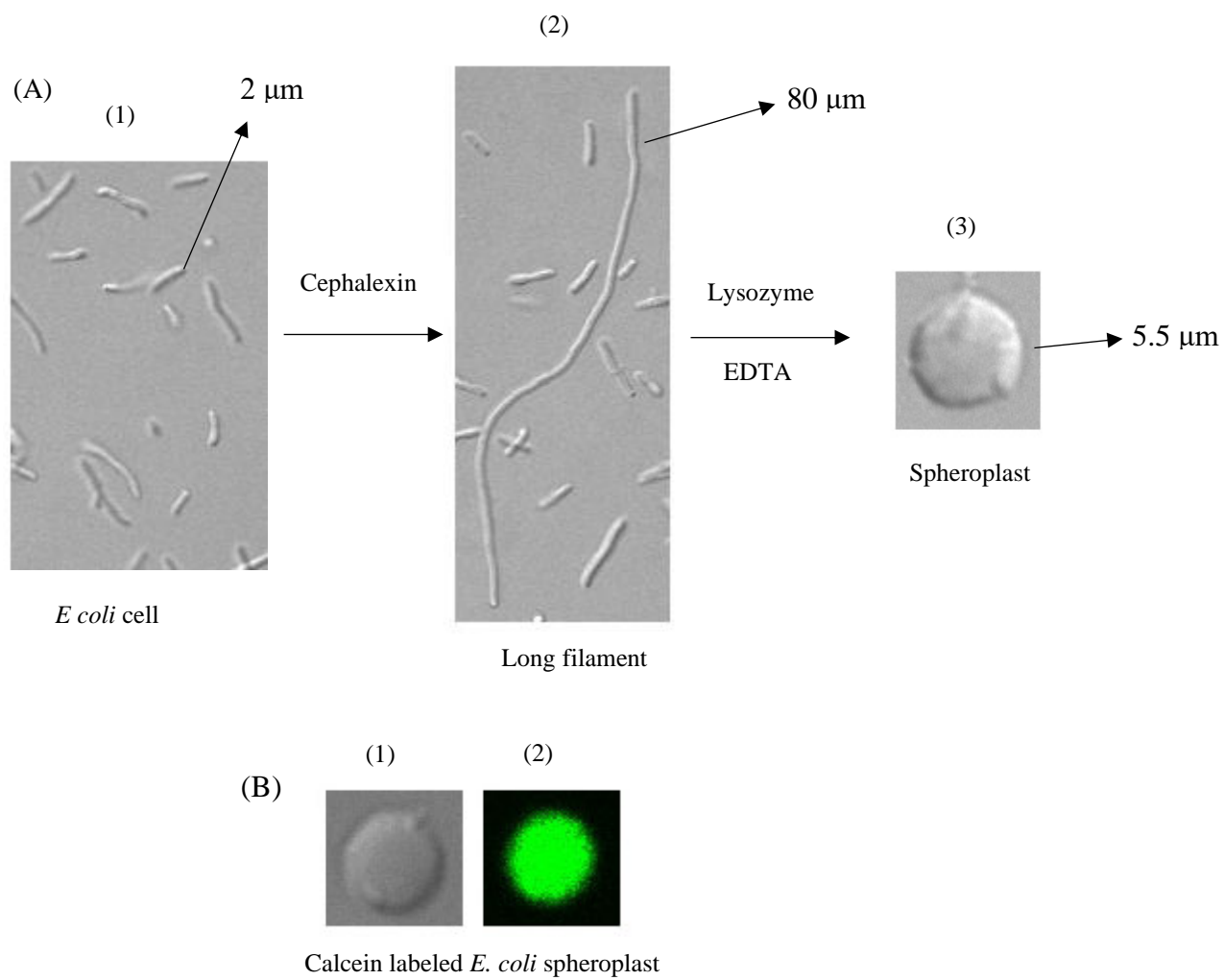Calcein labeled *E. coli* spheroplast

Figure 2.1 Preparation method of spheroplasts from *E. coli* cells

1 mL of a solution containing 20 mM MgCl₂, 0.7 M sucrose, and 10 mM Tris-HCl (pH 7.8) over 60 sec while stirring, and incubated it at room temperature for 240 sec. 2 mL of this suspension was layered over 4 mL buffer (10 mM Tris-HCl (pH 7.8) containing 1.5 mM KCl, 48.5 mM NaCl, and 0.73 M sucrose (or 10 mM Tris-HCl (pH 7.8) containing 10 mM MgCl2 and 0.8 M sucrose (Martinac et al., 1987; Wei et al., 2016)), and then concentrated it using Vivaspin 6 (100 kDa MWCO, GE Healthcare, Buckinghamshire, UK) by centrifugation at 6000×g for 1200 sec to obtain ~1.0 mL suspension of the spheroplasts. I repeated this purification procedure. 4 mL of a new buffer (10 mM Tris-HCl (pH 7.8) containing 1.5 mM KCl, 48.5 mM NaCl, and 0.73 M sucrose (or 10 mM 10 mM Tris-HCl (pH 7.8) containing 10 mM MgCl₂ and 0.8 M sucrose (Martinac et al., 1987; Wei et al., 2016)) was added to this ~1.0 mL suspension and mixed, and then concentrated it using Vivaspin 6 under the same condition to obtain 1 mL suspension of the spheroplasts (Fig 2.1A (3)).

2.2.5 Interaction of LfB with single spheroplasts containing calcein

A similar method of Martinac et al. (Martinac et al., 1987) were used to prepare spheroplasts of *E. coli* cells. During purification, MgCl₂ was replaced with KCl and NaCl because Mg²⁺ affected LfBs interaction with spheroplasts. For purification of spheroplasts I used buffer of 10 mM Tris-HCl (pH 7.8) containing 1.5 mM KCl, 48.5 mM NaCl, and 0.73 M sucrose. Within 3 h of purification, I used these spheroplasts for the experiment.

For labelling the spheroplasts with calcein, a similar method of calcein loading in *E. coli* cells (Dubey et al., 2011) were used. A 50 µL aliquot of calcein-AM (1.0 µg/µL in DMSO solution) was added to 1.0 mL suspension of spheroplast (final concentration of DMSO was 1%), and incubated for 1800 sec at room temperature under darkness. I used a handmade microchamber and transferred the spheroplast suspension into it and used for the interaction of LfB under CLSM (Fig 2.1B (2)). The interaction of LfB with single spheroplasts labelled with calcein was investigated using a similar method for single *E. coli* cells at 25 ± 1 °C, which in the above section was mentioned. The CLSM conditions; Laser (473 nm): 0.1%, HV: 550v, Gain: 4.125x, offset: 6%) were used in this experiment.

In the presence of CCCP, the interaction of LfB with single spheroplasts were examined, for that experiment, I used the same buffer as the suspension of spheroplasts containing calcein and mixed CCCP solution comprising DMSO (final concentrations of CCCP was 100 µM and DMSO was 0.5 %). I used a handmade microchamber and transferred the spheroplast suspension into it. Then incubate this for > 600 sec and then investigated LfBs interaction with single spheroplasts.

2.2.6 GUV preparation

GUVs of *E. coli* polar lipid extract (*E. coli*-lipid-GUVs) containing fluorescent dye were prepared by the natural swelling method at 37 °C for 2-3 h (Moniruzzaman et al., 2015). In brief, to prepare dry lipid films 200 µl of 1 mM *E. coli* polar lipid in chloroform were taken in a 5 ml glass vessel and dried by N_2 gas. After dry kept the vessel in desiccator for overnight (≥12 hours) for complete removal of liquid. 20 µl of milliQ were added into this lipid film and kept in ~47° C for 420 sec for prehydration. Then incubated at 37 °C for 2-3 h with buffer C (10 mM PIPES, pH 7.0, 1 mM EGTA, 50 mM NaCl) containing 0.1 M Sucrose and 6 µM AF647 dye. After that the GUV suspension were centrifuged at 13000 rpm for 1200 sec to remove Multilamellar vesicles and lipid aggregates. The membrane filtering method was used to remove untrapped fluorescent dye (Tamba et al., 2011). Briefly, after centrifugation the GUV suspension was filtered through a nucleopore polycarbonate membrane of 10 µm pores diameter using a handmade apparatus to get desired size of GUVs and remove un-trapped fluorescent dye. Here, the nucleopore membrane was clamped in a polypropylene filter holder and then the top and bottom side of the filter holder were connected to a 10 mL plastic syringe (syringe A) and a tube made of polypropylene, respectively. The other end of the tube was connected to another 10 mL plastic syringe (syringe B) and the GUV suspension was added to syringe B. A peristaltic pump (Tokyo Rikakikai Co., Ltd) was used to add buffer C containing 0.1 M glucose to syringe B at a constant velocity, maintained the flow rate 1 ml/min and the buffer in syringe A was simultaneously removed at the same constant velocity using the pump. Finally, I collected the suspension in the tube and the filter holder and used as a purified GUV suspension for the experiment.

Purified GUV suspension (300 µL: 0.1 M sucrose in buffer C as the internal solution; 0.1 M glucose in buffer C as the external solution) was transferred into a hand-made microchamber (Moniruzzaman et al., 2015). To prevent strong interaction between the glass surface and GUVs, the inside of the microchamber was coated with 0.10% (w/v) BSA in buffer C containing 0.10 M glucose (Moniruzzaman et al., 2015).

2.2.7 Interaction of LfB with single *E. coli*-lipid-GUVs

GUVs were observed using CLSM (FV-1000, Olympus) at 25 ± 1 °C using a stage thermocontrol system (Thermoplate, Tokai Hit). For CLSM measurements, fluorescence images of AF647 (excited by a laser at λ = 635 nm: 0.3%, HV: 700v, Gain: 4.5x, offset: 6%) and DIC images were obtained using the 60× objective (Islam et al., 2014b; Moniruzzaman et al., 2017; Waggoner et al., 1979). To investigate the effect of LfB on single GUVs, various concentrations of LfB in buffer C containing 0.10 M glucose were added continuously to the vicinity of the GUV through a 20-µm-diameter glass micropipette positioned using a micromanipulator. The distance between the single cells and the tip of the micropipette was 50 µm, and the applied pressure, ΔP, was 30 Pa (Karal et al., 2015). Consequently, the LfB concentration near the GUV approached steady state and was almost the same as the concentration inside the micropipette (Karal et al., 2015).

2.2.8 Application of membrane potential to single GUVs

For application of membrane potential in GUVs, a gradient of K^+ concentration across the GUV membrane was generated. For generating permeability of K^+ in the GUV membrane, gramicidin A molecules were incorporated into the membrane. Gramicidin A is a small ion channel for monovalent cations, here I also used TEAC, which cannot permeate through the gramicidin A channel nor it can block the channel. Due to this purpose, I prepared *E. coli*-lipid/ gramicidin A (molar ratio: 100/0.01) GUVs from a dry lipid film in buffer K (10 mM PIPES, pH 7.0, 50 mM KCl and 1 mM EGTA) containing 0.10 M sucrose and 6.0 µM AF647 by using the same method as mentuioned earlier i.e. the natural swelling method, and did the purification using membrane filteration. Then I diluted this purified GUV suspension with buffer T (10 mM PIPES, pH 7.0, 50 mM TEAC and 1 mM EGTA) containing 0.1 M glucose at various ratios. The total

concentration of KCl and TEAC in the buffer outside the GUVs was 50 mM, which had the same osmotic pressure as the buffer inside the GUVs. The membrane potential difference across a GUV membrane, $\Delta\varphi$, or the membrane potential inside a GUV, φ_{in}, was measured using the following Nernst equation:

$$\Delta\varphi = \frac{RT}{F}\ln\frac{[K^+]_{out}}{[K^+]_{in}} = 25.7\ln\frac{[K^+]_{out}}{[K^+]_{in}}\,(mV) \tag{2.1}$$

where F is the Faraday constant, R is the gas constant, T is the absolute temperature, $[K^+]_{out}$ and $[K^+]_{in}$ are the K^+ concentration outside and inside the GUV, respectively. The numerical value (25.7) in the last equation in eq. 2.1 is for 25 °C. For example, when I diluted the GUV suspension with buffer T at a GUV suspension to buffer T ratio of 1:9, $\Delta\varphi = -59$ mV at 25 °C. I used the samiliar method mentioned in the above section for investigating LfBs interaction with single GUVs using various $\Delta\varphi$. Prepared LfB soluton using the same buffer mixture as for the outside of the GUVs. After application of the K^+ concentration different, I waited for 600 sec to get an equilibrium, and observed the GUVs under CLSM.

The value of $\Delta\varphi$ was monitored using a fluorescent dye, $DiOC_6(3)$, which is sensitive to the $\Delta\varphi$ (Waggoner et al., 1979; Shapiro et al., 1994; Fulda et al., 1998; Ishihara et al., 2006). $DiOC_6(3)$ has a positive ion and two short hydrocarbon chains with 6 carbons, and thus it locates in both aqueous phase and membrane and also it can be translocated across the cell membranes and lipid bilayers. Due to its positive ion, $DiOC_6(3)$ can be distributed according to electric potential such as $\Delta\varphi$. First, I mixed the $\Delta\varphi$ dye $DiOC_6(3)$ with the same buffer as the the outside of the GUVs, and then mixed this $DiOC_6(3)$ solution with the GUVs suspension. The final concentrations of $DiOC_6(3)$ was 1 nM and methanol was 0.006%. I used a handmade microchamber and transferred the GUV suspension into it. I coated the microchamber with 0.10% (w/v) BSA to prevent strong interaction between the glass surface and the GUVs. After the application of the K^+ concentration gradient waited for 600 sec to get an equilibrium, and observed the GUVs under CLSM (FV-1000) at 25 ± 1 °C using the stage thermocontrol system (Thermoplate). Fluorescence images of $DiOC_6(3)$ (excited by a laser at λ = 473 nm: 0.5%, HV: 650v, Gain: 6x, offset: 7%) and DIC images were obtained using the 60×

objective. I measured the fluorescent intensity (FI) of the images from CLSM by using the software supplied with the CLSM (Fluoview, v. 4.1, Olympus). The FI of the rim a GUV due to the binding of $DiOC_6(3)$ dye was measured as the peak intensity in a line crossing the GUV (Islam et al., 2014a).

I investigated the interaction of LfB with single *E. coli*-lipid-GUVs with various $\Delta\varphi$ using the same method mentioned in the above section (investigation of the LfBs interaction with single *E. coli*-lipid-GUVs using CLSM). Various concentrations of LfB in the same buffer as for the outside of the GUVs (i.e., mixture of buffer T and buffer K with various ratios) containing 0.10 M glucose were added continuously to the vicinity of the GUV through a glass micro- pipette of 20-μm-diameter which was positioned using a micromanipulator.

2.3 RESULTS AND DISCUSSION

2.3.1 Interaction of LfB with single *E. coli* cells

To observe the interaction of LfB with single live *E. coli* cells using CLSM I used a synthetic cell culture medium, EZ medium. The composition of EZ medium are well defined, and thus, one can remove unfavorable reactions with the peptide (Neidhardt et al., 1974). To detect any damages in the cell membrane of *E. coli* cells induced by LfB, *E. coli* cells were interacted with Calcein-AM, which can enter their cytoplasm which converted into calcein after hydrolysis due to esterase (Dubey et al., 2011; Moniruzzaman et al., 2017).

A suspension of *E. coli* cells in EZ rich medium were transferred into a microchamber and then the cells were setteled down to the poly-L-lysine coated coverslip and fixed on it. Under this condition *E. coli* cells grew and the average increase in cell length for 600 sec was $11 \pm 3\%$. To induce an interaction of LfB with single *E. coli* cells on the coverslip a LfB solution was continuously added to the neighborhood of a cell using a micropipette, the LfB concentration near the cell became constant at a steady state, and was almost the same as that in the micropipette (Karal et al., 2015). Two kinds of cells were present, one type is the cells which have septum, i.e. a cell wall in the stage before cell division (Osella et al., 2017) called septating cells

Figure 2.2
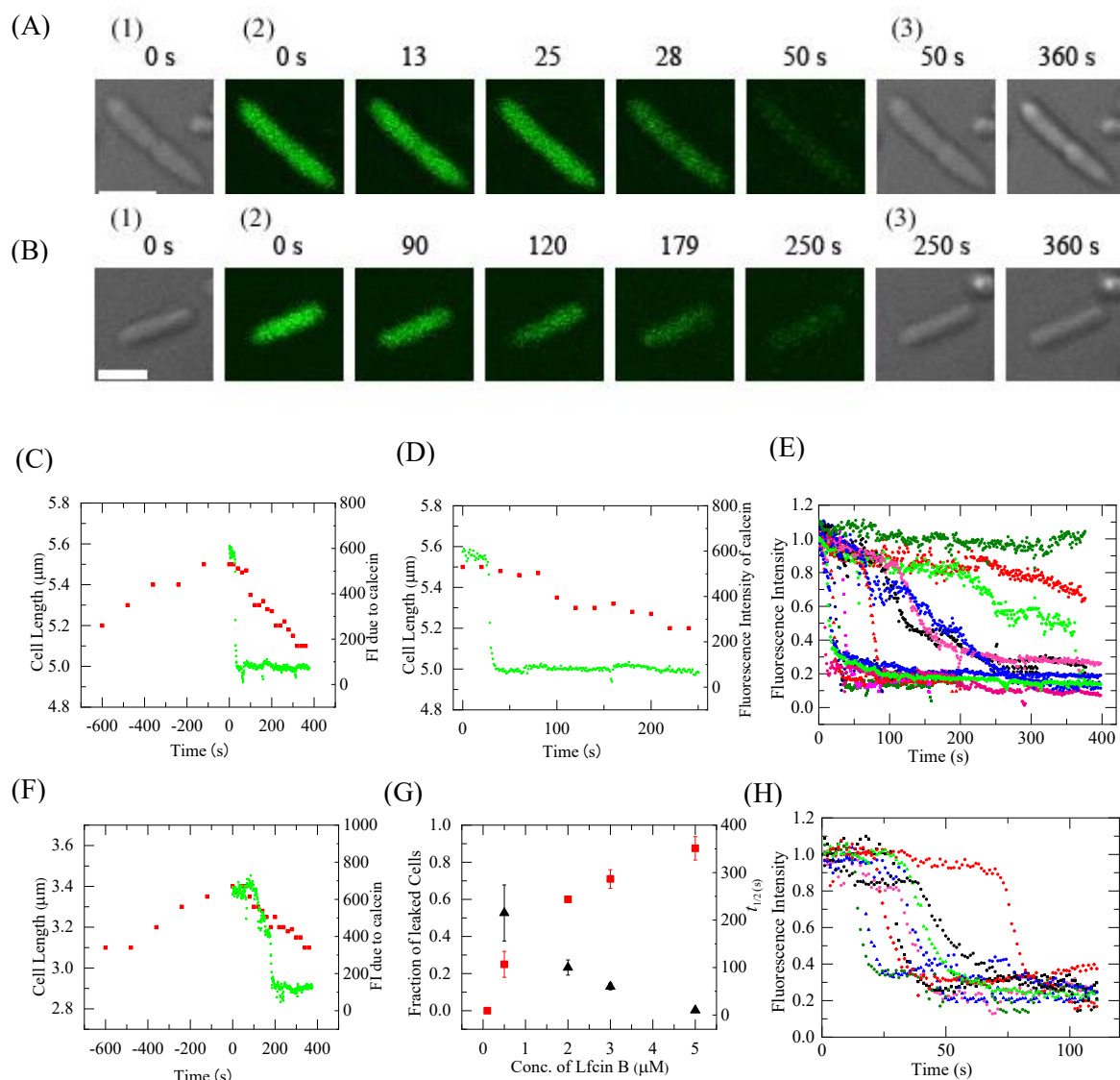
Figure 2.2 LfB-induced leakage of calcein from single *E. coli* cells. (A) (B) Images of an *E. coli* cell during the interaction of LfB due to calcein fluorescence (2) and DIC images (1) (3) obtained using CLSM. The number top on each image showing the interaction time with (A) 3.0 μM and (B) 0.5 μM LfB. The bar is 2.0 μm. The following CLSM conditions were used; Laser (473 nm): 0.4%, HV: 582v, Gain: 4.125x, offset: 6%) (C) (D) The time course of the FI of the total cell due to calcein (green line) and cell length (red squares) during the interaction of 3.0 μM LfB at 25 °C in (A). The LfB solution was added at $t = 0$. (D) An expanded figure of (C) after $t = 0$. (E) Time course of the change in the normalized FI change of several "single cells" under the same conditions as in (A). Each curve corresponds to the time course of FI for each cell. (F) The time course of the FI of the total cell due to calcein (green line) and cell length (red squares) during the interaction of 3.0 μM LfB at 25 °C in (B). The LfB solution was added at $t = 0$. (G) Concentration dependence of LfB of the fraction of leaked cells (red ■) and the leakage half-time (▲). Average values and SDs of the fraction of leaked cells (or SEs of leakage half-time) are shown. (H) Time course of the normalized FI change of several "single cells" during the interaction of 5.0 μM LfB.

31

and another one is non-septating cells which lack this septum between the cells. First I examined the interaction of 3.0 μM LfB with single cell, Figure 2.2A shows a typical result for septating cells. During the interaction of LfB, the FI (FI) of the cell due to calcein did not change during the initial interaction by26 s, then decreased rapidly (Fig. 2.2A and green line in Fig. 2.2C and 2.2D), indicating that LfB induced rapid permeabilization of calcein through *E. coli* cell membrane. This phenomenon can be explained as follows; LfB induced damage or pore formation in the cell membrane and then calcein permeated. On the other hand, the length of the cell increased before the addition of LfB (6% increase for 600 sec), but subsequently the length gradually decreased (7% decrease for 360 sec after the start of the interaction) (red squares in Fig. 2.2C and 2.2D). The same experiments were performed using 10 cells (i.e., 7 non-septating and 3 septating cells). I observed the same phenomenon (i.e., first a rapid leakage of calcein occurred, then a gradual decrease in cell length) in 7 cells (i.e., 5 non-septating and 2 septating cells). To estimate the rate of AMP-induced pore formation or damages of bacterial cells, one can use the fraction of AMP-induced leaked cells among all examined cells after a specific time, i.e., 360 sec reaction (P_{leak} (360 sec)), (tamba e al., 2005; 2009), P_{leak} (360 sec) was 0.70 for 3.0 μM LfB. Five independent experiments ($N = 5$) were conducted for 3.0 μM LfB concentration, and the average value and the standard deviation (SD) of the fraction of leaked cell was obtained. P_{leak} (360 sec) was 0.71 ± 0.05. To elucidate the LfB-induced leakage of calcein in more detail, I examined the time course of FI of several cells during the interaction of 3.0 μM LfB. This result indicates a wide distribution of rates of LfB-induced leakage of calcein from a single cell. The rate of leakage in septating cells was larger than that in non-septating cells. To compare the rate more quantitatively, I estimated the rate of LfB-induced leakage of calcein from a single cell using half-time (i.e., $t_{1/2}$), which is defined as the time required for leakage of 50% of total calcein from a single cell after the start of the leakage. The distribution of $t_{1/2}$ was plotted using a histogram (Fig. 2.3). This indicates that the $t_{1/2}$ values of all septating cells ($n = 28$) were less than 50 s, but the $t_{1/2}$ values of non-septating cells ($n = 44$) was widely distributed from 6 to 259 s. This quantitative analysis supports the conclusion that the rates of leakage from septating cells were larger than those from most non-septating cells and there is a wide distribution of the rates of leakage from non-septating cells. Before the interaction of LfB the cell length of *E. coli* cells
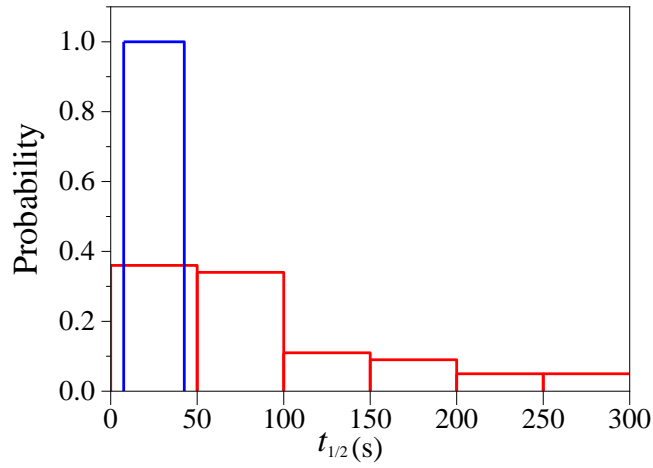
Figure 2.3

Figure 2.3 The rate of LfB-induced leakage of calcein from single cells interacting with 3.0 µM LfB. The distribution of half-time (i.e., $t_{1/2}$) of leakage of calcein in all the examined cells is shown using a histogram. Blue bar and red bar indicate the probability of each range of $t_{1/2}$ in septating cells and in non-septating cells, respectively.

increased, but after the start of the interaction of LfB the cell length started to decrease, indicating that the LfB-induced leakage from cells stopped cell growth. These results indicate that first LfB induced permeabilization in cell membrane of *E. coli* cells due to damage or pore formation in the cell membrane, through which calcein rapidly leaked, and then cell growth stopped, resulting in a decrease in cell length. A similar decrease in the cell length of *E. coli* cells was reported for the AMP, LL-37 (Sochacki et al., 2011).

Next, I investigated the interaction of a lower concentration (0.5 μM) of LfB with single *E. coli* cells in the media at 25 °C. Figure 2.2B shows a typical result for non-septating cells. During the interaction of 0.5 μM LfB, the FI of a cell due to calcein was constant initially (up to 110 s), and then gradually decreased (Fig. 2.2B and green line in Fig. 2.2F), indicating that LfB induced rapid permeabilization due to damage or pore formation in the cell membrane through which calcein leaked. On the other hand, cell length increased before the interaction of LfB (10% increase for 600), but subsequently cell length gradually decreased (9% decrease for 360 sec) (red squares in Fig. 2.2F).

Figure 2.2G shows the effect of LfB concentration on P_{leak} (360 sec). At 0.1 μM, no leakage was observed (i.e., $P_{leak} = 0$), while at and above 0.5 μM P_{leak} increased with an increase in LfB concentration. This result indicates that the rate of damage or pore formation in the cell membrane of *E. coli* cells increased with increasing LfB concentration. On the other hand, the rate of LfB-induced leakage of calcein through damages or pores gives us information on the size of pores and the extent of damages. Figure 2.2H shows the time course of FI of several cells due to calcein among all examined cells ($n = 17$ for 2 independent experiments) during the interaction of 5.0 μM LfB, indicating that LfB induced leakage of calcein from a single cell at a great rate and the values of this rate exhibited a sharp distribution. The average value and the standard error (SE) of leakage half-time ($t_{1/2}$) were obtained for each LfB concentration (the number of cells, n, was 15−17, except for 3.0 μM ($n = 72$) and for 0.5 μM ($n = 5$)) (Fig. 2.2G). For example, $t_{1/2}$ for 2 μM and 5 μM LfB was 100 ± 20 s and 10 ± 1 s, respectively. Leakage half-time decreased with an increase in LfB concentration (Fig. 2.2G), indicating that the rate of leakage from the pores increased with increasing LfB.

It is reported that the minimum inhibitory concentration (MIC) of LfB against *E. coli* (JM-109) is 3 ± 1 μM (Moniruzzaman et al., 2015). For measurement of MIC, a suspension of many *E. coli* cells is used. As

the interaction of LfB with many cells proceeds, the effective LfB concentration outside the cells decreases. For example, if I use 3 μM LfB initially, the effective concentration outside the cells is smaller than 3 μM. Moreover, the MIC values are determined after ~20 h culture. In contrast, in the experiments of interaction of LfB with single *E. coli* cells described above, LfB solution continuously was added and hence the LfB concentration remains constant from the beginning (e.g., 3 μM). Therefore, LfB concentration near *E. coli* cells in single cell experiment is larger than that in the MIC measurement using a suspension of cells. This is the reason why P_{leak} (360 sec)) was large for 3.0 μM LfB. To compare quantitatively the result of single cell experiments shown in Fig. 2.2 and that of MIC measurement, we need a systematic investigation near future.

To elucidate the role of $\Delta\varphi$ in the interaction of LfB with single live *E. coli* cells, the effect of a proton-ionophore, carbonyl cyanide m-chlorophenylhydrazone (CCCP) on the interaction of LfB with the cells were investigated. It is recognised that CCCP decreases the gradient of the electrochemical potential of proton (or the proton-motive force) in the cell membrane of bacterial cells such as *E. coli* cells by increasing proton permeability in the membrane, dissipating the $\Delta\varphi$, as well as the transmembrane pH difference across the cell membrane, ΔpH (Strahl et al., 2010). If the pH of the external media is neutral, ΔpH is small (Felle et al., 1980). The pH of EZ media used in the above experiments is pH 7.0, and hence, one can consider that CCCP mainly dissipated $\Delta\varphi$ under these experimental conditions.

First I examined the effect of 100 μM CCCP in the EZ medium (final concentration), on the interaction of 5.0 μM LfB with single *E. coli* cells in the medium at 25 °C. The FI of the cell due to calcein was constant during the interaction (up to 360 sec) (Fig. 2.4 A, B), indicating LfB did not induce any damage in the cell membrane through which calcein leaked. The same experiments were performed using 12 cells (i.e., 10 non-septating and 2 septating cells), and the same result was observed. Two independent experiments were conducted using 12–15 *E. coli* cells ($N = 2$), and the same results were obtained.

These results indicate that the $\Delta\varphi$ in the cell membrane plays an important role in the LfB-induced permeabilization due to damage or pore formation in the cell membrane of *E. coli* cells.

Figure 2.4

(A)
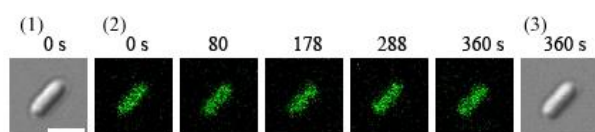
(B)
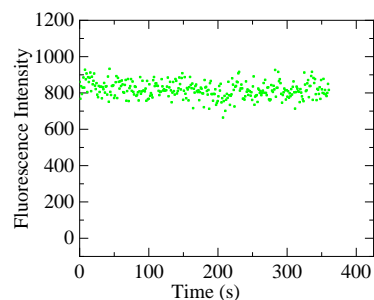
Figure 2.4 Effect of CCCP on LfB-induced leakage from single *E. coli* cells. (A) Images of an *E. coli* cell during the interaction of LfB due to calcein fluorescence (2) and DIC images (1) (3) obtained using CLSM. The number above each image shows the interaction time with 5.0 μM. The bar is 2.0 μm. The following CLSM conditions were used; Laser (473 nm): 0.4%, HV: 582v, Gain: 4.125x, offset: 6%) (B) Time course of the FI change of the total cell during interaction with 5.0 μM LfB due to calcein at 25 °C in (A). The LfB solution was added at $t = 0$.

2.3.2 Interaction of LfB with single *E. coli* spheroplasts

The results in the previous section indicates that LfB induces rapid permeabilization in cell membrane of *E. coli* cells. However, as described in the introduction of this chapter, *E. coli* cells have complicated structure composed of outer membrane, peptidoglycan and the cell membrane. It is reported that some AMPs interact with lipopolysaccharide (LPS) in the outer membrane and peptidoglycan. To examine the direct interaction of LfB with the cell membrane of *E. coli* cells, it is important to use *E. coli* spheroplasts which do not have the outer membrane and peptidoglycan. Here, I investigated the interaction of LfB with single spheroplasts derived from *E. coli* cells using CLSM. To detect the damage of the cell membrane of spheroplast induced by LfB, I tried to load calcein inside the spheroplasts using the Calcein-AM by the same method applied to *E. coli* cells (2.3.1). After the reaction of spheroplasts suspension with Calcein-AM. I obtained many spheroplasts with high FI due to calcein (Fig. 2.5A). This result indicate that esterase in the cytoplasm of spheroplasts are active as same as *E. coli* cytoplasm. Here, I use their spheroplasts in my experiment.

First, I investigated the interaction of 2.0 μM LfB with single spheroplasts in the spheroplasts buffer (i.e., 10 mM Tris-HCl (pH 7.8) containing 1.5 mM KCl, 48.5 mM NaCl and 0.73 M sucrose) at 25 °C (the concentrations of K^+ and Na^+ are almost the same as those in the EZ rich media). A LfB solution was continuously provided to the vicinity of a spheroplast through a micropipette. During the interaction of 2.0 μM LfB, the FI of the spheroplast lumen due to calcein was constant up to 66 s, and then rapidly decreased to zero within a few seconds (Fig. 2.5A and 2.5B), indicating that LfB induced rapid permeabilization due to damage or pore formation in the cell membrane of the spheroplast through which calcein leaked. When the same experiments were performed using other spheroplasts, similar rapid leakage of calcein occurred stochastically within 360 sec after gradual decrease in FI (Fig. 2.5C). This initial gradual decrease in FI was also observed in spheroplasts in the absence of LfB, and hence we can consider reasonably that it is due to the photobleaching of calcein (Fig. 2.5C). For 2.0 μM LfB, 13 spheroplasts exhibited leakage by 6 min among all examined ones ($n = 16$) (i.e., P_{leak} (360 sec) = 0.81).

Figure 2.5

Figure 2.5 LfB-induced leakage of calcein from single *E. coli* spheroplasts. (A) Images of an *E. coli* spheroplasts during the interaction of LfB due to calcein fluorescence (2) and DIC images (1) (3) observed using CLSM. The number above each image shows the interaction time with 2.0 µM LfB. The bar is 5.0 µm. The following CLSM conditions were used; Laser (473 nm): 0.1%, HV: 550v, Gain: 4.125x, offset: 6%) (B) Time course of the normalized FI change of the total spheroplast during the interaction of 2.0 µM LfB due to calcein at 25 °C shown in (A). The ratio of the FI at time *t* to that of before addition of the LfB was defined as normalized FI. (C) Time course of the change in the normalized FI change of several "single cells" under the same conditions as in (A). (D) Time course of the change in the normalized FI change of several "single cells" during the interaction of 5.0 µM LfB. In (C) and (D), each curve corresponds to the time course of FI change of each spheroplast. (E) Concentration dependence of LfB of the fraction of leaked spheroplasts (red ■). Average values and SDs are shown for the fraction of leaked spheroplasts.

Next, I investigated the interaction of higher concentrations of LfB with single spheroplasts at 25 °C. During the interaction of 5.0 μM LfB, the FI of spheroplasts due to calcein was constant, and then rapidly decreased (Fig. 2.5D), indicating that LfB induced rapid permeabilization due to damage or pore formation in the cell membrane of the spheroplasts. Figure 2.5E shows the LfB concentration dependence of P_{leak} (360 sec) (N=2). At 0.1 μM, no leakage was observed (i.e., $P_{\text{leak}} = 0$), while at 2.0 μM, $P_{\text{leak}} = 0.76 \pm 0.07$, and at 5.0 μM, $P_{\text{leak}} = 1.0$; thus, P_{leak} increased in a LfB concentration-dependent manner. This result indicates that the rate of damage or pore formation in the cell membrane of spheroplasts increased with increasing LfB concentration.

These results indicate that the direct interaction of LfB with the cell membrane of spheroplasts induces rapid permeabilization due to damage or pore formation in the membrane, through which the internal contents rapidly leak. The effect of LfB concentration of the fraction of leaked spheroplast for 360 sec was similar to that of *E. coli* cells, indicating that one of the targets of LfB in *E. coli* cells is the cell membrane. In contrast, the time-course of the LfB-induced leakage from spheroplasts was different from that of *E. coli* cells. The starting time and the rate of leakage in *E. coli* cells was slower and had wider distribution compared with that in spheroplasts. This difference can be explained as follows. In *E. coli* cells, at first LfB molecules interact with the outer membrane and peptidoglycan layer and then to reach the cell membrane. Therefore these interactions decrease and vary the rate of increase in LfB concentration in the cell membrane. Moreover, for the leakage of calcein molecules to the outside of the cells, they must permeate through the peptidoglycan layer and the outer membrane, which decreases and varies the rate of leakage of calcein. Therefore, the difference of the time-course of the leakage is due to the barriers (i.e., the peptidoglycan layer and the outer membrane) of the cells.

Several experimental results indicate that spheroplasts from *E. coli* cells have $\Delta\varphi$ (Daniels et al., 1981). To elucidate the role of $\Delta\varphi$ in the interaction of LfB with single spheroplasts, I examined the effect of a CCCP on the interaction of LfB with the spheroplasts. In the presence of 100 μM CCCP in spheroplasts buffer, I investigated the interaction of 5.0 μM LfB with single spheroplasts at 25 °C. A gradual decrease in FI occurred during the interaction (up to 360 sec) (Fig. 2.6A, B) one can reasonably infer that the

Figure 2.6

(A)

(B)

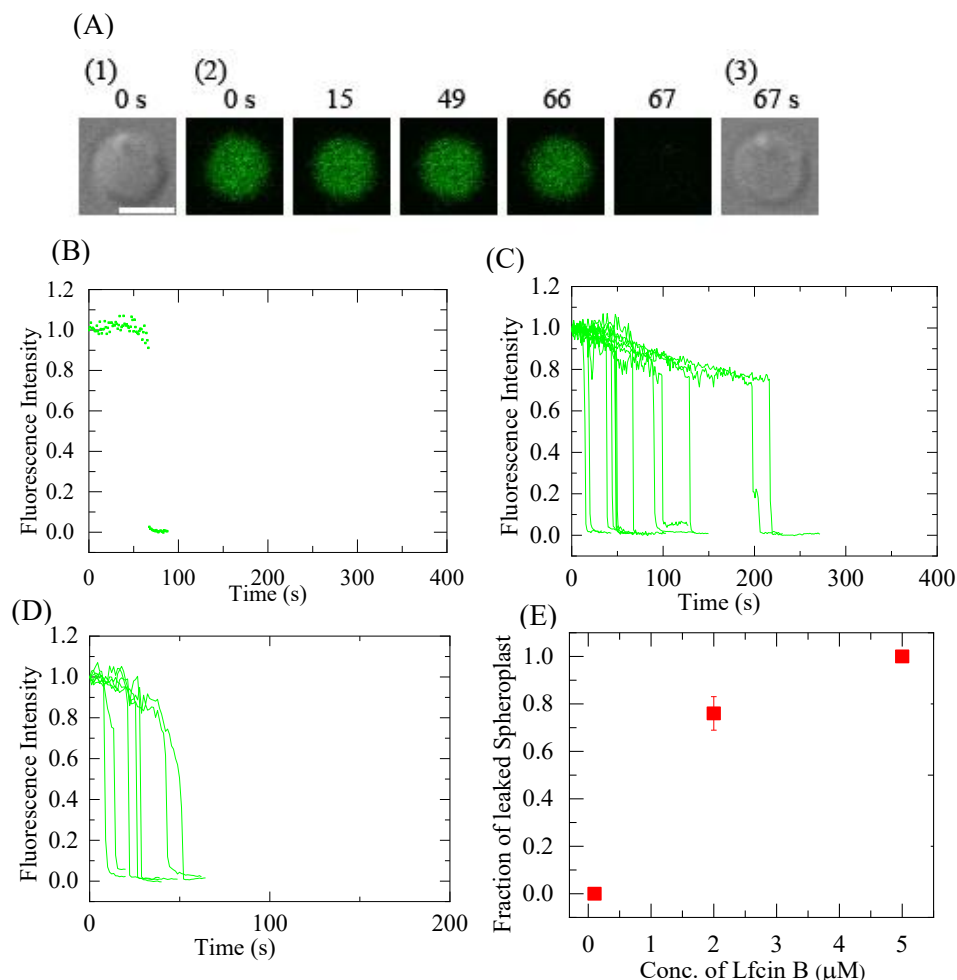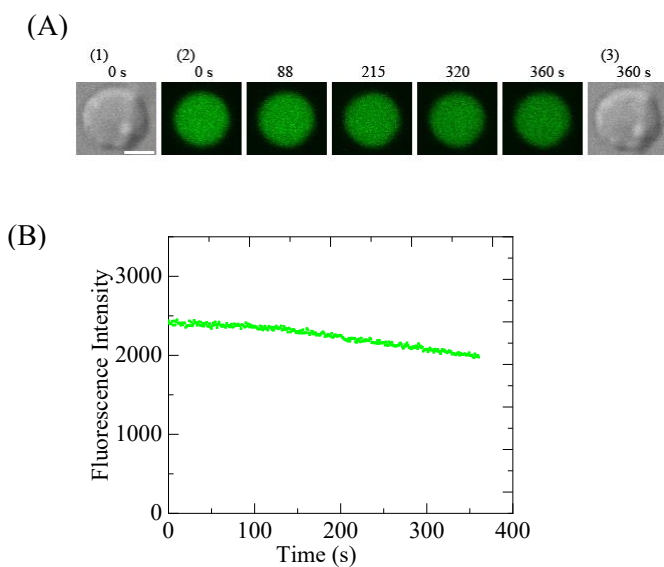**Figure 2.6** Effect of CCCP on LfB-induced leakage from single *E. coli* spheroplast. (A) Images of an *E. coli* spheroplast during the interaction of LfB due to calcein fluorescence (2) and DIC images (1) (3) obtained using CLSM. The number above each image shows the interaction time with 5.0 μM. The bar is 5.0 μm. The following CLSM conditions were used; Laser (473 nm): 0.1%, HV: 550v, Gain: 4.125x, offset: 6%). (B) Time course of the FI change of the total cell during the interaction of 5.0 μM LfB due to calcein at 25 °C in (A). The LfB solution was added at $t = 0$.

photobleaching of calcein caused this gradual decrease because a similar gradual decrease in FI was observed in spheroplasts without interacting LfB. Therefore this results indicates LfB did not induce any damage in the cell membrane through which calcein leaked. The same experiments were performed using 15 spheroplasts, and the same result was observed (i.e., $P_{leak} = 0$). Two independent experiments were conducted using 15 spheroplasts ($N = 2$), and the same results were obtained.

This result indicates that the $\Delta\varphi$ in the spheroplasts plays an important role in the LfB-induced rapid permeabilization due to damage or pore formation in their membranes.

2.3.3 LfB-induced leakage of internal contents from single *E. coli*-lipid- GUVs

The result in the previous section indicates that LfB interacts directly with the cell membrane to induce rapid permeabilization. However, the cell membrane of spheroplast is composd of lipid bilayer and membrane proteins. There are two possible targets for LfB to induce permeabilization. To identify the target of LfB in the cell membrane, here I prepared GUVs of lipid bilayers where lipid composition is almost same as *E. coli* cell membrane and examined the interaction of LfB with these single GUVs. For this purpose, I prepared GUVs comprising *E. coli* polar lipid extract (*E. coli*-lipid), whose lipid composition is phosphatidylethanolamine (PE) / phosphatidylglycerol (PG) / cardiolipin (CA) [67/23/10 (wt% ratio)]. To monitor any damages in *E. coli*-lipid-GUV membrane or the leakage of internal contents, the lumen of GUVs contained a water-soluble fluorescent dye, AF647. To use the same monovalent ion concentration of EZ medium (50 mM) buffer C (10 mM PIPES, pH 7.0, 1 mM EGTA, 50 mM NaCl) was used to prepare GUVs and to examine their interaction with LfB. Figure 2.7A shows a typical experimental result of the interaction of 40 µM LfB with single GUVs. The FI of the GUV lumen (i.e. lumen intensity) due to AF647 remained essentially constant during the addition of LfB solution for the first 124 s, then the lumen intensity rapidly decreased (Fig. 2.7A (2) and Fig. 2.7B). At 125 s, the lumen intensity fell to effectively zero; a DIC image of the same GUV (Fig. 2.7A (3)) showed that the spherical GUV structure remained, albeit with an apparent decrease in diameter. This is essentially the same phenomenon as that observed in the interaction of LfB with DOPG/DOPC (1/1)-GUVs (Moniruzzaman et al., 2015). As discussed in the previous report (Moniruzzaman

Figure 2.7

(A)

(B)

(C)

(D)

(E)
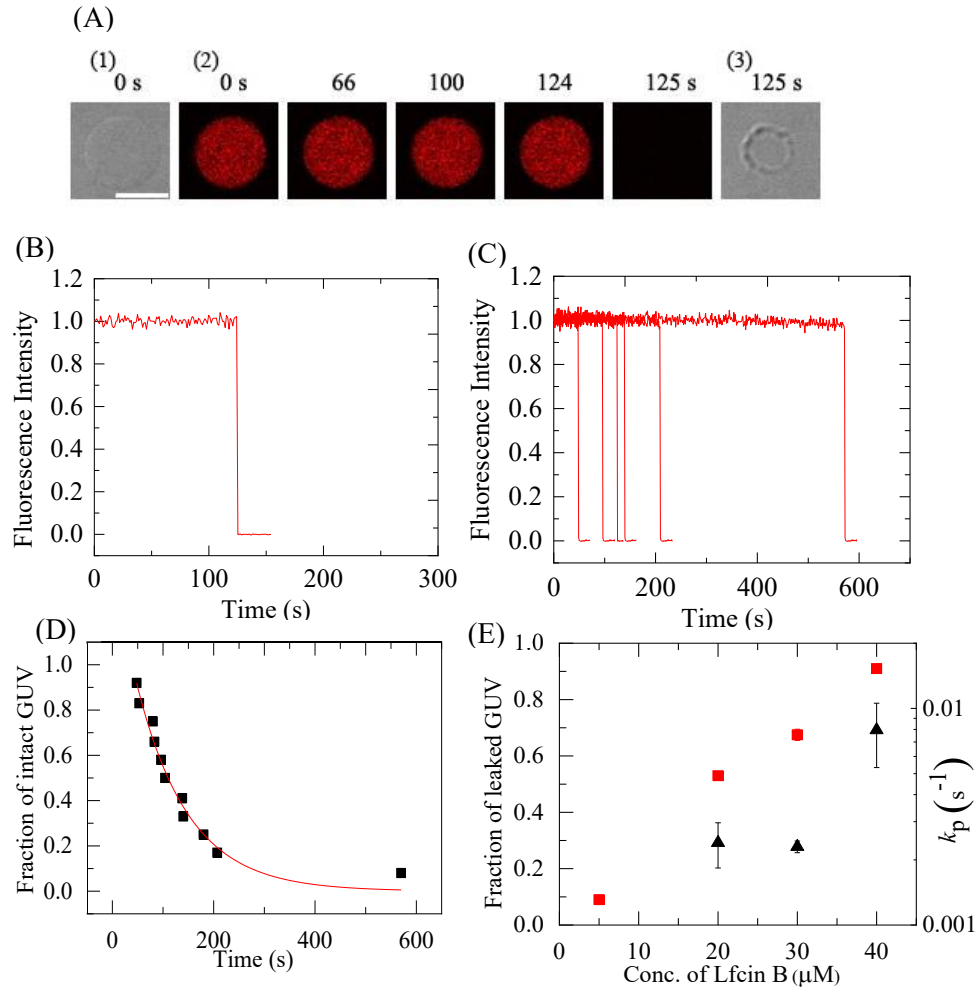
Figure 2.7 LfB-induced leakage of AF647 from single *E. coli*–lipid-GUVs. (A) CLSM Images of a GUV due to AF647 during the interaction of LfB (2) and DIC images (1) (3). The number above each image shows the interaction time with 40.0 μM LfB. The following CLSM conditions were used; Laser (635 nm): 0.3%, HV: 700v, Gain: 4.5x, offset: 6%). The number on top each image shows the time in sec after the addition of 40 μM LfB. The bar corresponds to 20 μm. (B) Time course of the change in the normalized FI of the GUV lumen (i.e. lumen intensity) shown in (A). T (C) Time course of the normalized lumen intensity of several "single GUVs" under the same conditions as in (A). Each curve corresponds to the time course of each GUV. (D) Time course of fraction of intact GUV, P_{intact}, among all examined GUVs. The solid line represents the best fit curve of eq. 2.2. (E) LfB concentration dependence of the rate constant of local rupture, k_P, (▲) and fraction of leaked GUV at 600 sec (red ■). Average values and SDs are shown for these values.

42

et al., 2015), the rapid decrease in lumen intensity occurred as a result of the rapid leakage of the AF647 through the LfB-induced local rupture of the GUV. Thus, the onset time of decrease in lumen intensity can be considered as the onset time of local rupture of the GUV. When the same experiments were carried out using 12 single GUVs, I observed the similar rapid leakage of AF647 from each GUV occurred at different time (Fig. 2.7C). This indicates that the LfB-induced local rupture is a stochastic phenomenon.

To analyze the stochastic phenomena, introduction of probability concept is useful. If one observe the fate of single GUVs interacting with LfB, the local rupture occurs at random time. However, if one consider an ensemble of all examined single GUVs, the probability of GUVs without local rupture (or the fraction of intact GUV) $P_{intact,}$ can be calculated as a function of time. The analysis of the result shown in Fig. 2.7C indicates that $P_{intact}(t)$ decreases with time. One can consider the LfB-induced local rupture of GUVs as the transition from the intact to locally ruptured GUV without an intermediate state (i.e. two-state transition). This transition is similar to an irreversible first-order reaction. Thus, if one use k_P as the rate constant of two-state transition, $P_{intact}(t)$ can be described using the following equation:

$$P_{intact}(t) = \exp\{-k_p(t-t_{eq})\} \tag{2.2}$$

where t_{eq} is a fitting parameter that denotes the time required for the binding equilibrium of LfB from the aqueous solution to the GUV membrane. k_P can be interpreted as the rate constant of local rupture of GUV caused by LfB. The data found experimentally for the time course of P_{intact} in Fig 2.7D fit well to a theoretical curve (Eq. 2.2). Two independent experiments ($n = 2$) were carried out using 12-15 single GUVs to get the time course of P_{intact} and determined the average value for $k_{P,}$, and these curves also showed a good fit by eq. 2. The average value and SD of k_P for 40 μM LfB was $(8 \pm 3) \times 10^{-3}$ s^{-1} ($n = 2$). Figure 2.7E (▲) indicated that the k_P increased with an increase in LfB concentration. To obtain the value of k_P accurately, it is required that in most GUVs local rupture occurs. In other words, if local rupture occurs in a small fraction of GUVs, one cannot determine the value of $k_{P.}$ In this case, one can use the fraction of leaked GUVs (P_{leak}) or the fraction of local ruptured GUV among all examined GUVs after a specific interaction time as a measure of the rate of lcal rupture of GUV. The value of $P_{leak}(t)$ can be determined from $P_{intanct}(t)$ using $P_{leak} = 1 - P_{intact}(t)$.

Figure 2.7E (■) also revealed that the fraction of leaked GUV among all examined GUVs (P_{leak} [$= 1 - P_{intact}$]) after 600 sec (i.e., P_{leak} (600 sec)) increased with an increase in LfB concentration. At less than 5 µM LfB, no leakage of AF647 was observed, indicating that local rupture did not occur in *E. coli*-lipid-GUVs at low LfB concentrations.

2.3.4 Application of the membrane potential to *E. coli*-lipid-GUVs

As described in the previous section, LfB induced rapid, stochastic leakage of AF647 from single *E. coli*-lipid-GUVs; however, higher concentrations of LfB were required to induce a significant rate of local rupture in GUVs compared to *E. coli* cells and spheroplasts. On the other hand, the results shown in Fig. 2.4 and Fig. 2.6 indicate that $\Delta\varphi$ across the cell membrane of *E. coli* cells and spheroplasts increases the rate of LfB-induced pore formation or local rupture of the cell membrane. On the basis of these results, I inferred that $\Delta\varphi$ may increase the rate of LfB-induced local rupture in *E. coli*-lipid-GUVs. To test this hypothesis, the effect of $\Delta\varphi$ on LfB-induced leakage from single *E. coli*-lipid-GUVs were examined.

To apply a $\Delta\varphi$ across a GUV membrane I used a differential potential. For this purpose a small amount of gramicidin A (gA) were incorporated in the *E. coli*-lipid-GUV membrane and a difference in K^+ concentration between the lumen and the outside of the GUVs was applied by diluting GUVs prepared in buffer K (containing 50 mM KCl) with buffer T (containing 50 mM tetraethyl-ammonium chloride (TEAC)) at various ratios. It is well known that gA is a monovalent cation-selected ion channel (Finkelstein et al., 1981; Hille et al., 1992), and tetraethyl-ammonium ions (TEA^+) cannot pass through the gA channel nor block the channel (Andersen et al., 1983). In this situation, K^+ concentration in the GUV lumen ($[K^+]_{in}$) is larger than that in the exterior of the GUV ($[K^+]_{out}$), and thus, K^+ diffuses through gA channel from the lumen to the exterior, resulting in membrane potential difference, $\Delta\varphi$. At equilibrium, the flux of K^+ from the lumen to the exterior due to the diffusion of K^+ is counterbalanced by the flux of K^+ from the lumen to the exterior due to the movement of K^+ driven by the electric field produced by $\Delta\varphi$. Therefore, only the ratio of K^+ concentration in the outside of a GUV, $[K^+]_{out}$, to that in the GUV lumen, $[K^+]_{in}$, determines $\Delta\varphi$, according to the Nernst equation (i.e., eq. 2.1 in the section 2.2.8). For example, when $[K^+]_{in} = 50$ mM, $\Delta\varphi = -59$ mV for $[K^+]_{out} = 5.0$ mM, and $\Delta\varphi = -102$ mV for $[K^+]_{out} = 0.94$ mM at 25 °C.

To detect a change in $\Delta\varphi$ produced by various K^+ differnce across GUV membranes, I examined the interaction of 1 nM of $\Delta\varphi$-sensitive dye $DiOC_6(3)$ with *E. coli*-lipid-GUVs at various $\Delta\varphi$ using CLSM. Figure 2.8A shows representative CLSM images of one of the *E. coli*-lipid-GUVs in the presence of various values of $\Delta\varphi$. The FI of the GUV membrane (i.e., the rim intensity of the GUV) due to $DiOC_6(3)$ increased with an increase in negative $\Delta\varphi$ (Fig. 2.8A and 2.8B).

$DiOC_6(3)$ has a positive charge and two short hydrocarbon chains, and thus, it can enter the cytoplasm of cells under negative potentials by translocating across the cell membranes and hence the $DiOC_6(3)$ concentration in the cytoplasm increases (Waggoner et al., 1979; Shapiro et al., 1994; Fulda et al., 1998; Ishihara et al., 2006). In the case of GUVs, with an increase in negative $\Delta\varphi$, the $DiOC_6(3)$ concentration in the GUV lumen becomes larger than that in the outside of the GUV. The binding equilibrium of $DiOC_6(3)$ in between the GUV lumen and the inner monolayer of the GUV holds, and thus, the $DiOC_6(3)$ concentration in the inner leaflet of the GUV increases with an increase in negative $\Delta\varphi$. It can be reasonably inferred that the rim intensity due to $DiOC_6(3)$ is proportional to $DiOC_6(3)$ concentration in the GUV membrane at a low concentration, although at higher $DiOC_6(3)$ concentrations the rim intensity would decrease due to quenching of $DiOC_6(3)$ (Waggoner et al., 1979). Therefore, Fig. 2.8 indicates qualitatively that the $DiOC_6(3)$ concentration in the GUV membrane increased with an increase in $\Delta\varphi$ (calculated by the Nernst equation), i.e., with an increase in the K^+ concentration gradient. I can reasonably infer that the binding constant of $DiOC_6(3)$ from aqueous solution to lipid monolayers is large because $DiOC_6(3)$ has two hydrocarbon chains per molecule, and thus, most $DiOC_6(3)$ dyes exist in the membrane, not in aqueous solution of the GUV lumen. Therefore, the sensitivity of detection of $\Delta\varphi$ in the measurement of the rim intensity is greater than that in the measurement of FI of GUV lumen. The result shown in Fig. 2.8 also indicates that the GUVs prepared using this method showed negative $\Delta\varphi$ and their absolute value increased with a decrease in K^+ concentration in the outside of a GUV, $[K^+]_{out}$. Hence, these GUVs can be used to investigate the effect of $\Delta\varphi$ on the LfB-induced local rupture of GUVs.

Figure 2.8

(A)

-102   -59   -23.5   0 mV

(B)
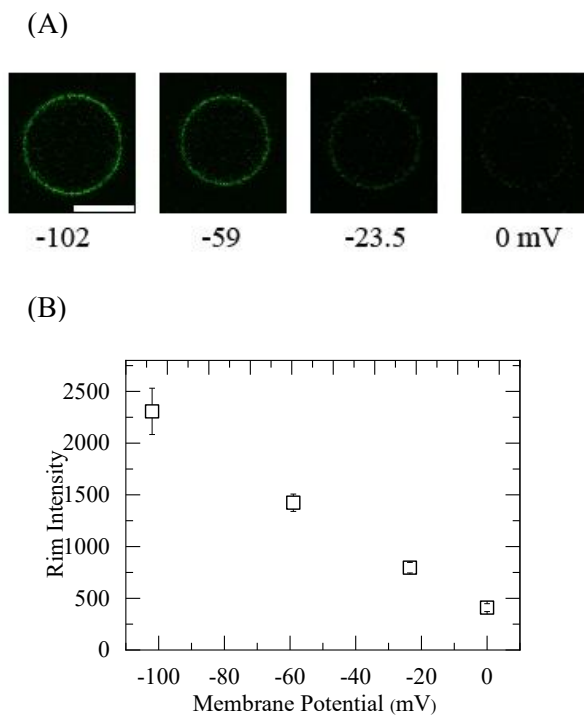
Figure 2.8 Effects of $\Delta\varphi$ on the rim intensity due to $DiOC_6(3)$ in single *E. coli*-lipid-GUVs. (A) Images of the GUV due to $DiOC_6(3)$ fluorescence obtained using CLSM. The following CLSM conditions were used; Laser (473 nm): : 0.5%, HV: 650v, Gain: 6x, offset: 7%). The number below each image shows the $\Delta\varphi$ on the GUV membrane (from 0.0 to -102 mV). The bar corresponds to 20 μm. (B) Dependence of rim intensity of single GUVs on $\Delta\varphi$ at 25 °C. The average values and SDs of the rim intensity are shown.

2.3.5 Effect of $\Delta\varphi$ on the LfB-induced leakage of AF647 from single *E. coli*-lipid-GUVs

To elucidate the effect of $\Delta\varphi$ on LfB-induced membrane permeabilization or LfB-induced local rupture in single *E. coli*-lipid-GUVs. I examined the interaction of LfB with single GUVs containing AF647 with various membrane potential. First, I used 5.0 µM LfB (Fig. 2.9). In the absence of $\Delta\varphi$, 5.0 µM LfB did not induce significant leakage of AF647 from single GUVs, i.e., P_{leak} (600 sec) = 0.09 (Fig. 2.7E). When I applied $\Delta\varphi = -102$ mV to the GUVs, 5.0 µM LfB induced the leakage of AF647 greatly. For example Fig 2.9A and B show that the lumen intensity of the GUV lumen due to AF647 did not change for the first 50 s interactions, then the lumen intensity rapidly decreased, and at 51 s, the FI reached essentially zero. A DIC image of the same GUV (Fig. 2.9A (3)) showed that the spherical GUV structure remained, albeit with an apparent decrease in diameter. The starting time of decreased lumen intensity corresponded to the onset time of local rupture of GUV. When the same experiments were carried out using 15 single GUVs, I observed the stochastic occurrence of a similar rapid leakage of AF647 from each GUV (Fig. 2.9C). Figure 2.9D shows that the P_{intact} of *E. coli*-lipid-GUVs decreased with time in the presence of 5.0 µM LfB, which was fit to the theoretical curve (eq. 2.2). To determine the average value for k_P, two independent experiments ($n = 2$) using 12-15 single GUVs to obtain the time course of P_{intact} were carried out and these data were also fit well with eq. 2.2. The average value of k_P for 5.0 µM LfB at $\Delta\varphi = -102$ mV was $(4.9 \pm 0.2) \times 10^{-3}$ s^{-1} ($n = 2$). I also examined the effect of different concentration of LfB (20.0 µM). For example, Fig. 2.10 shows the results of the interaction of 20.0 µM LfB with single GUV at $\Delta\varphi = -86$ mV. Figure 2.9E indicated that the k_P increased with an increase in negative $\Delta\varphi$ (or the absolute value of $\Delta\varphi$). Figure 2.9F indicated that P_{leak} (600 sec) also increased with $\Delta\varphi$. At $\Delta\varphi = -102$ mV, the fraction of leaked GUV at 600 sec increased with increasing LfB concentration (Fig. 2.9G).

The single GUV method can provide information on the rate of membrane permeation through the damage of the membrane such as pore formation. For this purpose, one has to analyse the time course of FI of a GUV lumen due to a fluorescent dye. In the case of LfB-induced leakage of AF647, in the absence of $\Delta\varphi$ the rate of leakage of AF647 was very large, Thus, I cannot detect the effect of $\Delta\varphi$ on the rate of leakage.

Figure 2.9
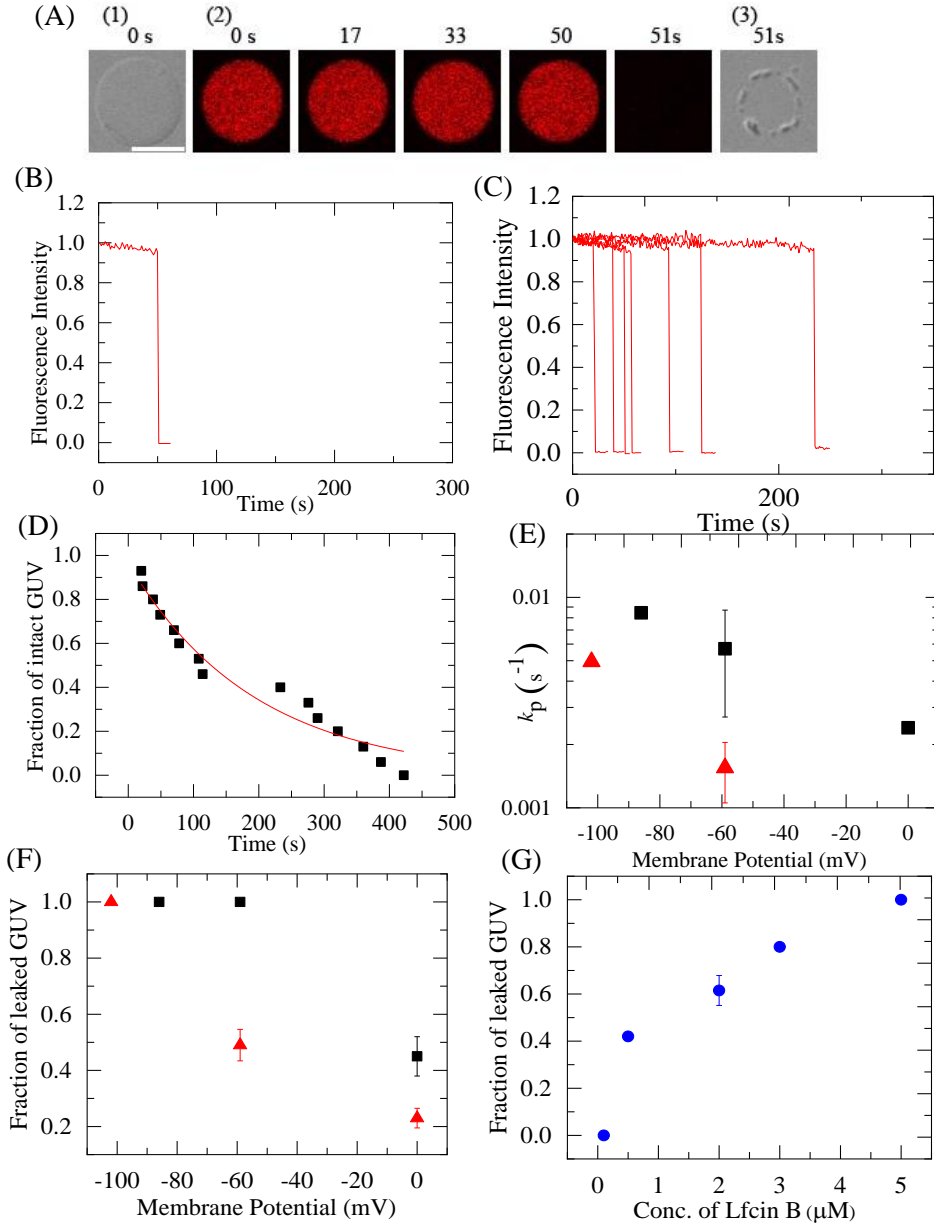
Figure 2.9 Effect of $\Delta\varphi$ on the LfB-induced leakage of AF647 from single *E. coli*-lipid-GUVs. (A) CLSM images due to AF647 of single *E. coli*-lipid-GUVs with $\Delta\varphi = -102$ mV induced by 5 μM LfB at 25 °C. (2) and DIC images (1) (3). The following CLSM conditions were used; Laser (635 nm): 0.3%, HV: 700v, Gain: 4.5x, offset: 6%). The number on top of each image shows the time in sec after the addition of 5 μM LfB.. The bar corresponds to 20 μm. (B) Time course of the normalized lumen intensity of the GUV shown in (A). (C) Time course of the normalized lumen intensity of several GUVs under the same conditions as in (A). Each curve corresponds to the time course of each GUV. (D) Time course of fraction of intact GUV, P_{intact}, among all examined GUVs. The solid line represents the best fit curve of eq. 2.2. (E) Effect of $\Delta\varphi$ on the rate constant of pore formation, k_P. Average values and SDs of k_P are shown. (red ▲) 5 μM and (■) 20 μM LfB. (F) Dependence of P_{leak} (600 sec) on $\Delta\varphi$. (red ▲) 5 μM and (■) 20 μM LfB. (G) LfB Concentration dependence of fraction of leaked GUV at 600 sec in the presence of $\Delta\varphi = -102$ mV.

48

Figure 2.10

(A)

(B)   (C)

(D
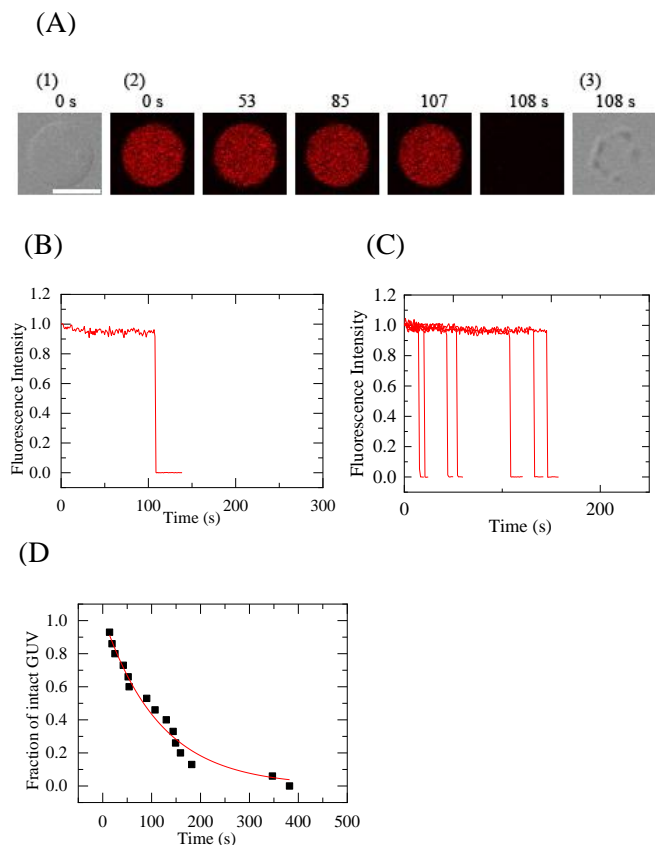
Figure 2.10 LfB -induced leakage of AF647 from single *E. coli*-lipid-GUVs with $\Delta\varphi = -86$ mV. (A) CLSM images due to AF647 of single *E. coli*-lipid-GUVs with $\Delta\varphi = -102$ mV induced by 20 μM LfB at 25 °C. (2) and DIC images (1) (3). The following CLSM conditions were used; Laser (635 nm): 0.3%, HV: 700v, Gain: 4.5x, offset: 6%). The number on top of each image shows the time in sec after the addition of 20 μM LfB. The bar corresponds to 20 μm. (B) Time course in the normalized lumen intensity of the GUV shown in (A). (C) Time course of the normalized lumen intensity of several GUVs under the same conditions as in (A). Each curve corresponds to the time course of each GUV. (D) Time course, P_{intact},. The solid line represents the best fit curve of eq. 2.2.

2.4 GENERAL DISCUSSION

The results in this chapter show that in the interaction of LfB with single *E. coli* cells and single *E. coli* spheroplasts, calcein leaked rapidly and completely from the cytosol. Based on these results, I can reasonably infer that LfB induced local damage or pore formation in the cell membrane, resulting in rapid permeabilization. Therefore, it can be concluded that the antimicrobial activity of LfB is mainly due to permeabilization in cell membrane of *E. coli* cells induced by the direct interaction of LfB with the cell membrane. In the interaction of LfB with single *E. coli*-lipid GUVs, AF647 leaked rapidly and stochasticallydue to local rupture of the GUVs. This result clearly indicate that LfB interact with lipid bilayer region in the cell membrane directly to induce local rupture, i.e. the target of LfB is the lipid bilayer region in the cell membrane. However, higher LfB concentrations were required to induce a significant rate of permeabilization in *E. coli* lipid-GUVs compared with that observed in *E. coli* cells and spheroplasts. Based on these result, I considered that other factors are necessary to induce LfB-induced rapid local rupture in *E. coli* lipid-GUVs and that $\Delta\varphi$ is as one of these factors. I found that the rate constant of LfB-induced local rupture in GUVs increased greatly with an increase in negative $\Delta\varphi$, and at $\Delta\varphi = -102$ mV, the rate of local rupture at the same LfB concentrations became similar in the GUVs and *E. coli* cells. In the case of the interaction of LfB on single spheroplasts and *E. coli* cells, the CCCP-induced dissipation of $\Delta\varphi$ greatly decreased the rate of permeabilization in the cell membrane. To the best of our knowledge, this is the first report that indicates the significant role of $\Delta\varphi$ in the permeabilization activity of AMPs in GUVs of lipid bilayers and spheroplasts, while some researchers have suggested the role of $\Delta\varphi$ in the interaction of AMPs with bacterial cells (Yeamen et al., 1998; Wu et al., 1999).

Many researchers have suggested the effect of $\Delta\varphi$ in the interaction of AMPs with bacterial cells (Yeaman et al., 1998; Wu et al., 1999). They found that platelet microbicidal protein-2 (PMP-2) induce greater permeabilization in *Staphylococcus aureus* strain (6850) with $\Delta\varphi = -150$ mV compare to another strain of *S. aureus* (JB-1) with $\Delta\varphi = -100$ mV. These results indicates that $\Delta\varphi$ plays a vital role in the membrane permeabilization or antimicrobial activity of PMP-2 against *S. aureus* (Yeamen et al., 1998). Hancock and colleague found that in the interaction of AMPs with planar bilayers, high transmembrane

voltage (usually −180 mV) was indispensable to induce conductance, and the increase in KCl concentration in the outside of *E. coli* cells (i.e., decrease in Δφ) did not alter the antimicrobial activity of several α-helical cationic peptides and a β-structured peptide (Gram 474) (judging from MIC values) but decreased the antimicrobial activity of gramicidin S, Gram 4112, and indolicidin (Wu et al., 1999), suggesting that Δφ plays an important role in the antimicrobial activity of some AMPs.

In most bacterial strain's Δφ or proton motive force (pmf) is vital for the normal localization of various morphogenetic proteins and the correct localization of these protein is essential for their function (Strahl et al., 2010). Strahl investigated cellular localization of different protein of *Bacillus subtilis* cells such as GFPMinD, YFP-FtsA, and GFP-MreB in the presence and absence of the proton ionophore CCCP and found a rapid change (fluorescence signal was diffuse and spotty) i.e. it greatly affect the cellular localization of different protein in bacterial cells after incubation with CCCP. Therefore, the results of the effects of Δφ on AMPs activities in various bacteria can be interpreted by different ways. However, the results in this chapter shows that the Δφ greatly affects the activity of LfB in *E. coli* spheroplasts, indicating that the effect of Δφ on the interaction of LfB with the cell membrane (neither periplasm nor outer membrane) of bacterial cells plays an important role in the LfB-induced leakage. Moreover, the results in this study shows that the negative Δφ greatly increases the activity of LfB in *E. coli* lipid-GUVs, indicating that the effect of Δφ on the interaction of LfB with lipid bilayer regions of the cell membrane of bacterial cells plays a vital role in the LfB-induced leakage. Therefore, to the best of our knowledge, this is the first report to indicate that Δφ plays a vital role in the interaction of AMPs with lipid bilayer regions of the cell membrane of bacterial cells to induce their bactericidal activity.

In this chapter, I observed the interaction of LfB with single cells, and hence, variation of the LfB-induced permeabilization of cell membrane of each cell was detected. For low concentrations of LfB (e.g., 3.0 μM), the rates of LfB-induced leakage from septating cells were larger than those from most non-septating cells and the rate of LfB-induced leakage of calcein from single non-septating *E. coli* cells exhibited a wide distribution (Fig. 2.2E and 2.3). Generally, the rate of leakage depends on degree of the damage such as pore formation induced by peptides/proteins in lipid membranes and cell membrane such as the size and the

number of pores or local rupture (Alam et al., 2012; Tamba et al., 2010). Therefore, the rate of permeabilization in cell membrane depends on AMP concentration in the membrane and the degree of interaction of AMPs with the membrane. It can reasonably considered that each *E. coli* cell exists in different step of bacterial cell cycle (e.g., replication, Z-ring formation, end of replication, septation, division) (Kiviet et al., 2014; Osella et al., 2017). The degree of the damage in the cell membrane induced by LfB may greatly depend on the step of cell cycle of *E. coli* cells. In the cell cycle, only the septating cells are clearly recognized from their optical microscopic images. The result that the rates of LfB-induced leakage from septating cells were larger than those from most non-septating cells is evident, but currently its mechanism is not clear. Further investigation is required. In contrast, for higher concentration of LfB (5.0 μM), the leakage started stochastically (i.e., the onset times of the leakage were random) but the rate of LfB-induced leakage of calcein was similar in all examined cells. This result suggests that the degree of the damage induced by LfB does not depend on the step of cell cycle at higher concentration of LfB.

Currently, the mechanism of the effect of $\Delta\varphi$ on LfB-induced local rupture in lipid bilayers of GUVs is not revealed. It can be expected that the negative $\Delta\varphi$ induces a large electric field inside the lipid bilayer, which could alter the interaction modes of LfB with the membrane, such as degree of insertion of peptides into the membrane interface, which may change the physical property of the membranes and their stretching.

After I had published a paper on the role of $\Delta\varphi$ on LfB-induced permeabilization of cell membrane of *E. coli* cells and LfB-induced local rupture of single GUVs (Hossain et al., 2019), Rashid et al., published a paperon the effect of $\Delta\varphi$ on another AMP, magainin2-induced pore formation in single GUVs very recently (Rashid et al., 2020). They examined the effect of $\Delta\varphi$ on the binding of fluorescent dye-labeled magainin2 (CF-magainin2) to the GUV membranes, and found that the binding constant of CF-magainin2 to the membrane greatly increase with increasing negative $\Delta\varphi$. In the case of LfB, $\Delta\varphi$ may increase the binding constant of LfB to the GUV membrane. In near future, it is necessary to examine the effect of $\Delta\varphi$ on the binding of fluorescent dye-labeled LfB to the GUV membranes. Moreover, I have to examine the effect of $\Delta\varphi$ on the mechanisms of LfB-induced local rupture from various point of views.

In this study, I demonstrated that the electrochemical potential of proton or $\Delta\varphi$ plays a vital role in the activity of LfB (i.e., LfB-induced permeabilization) in bacterial cells and lipid vesicles by affecting the interaction of LfB with the membranes. So far almost all studies on the interactions of AMPs with lipid bilayers and the structures of AMPs in lipid bilayers have been performed in the absence of $\Delta\varphi$. Therefore, it is indispensable to reconsider and reinterpret all the results obtained in these studies. Furthermore, I have to reveal the mechanisms of activities of AMPs by including the effects of $\Delta\varphi$. Currently it is recognized that there are several modes of actions of AMPs (Hasan et al., 2019). Thus, it is necessary to examine the effects of $\Delta\varphi$ on each mode of action of AMPs. To design new peptides which have an antimicrobial activity, it is indispensable to consider the effect of $\Delta\varphi$ on the interaction of the peptides with lipid bilayers.

2.5 CONCLUSION

The results of the effect of LfB on single *E. coli* cells and single spheroplasts indicate that the direct interaction of LfB with cell membranes induced rapid permeabilization. Based on the results of changes in the cell length during LfB interaction with single cells, I can reasonably infer that this permeabilization induced growth cessation of the cells. At present it is not clear that this rapid permeabilization occurs due to large pore formation or local rupture in the cell membrane. The presence of CCCP (hence the decrease in the $\Delta\varphi$) suppressed this leakage. On the other hand, LfB induced local rupture in single *E. coli*-lipid-GUVs, through which AF647 leaked rapidly from GUV lumen. The rate of this LfB-induced local rupture in single GUVs increased with an increase in negative $\Delta\varphi$ of the GUVs. These results indicate that $\Delta\varphi$ plays an important role in LfB-induced local rupture of lipid bilayers and in the interaction of LfB with lipid bilayer regions of the cell membrane of bacterial cells to induce rapid permeabilization, resulting in their bactericidal activity. The results in this chapter are indispensable in revealing the mechanism of action of LfB and also other AMPs against bacterial cells.

Chapter 3

Effect of Membrane Potential on Entrance of Lactoferricin B Derived Short Peptide, LfB4-9 into Lipid Vesicles and live *E. coli* Cells

Chapter 3

Effect of Membrane Potential on Entrance of Lactoferricin B Derived Short Peptide, LfB4-9 into Lipid Vesicles and live *E. coli* Cells

3.1 Introduction

AMPs are effective, broad spectrum antibiotics and exhibit as potential novel therapeutic agents. These peptides are capable to kill bacteria of both gram negative and positive, fungi, enveloped viruses and also cancerous cells (Amsterdam et al., 1996). This AMPs provide attractive models where they target the negatively charged membranes of bacteria and permeabilize them (Sochacki et al., 2011). There are various modes of action by which AMPs kill microbes. The most frequent target is cytoplasmic membrane, but it may also interfere with DNA and protein synthesis, cell wall synthesis and protein folding (Hancock et al., 2002). These peptides amphipathicity, amino acid composition, cationic charge and size would permit them to attach and enter into lipid membrane bilayers to form pores.

LfB is an AMPs, composed of 25 amino acid residue (FKCRRWQWRMKKLGAPSITCVRRAF). This peptide is extremely cationic due to 5 Arg and 3 Lys residues (Yamauchi et al., 1993). It is effective against bacteria of both gram-negative and positive (Vorland et al., 1999). The mechanism by which AMPs damage the membrane and the mode of translocation of it are still controversial. Short fragments derived from LfB also have some antibacterial, antiviral, antitumor and immunological activities. One fragment is LfB17-34 with 18 residue (FKCRRWQWRM KKLGAPSI), which actively increased synthesis of melanin, which elevated expression of melanogenic enzymes such as tyrosinase and Trp1 (Huang et al., 2017). LfB4-9 is a short peptide derived from LfB, which has very high bactericidal activity. It is comprising 6 residues of amino acid (RRWQWR), this sequence is considered to be the antimicrobial active center of LfB (Maria et al., 2015). It has three positively-charged arginine residues which is considered to promote selective interaction with bacterial cell membrane (Chan et al., 2006). LfB4−9 entered into the cytoplasm of *E. coli* cells and enter inside the single GUVs without causing damages of these membranes, which indicate that LfB4-9 has cell

penetrating activity (Moniruzzaman et al., 2017). However, the fundamental procedures and mechanisms of antimicrobial activity of this shorter version of LfB with lipid bilayers and live bacterial cells are not yet clear.

The single GUV method is convenient for demonstrating the preliminary processes associated with the entrance process of these peptides into lipid vesicles using CLSM (Islam et al., 2018; Islam et al., 2017; Islam et al., 2014; Sharmin et al., 2016; Moniruzzaman et al., 2017). Various data regarding the entrance of peptides, labeled with fluorescent dye (e.g., LfB (4−9) labeled with Rhodamin, (Rh-LfB4-9) inside the single GUVs before formation of pore can be obtained using single GUV method. This method, provides the information regarding the entry rate, the link between the entry and development of pore, and the time course of the increase in peptide amount in the GUV membrane and inside of GUV (Islam et al., 2017; Islam et al., 2014; Sharmin et al., 2016; Moniruzzaman et al., 2017). Two model mechanisms have been proposed to date for the entry of peptides which have cell penetrating activity into the vesicle's lumen (Islam et al., 2018). In the first one, the peptide can permeate through the pores in the lipid bilayer (Mishra et al., 2008; Mishra et al., 2011). The other proposed model is the permeation via inverted micelle formation (Berlose et al., 1996; Swiecicki et al., 2014). A new method demonstrating the translocation through transient hydrophilic pre-pores in the lipid vesicle has been proposed according to the results found from single GUV method (Sharmin et al., 2016; Islam et al., 2017).

Negative membrane potentials usually exist in eukaryotic cells ($-55 \sim -90$ mV), which play various important roles (Sperelakis et al., 2012; Hille et al., 1992; Sakmann et al., 1995; Zhou et al., 2015). Many researchers proposed that the membrane potential has a vital role in the entry of cell penetrating peptides into cells (Rothbard et al., 2004; Rothbard et al., 2005; Henriques et al., 2005). In live bacterial cells membrane potential greatly hamper the arrangement of several proteins. As described in Chap. 2, the membrane potential significantly affects LfB's activity in live bacteria and also in lipid membrane, indicating that the effect of membrane potential has a vital role in damage of lipid membrane and pore formation in *E. coli* inner membrane caused by LfB. Previously I examined non-labeled peptide LfB which have antimicrobial activity, therefore, it is necessary to examine the effect of membrane potential on fluorescent labelled peptide which have cell penetrating activity and also antimicrobial activity.

In this Chapter, to reveal the elementary processes and mechanism of entry of LfB4-9 across the cell membrane of cells, I investigated the interaction of rhodamine labeled LfB4-9 (Rh-LfB4-9) with single bacterial membrane mimic lipid *E. coli* lipid GUVs, comprising of AF647 and small GUVs of DOPG/DOPC (molar ratio: 1/1), using the single GUV method. Previously, the interaction of Rh-LfB4-9 with single *E. coli* cells in buffer were examined, where the cells were not active or in sleeping state (Moniruzzaman et al., 2017). Here, I examined the interaction of Rh-LfB4-9 with live single *E. coli* cells in EZ medium (where the cells are active and can grow) labelling with fluorescent dye calcein into its cytoplasm, using CLSM. To study the interaction of Rh-LfB4-9 with the inner membrane of *E. coli* cells directly, I examined its interaction with single *E. coli* spheroplast, the cells from which the outer membrane and peptidoglycan had been removed. I found that Rh-LfB4-9 entered the single GUVs without pore formation and also entered the *E. coli* cells and spheroplasts. Next, I examined the effect of membrane potential on the penetrating activity or entry of Rh-LfB4-9 across lipid membrane and in live *E. coli* cells and *E. coli* spheroplasts using CLSM. Various negative membrane potentials were induced across the lipid bilayer and the effect of membrane potential was investigated. Based on the results obtained in this study, the mechanistic action of LfB4-9's bactericidal activity as well as its mode of translocations across the membranes was discussed.

3.2 MATERIALS AND METHODS

3.2.1   Materials

DOPG, and DOPC were procured from Avanti Polar Lipids, Inc. (Alabaster, AL). Obtained the Lissamine rhodamine B Red (LRB Red) succinimidylester from AAT Bioquest Inc. (Sunnyvale, CA). Other materials were described in chapter 2, section 2.2.1.

3.2.2   Peptide synthesis and identification

3.2.2.1 Peptide synthesis:

LfB4-9 was prepared by the FastMoc method using a 433A peptide synthesizer (PE Applied Biosystems, Foster City, CA) (Moniruzzaman et al., 2017). LfB4-9 was also synthesized by an Initiator + Alstra (Biotage, Uppsala, Sweden). LfB4-9 composed of 6 amino acids residue and the sequence is RRWQWR.

Procedure of LfB4-9 synthesis by an Initiator + Alstra:

Checked all the materials and reagents are available required for peptide synthesis. All the amino acids and other reagents vessels (HOBt, HBTU, DIEA), and reagent bottles (piperidine, DCM) were loaded into the correct position in the racks according to the calculation table. Resin were taken in the reactor vial according to the calculation table and inserted into the microwave cavity using the vial loading tool. For most amino acids, the reaction temperature was 70°C, but for some amino acids (Arg, Cys, His) the reaction temperature was room temperature. The total program for the synthesis were checked and after that synthesis was started. When the synthesis was finished a dialog box of **Display Report** was shown. The reactor vial was unloaded from the machine and dried in vacuum desiccator for overnight (minimum for 3 hours). After dried measured the weight of peptide resin to calculate the yield of synthesis.

3.2.2.2 Labelling of LfB4-9 with LRB Red™ Succinimidyl Ester:

The labeled LfB4-9 (Rh-LfB4-9), containing one fluorophore Rh at the N-terminus of the peptide was synthesized by a standard method. Briefly, 10 ml of DMF were taken into a reaction vessel, 8.5 µl of N-Ethyldiisopropylamine, DIEA (0.05 mM) were added into it and was mixed well for 600 sec by shaking. Then 50 mg of peptide resin were added into it and gently shaken for 600 sec. After that added 10 mg of LRB Red™ SE into it and was shaken for 24 hours at room temperature. Then washed this mixture with DMF until complete removal of unlabeled dye (5-6 times) and finally washed with methanol for 3 times. After that dried for 1 hour under fume hood and then kept in desiccator for 24 hour for complete drying.

3.2.2.3 Cleavage and purification of Rh-LfB4-9:

The procedure for cleavage, purification and identification of these peptide were mentioned in chapter 2 and also in previous paper (Moniruzzaman et al., 2017).

3.2.2.4 Determination of Rh-LfB4-9 concentration:

A small amount of Rh-LfB4-9 were dissolved in pipes buffer and media. Determined the concentrations of Rh-LfB4-9 by taking absorbance using the molar extinction coefficient of Rh at 568 nm (i.e., 95,000 $M^{-1}cm^{-1}$).

3.2.3 CLSM Investigation of the interactions of Rh-LfB4-9 with single GUVs comprising AF647

To investigate the entry of Rh-LfB4-9 into single GUVs, I prepared GUVs of *E. coli*-lipid- containing small DOPG/DOPC-GUVs inside the mother GUV using the previously described procedure (Moniruzzaman et al., 2017). Using the natural swelling method, first prepared GUVs of DOPG/DOPC (1/1; molar ratio) by incubating in buffer C (10 mM PIPES, pH 7.0, 50 mM NaCl, 1 mM EGTA) comprising 0.10 M sucrose at 37 °C for 2 h (Moniruzzaman et al., 2017). Then, to remove lipid aggregates and multilamellar GUVs, centrifuged the GUV suspension at 14,000×g for 1200 sec at 20 °C. This partially purified GUV combined with 6 μM AF647 solution in buffer C comprising 0.1 M sucrose and incubated with *E. coli* dry lipid films at 37 °C for 2-3 h (Moniruzzaman et al., 2017). Untrapped fluorescent dyes were separated by using membrane filter method (Tamba et al., 2011).

I transferred the purified GUV suspension into a hand-made microchamber which was coated with 0.10 %(w/v) BSA in same experimental buffer to prevent GUVs strong interaction with the glass surface (Yamazaki et al., 2008). To conduct the experiment of Rh-LfB4-9 with single GUVs, observed the GUVs in CLSM (FV-1000, Olympus, Tokyo, Japan) at 25± 1 °C (Islam et al., 2014a). For CLSM measurements, fluorescence images of AF647 (excited by a laser at λ = 635 nm: 0.3%, HV: 750v, Gain: 5.5x, offset: 6%), fluorescence images of Rh (excited by a laser at λ = 559 nm: 1.2%, HV: 475v, Gain: 5.875x, offset: 6%) and DIC images were obtained using the 60× objective. Continuously added various concentrations of Rh-LfB4-9 were into the vicinity of the single GUV through a glass micropipette (~ 20 μm) and change of the FI observed during the interaction under CLSM. The detailed experimental and analysis procedures were described earlier (Islam et al., 2014a).

3.2.4 Investigation of the interactions of Rh-LfB4-9 with single GUVs under membrane potential

To induce a membrane potential in GUVs, I used the same procedure mentioned in Chap. 2. A K^+ concentration gradient was generated across the GUV membrane containing gramicidin A (Hossain et al., 2019). For this purpose, *E. coli*-lipid/gramicidin A (molar ratio: 100/0.01) GUVs were made in buffer K (10 mM PIPES, pH 7.0, 1 mM EGTA, 50 mM KCl) with 0.10 M sucrose. A partially purified DOPG/DOPC (1/1)-GUVs prepared in the same buffer K with 6.0 μM AF647. I diluted the above purified GUV suspension with buffer T (10 mM PIPES, pH 7.0, 50 mM TEAC, 1 mM EGTA) with 0.1 M glucose at various ratios. Here, I measured the difference of membrane potential across a GUV membrane, $\Delta\varphi$, using the same Nernst equation (Eq. 2.1) as I mentioned in the in Chap. 2. The same experimental procedure as mentioned in the previous chapter (2.2.8) were followed for the interaction of Rh-LfB4-9 with single GUVs under various membrane potential.

3.2.5 CLSM investigation of the interaction of Rh-LfB4-9 with single *E. coli* cells comprising calcein

For preparation of calcein-loaded *E. coli* cells, I used the same procedure mentioned in chap. 2, section 2.2.3. I transferred the labeled *E. coli* cells into a hand-made microchamber which was coated with 0.1% poly-l-lysine to prevent strong interaction with the glass surface (Yamazaki et al., 2008). Performed the experiment of Rh-LfB4-9 with single *E. coli* cells using CLSM at 25± 1 °C as reported earlier (Islam et al., 2014a). I obtained he fluorescence images for calcein (473 nm laser), Rh-LfB4-9 (559 nm laser), and DIC images by using a 60×objective (Islam et al., 2014a; Moniruzzaman et al., 2017). Continuously added various concentrations of Rh-LfB4-9 into the vicinity of the single GUV *E. coli* through a glass micropipette (~ 20 μm) and change of the FI observed during the interaction under CLSM. The detailed experimental and analysis procedures were described earlier (Moniruzzaman et al., 2017).

I followed the same experimental procedure for doing the investigation of Rh-LfB4-9 with single *E. coli* cells containing CCCP as mentioned in chap. 2, section 2.2.3. For CLSM measurements, fluorescence images of calcein (excited by a laser at λ = 473 nm: 0.1%, HV: 660v, Gain: 4.125x, offset: 6%), fluorescence

images of Rh (excited by a laser at $\lambda = 559$ nm: 0.5%, HV: 440v, Gain: 4.875x, offset: 7%) and DIC images were obtained using the 60× objective.

3.2.6 CLSM investigation of the interaction of Rh-LfB4-9 with single spheroplasts comprising calcein

For preparation of *E. coli* spheroplasts and loading of calcein in their cytoplasm, in chap. 2, section 2.2.5. I followed the same experimental procedure for doing the investigation of Rh-LfB4-9 with single spheroplast and also the experiment in the presence of CCCP as mentioned in chap. 2, section 2.2.5. For CLSM measurements, fluorescence images of calcein (excited by a laser at $\lambda = 473$ nm: 0.1%, HV: 580v, Gain: 4.5x, offset: 7%), fluorescence images of Rh (excited by a laser at $\lambda = 559$ nm: 0.5%, HV: 400v, Gain: 4.25x, offset: 7%) and DIC images were obtained using the 60× objective.

I also observed the dependence of CCCP on membrane potential of spheroplast using a membrane potential sensitive fluorescent dye, $DiOC_6(3)$. First, mixed the dye $DiOC_6(3)$ in methanol with the same buffer as outside of the spheroplasts and then mixed this $DiOC_6(3)$ solution with purified spheroplasts suspension. The final conc. of $DiOC_6(3)$ was 1 nM. Then I prepare the same mixture with different concentration of CCCP. Then, this suspension was transferred into a hand-made microchamber. I waited for 600 sec, and then observed the spheroplasts under CLSM. The detailed experimental and analysis procedures were described earlier (chap. 2, section 2.2.8).

3.3 RESULTS AND DISCUSSION

3.3.1   Interaction of Rh-LfB4-9 with single *E. coli*-lipid-GUVs

Moniruzzaman et al. demonstrated that Rh-LfB4-9 entered the lumen of single DOPG/DOPC (1/1) GUVs without pore formation (Moniruzzaman et al., 2017). Generally, interactions of peptides with lipid bilayers depend on lipid composition. Here I investigated the entry of Rh-LfB4-9 into the lumen of single *E. coli*-lipid GUVs. For monitoring the entry of Rh-LfB4-9 into the inside of single GUVs and pore formation in their membranes, I used the single GUV method for CPPs (Islam et al., 2014; Moniruzzaman et al., 2017). In this method, one use single GUVs (i.e. mother GUVs) containing smaller GUVs with 1-10 μm in diameter and a water-soluble fluorescent dye, AF647, in their lumen. During the interaction of peptide with single GUVs, if one detect fluorescence at smaller GUVs in the mother GUV lumen, this results indicate the entry of peptides into the lumen. Here, I used DOPG/DOPC (1/1) GUVs as the smaller GUVs and *E. coli*-lipid-GUVs as the mother GUVs.

First, I examined the interaction of 5.0 μM Rh-LfB4-9 with single *E. coli*-lipid-GUVs. A peptide solution was continuously provided via a micropipette to the neighbourhood of a single GUV. The peptide concentration in the neighborhood of the GUV was a little lower than inside the micropipette at steady state (Karal et al., 2015). Figure 3.1A (1) shows that the FI in the inside of the GUV (i.e., the lumen intensity) due to AF647 remained almost constant for 600 sec interaction of the peptide with the GUV (Fig. 3.1A (1) and 3.1B), showing that membrane permeation of AF 647 did not occur. This result indicates no pore formation in the GUV membrane. Figures 3.1A (2) and 3.1B show that the FI of the GUV membrane due to Rh-LfB4-9 increased with time to reach a steady value at 12 s. On the other hand, there was no fluorescence inside the GUV, but after 106 s the FI at the small GUVs inside the GUV was observed without pore formation (Fig. 3.1A (2)). Based on these results, one can conclude that the peptide enters the inside of the GUV and binds to the small GUVs without pore formation (Islam et al., 2014a). As a measure of the rate of entry of Rh-LfB4-9 into the inside of the GUV, V_{entry}, one can use the fraction of GUVs which the peptide enters before a specific time *t* without pore formation among the whole investigated GUVs (hereafter, fraction of entry), P_{entry} (*t*) (29). I repeated the experiment shown in Fig. 3.1A with 16 single GUVs (*n* = 26) and obtained P_{entry} (600 sec) = 0.56. Two independent experiment were conducted, using 10−16 GUVs each time, and the average

Figure 3.1

(A)

(B)

(C)

Figure 3.1: Interaction of Rh-LfB4-9 with single *E. coli*-lipid-GUVs comprising of small GUVs. (A) Showing images from CLSM of (1) AF647, (2) Rh-LfB4-9 and (3) DIC image for the interaction of an *E. coli*-lipid-GUV with 5.0 µM of Rh-LfB4-9 without membrane potential. The numbers above each image show the time in sec during the interaction. The following CLSM conditions were used; Laser (635 nm): 0.3%, HV: 750v, Gain: 5.5x, offset: 6%; laser 559 nm: 1.2%, HV: 475v, Gain: 5.875x, offset: 6%). The bar is 30 µm. (B) Time course of FI change of GUV lumen due to AF647 (red points) and GUV rim due to Rh-LfB4-9 (green triangles). (C) Rh-LfB4-9 concentration dependence of P_{entry}.

value and SD of P_{entry} were determined: P_{entry} (600 sec) = 0.53 ± 0.04. On the other hand, I did not observe any leakage of AF647 after 600 sec interaction, i.e. P_{leak} (600 sec) = 0.

Next, I investigated the interaction of various concentrations of Rh-LfB4-9 with single *E. coli*-lipid-GUVs. I found that the peptide entered a GUV lumen without the membrane permeation of AF647 for all concentrations. Figure 3.1C shows that P_{entry} (600 sec) increased with a peptide concentration dependent manner at and above 2.0 μM and P_{entry} (600 sec) = 0.76 ± 0.03 for 9.0 μM. I did not observe any leakage of AF647 after 600 sec interaction for all peptide ≤ 9.0 μM.

3.3.2   Effect of membrane potential on entrance of Rh-LfB4-9 into single *E. coli*-lipid-GUVs

I investigated the role of membrane potential, $\Delta\varphi$, on the entrance of Rh-LfB4-9 into single *E. coli*-lipid-GUVs. Membrane potentials were generated only in the mother *E. coli*-lipid-GUVs whose membranes contained monovalent cation channel gramicidin A using various K^+ differences between the inside and the outside of these GUVs.

First, I examined the effect of $\Delta\varphi$ (−102 mV) on the entry of 0.50 μM Rh-LfB4-9 into single GUVs, because in the absence of membrane potential the peptide does not enter a GUV significantly for 600 sec interaction (Fig. 3.1C). Figure 3.2A (1) shows that the lumen intensity due to AF647 did not decrease for 10 min interaction of Rh-LfB4-9 with the GUV, indicating no pore formation in the mother GUV membrane. The rim intensity due to the peptide rapidly increased to a maximum at 70 s, then decreased a little, and finally attained a steady value at 100 s (Fig. 3.2A (2) and 3.2C). This decrease in rim intensity may be due to quenching of Rhodamine fluorescence due to a high concentration of Rh-LfB4-9 in the GUV membrane.

On the other hand, during initial interaction no fluorescence inside of the mother GUV was found, but after 239 s fluorescence was observed at small GUVs diffusing in the aqueous solution inside mother GUV (Fig. 3.2A (2)). This result indicates that Rh-LfB4-9 enters the GUV lumen and then binds to the small GUVs without pore formation in the mother GUVs (Islam et al., 2014a). The experiment shown in Fig. 3.2A was repeated using 12 single GUVs and the value of P_{entry} was determined (P_{entry} (600 sec) = 0.92). Two independent experiment were conducted, using 8−12 GUVs each time, and the average value and SD of P_{entry} were determined; P_{entry} (600 sec) = 0.90 ± 0.03.

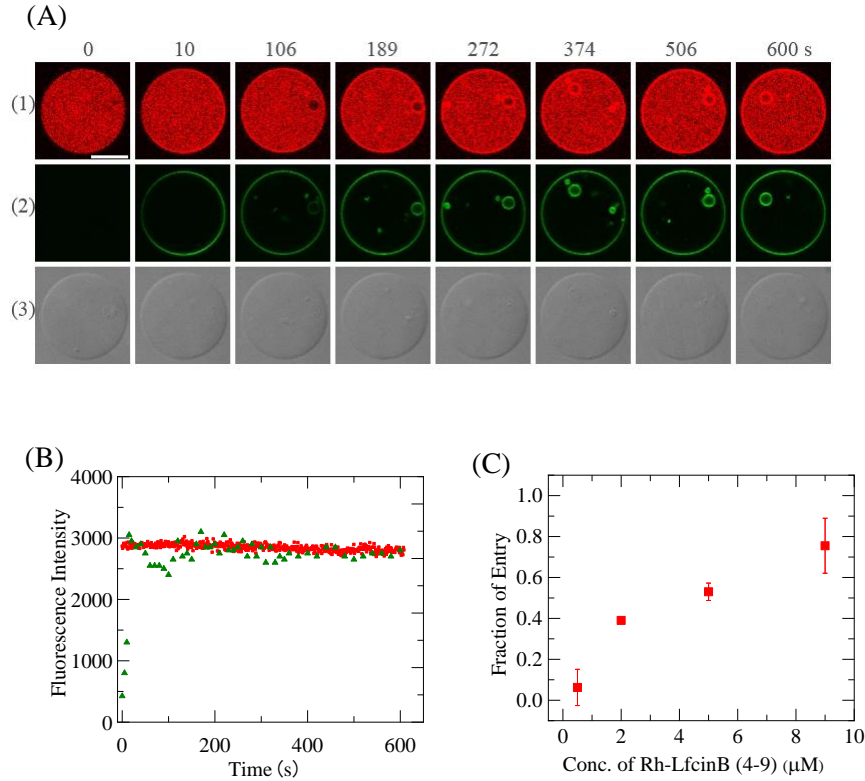**Figure 3.2**
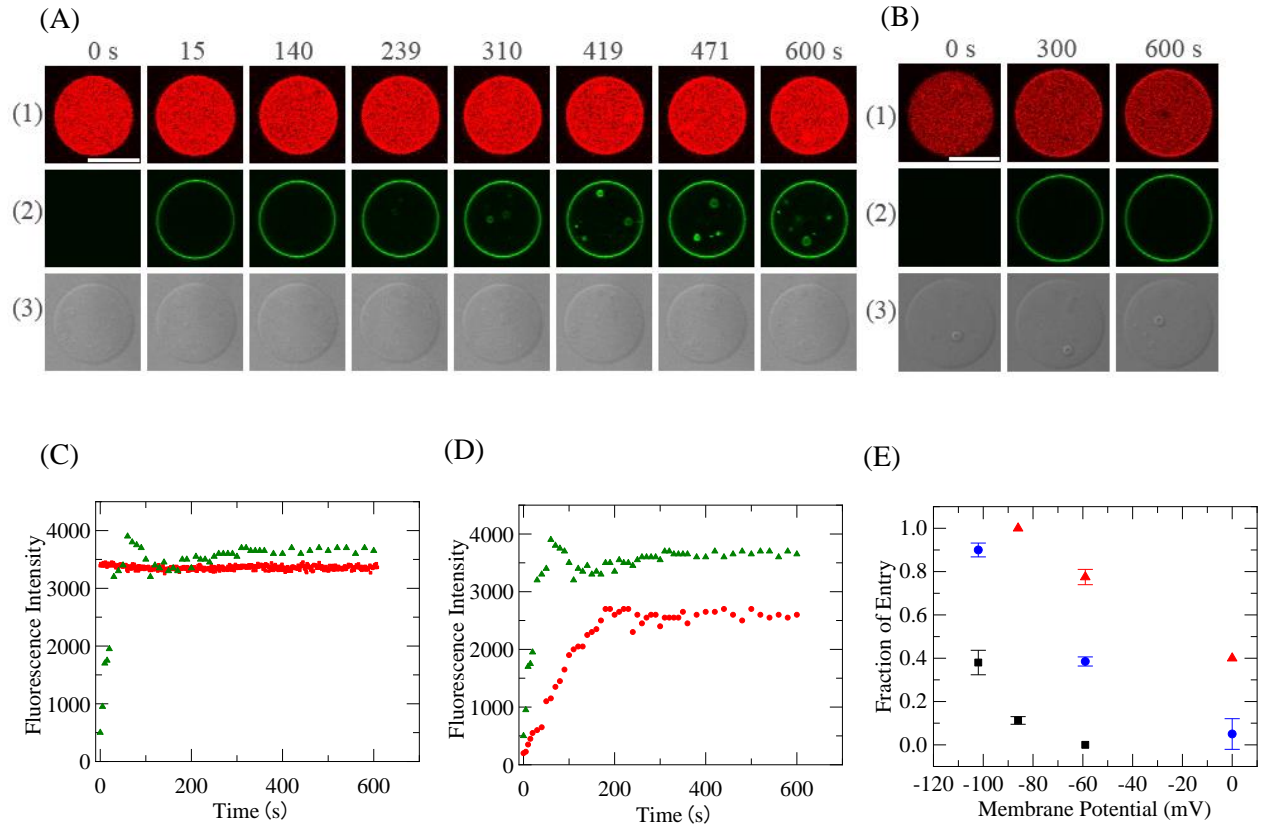
Figure 3.2: Role of membrane potential on the entrance of Rh-LfB4-9 into single *E. coli*-lipid-GUVs comprising of small GUVs. (A) and (B) showing images from CLSM of (1) AF647, (2) Rh-LfB4-9 and (3) DIC image on the interaction of an *E. coli*-lipid-GUV with 0.50 μM Rh-LfB4-9 under (A) $\Delta\varphi = -102$ mV and (B) 0 mV. The numbers top on each image showing the time in sec during the interaction. The following CLSM conditions were used; Laser (635 nm): 0.3%, HV: 750v, Gain: 5.5x, offset: 6%; laser 559 nm: 1.2%, HV: 475v, Gain: 5.875x, offset: 6%). The bar is 30 μm. (C) Time course of FI change of GUV lumen due to AF647 (red squares) and GUV rim due to Rh-LfB4-9 (green triangles). (D) Time course of change in the rim intensity due to Rh-LfB4-9 under $\Delta\varphi = -102$ mV (green triangles) and 0 mV (red circles). (E) Role of membrane potential on P_{entry}. (red ▲) 2.0 μM, (blue ●) 0.50 μM, and (■) 0.20 μM Rh-LfB4-9.

As a control experiment, the interaction of Rh-LfB4-9 with single GUVs with the same lipid composition (i.e., *E. coli*-lipid and gramicidin A mixture) was investigated at $\Delta\varphi = 0$ mV. Under this condition, P_{entry} (600 sec) = 0.05 ± 0.07) (Fig. 3.2B). The rim intensity due to the peptide gradually increased to reach a steady value at 200 s (red circles in Fig. 3.2D). A transient decrease in rim intensity due to the quenching was not observed. For $\Delta\varphi = -59$ mV, P_{entry} (600 sec) = 0.39 ± 0.02 ($n = 18$). These results show that P_{entry} (600 sec) increased as the negative membrane potential increased (Fig. 3.2E). I did not observe any leakage of AF647 after 600 sec interaction in the presence of $\Delta\varphi$.

Using different peptide concentrations (2.0 and 0.20 μM), I examined the effect of $\Delta\varphi$ on the entrance of Rh-LfB4-9 into single GUVs. The results for both cases are similar to those for 0.50 μM. Figure 3.2E shows that, irrespective of peptide concentration, the fraction of entry of Rh-LfB4-9 increased with increasing negative membrane potential, which indicates that the rate of entry of Rh-LfB4-9 was increased with negative $\Delta\varphi$.

3.3.3   Effect of $\Delta\varphi$ on entrance of Rh-LfB4-9 into single cells of *E. coli*

Recently Moniruzzaman et al. demonstrated that Rh-LfB4-9 enters the cytoplasm of single *E. coli* cells without leakage of calcein, i.e., without damage of their cell membranes (Moniruzzaman et al., 2017). However, in their study, they studied peptide's interaction with single *E. coli* cells in buffer (limitation of nutrients), which can cause loss of ability to culture the cell, i.e. the cells might not active or in sleeping state (Ramos et al., 2001; Ihssen et al., 2007; Van et al., 2011). Here I examined the Rh-LfB4-9's interaction with single *E. coli* cells in EZ medium, where the cells are active and can grow (Neidhardt et al., 1974). Calcein was loaded to the cytoplasm of *E. coli* cells using the same method described in section 2.3.1

First, I examined the interaction of 5.0 μM Rh-LfB4-9 with single E. coli cells at 25 °C using CLSM. The peptide solution (in EZ rich medium) was continuously provided to the neighborhood of an E. coli cell via a micropipette. Figure 3.3A shows a result for non-septating cells. During the interaction of the peptide, the FI of E. coli cell due to calcein decreased gradually (up to 600 sec) (Figure 3.3A (1) and a green line in Figure 3.3C). This gradual decrease in FI is due to photobleaching of calcein, because I observed a similar gradual decrease in FI was observed in single *E. coli* cells without interacting the peptides. On the other hand,

the FI of the total *E. coli* cell due to Rh-LfB4-9 increased a little with time to attain a steady value at ~35 s, which was kept constant for 120 s, then gradually increased from 155 s to reach a high FI (Fig. 3.3A (2) and a red line in Fig. 3.3C). To compare the FI of the *E. coli* membranes due to Rh-LfB4-9 (i.e., the rim intensity) with that of the cytoplasm, I made the FI profiles along a line traversing the cell. As the line, a white line in Fig. 3.3A (0 s of calcein image) was used. The FI profiles (along the line) show that at less than 155 s the rim intensity was higher than the central region's (corresponding to the cell cytoplasm) FI, but after 155 s the central region's FI became higher than the rim intensity (Fig. 3.3B). It is considered that the binding of Rh-LfB4-9 to the *E. coli* membrane produces the initial weak rim intensity and the entry of the peptide into the cytoplasm induces the gradual, great increase in FI from 160 s. As the criterion of the entry of the peptide into the cytoplasm, I adopted the condition that the central region's FI of cell is larger than the rim intensity.

I conducted the same experiments using 13 cells of *E. coli* (i.e., 9 non-septating and 4 septating cells). I found that Rh-LfB4-9 entered the cytoplasm without great decrease in FI due to calcein in 8 cells (i.e., 5 non-septating and 3 septating cells). Figure 3.1D shows the change of FI of several single cells during the interaction of 5.0 μM peptide. Each curve represents the time course of FI for each cell. This figure shows that there are various rates of entry of the peptide into the cytoplasm of a single cell. The rate of entry of the peptide into septating cells was larger than that into non-septating cells. Based on these results, I can conclude that Rh-LfB4-9 outside the cell translocates across the *E. coli* cell membrane and enters its cytoplasm without pore formation. In contrast, for other cells, the FI of the central region of the cells was smaller than the rim intensity after 600 sec, and moreover, the FI of total cell was also lower (Fig. 3.3D). This result suggests that Rh-LfB4-9 cannot enter its cytoplasm. Therefore, one can conclude that for the interaction of 5.0 μM Rh-LfB4-9 with single *E. coli* cells, the entry of the peptide into its cytoplasm occurred in 62 % of total examined cells. In other words, the fraction of cells which the peptide entered their cytocellmong all examined cells at 600 sec interaction (i.e., the fraction of entry at 600 sec, P_{entry} (600 sec)) is 0.62. Two independent experiment were conducted, using 12–13 GUVs each time, and the average value and SD of P_{entry} (600 sec) was 0.64 ± 0.03.

Figure 3.3

Figure 3.3: Interaction of Rh-LfB4-9 with single *E. coli* cells comprising calcein. (A) showing images from CLSM of (1) calcein, (2) Rh-LfB4-9 and (3) DIC image on the interaction of an *E. coli* cell with 5.0 µM Rh-LfB4-9. The numbers top on each image showing the time in sec during the interaction. The following CLSM conditions were used; Laser (473 nm): 0.1%, HV: 660v, Gain: 4.125x, offset: 6%; laser (559 nm): 0.5%, HV: 440v, Gain: 4.875x, offset: 7%). The bar is 2 µm. (B) FI profiles of calcein (green line) and Rh-LfB4-9 (red line) along a white line in the cell in (A). (C) Time course of FI change of the cell due to calcein (green line) and Rh-LfB4-9 (red line). (D) Time course of FI change of several "single cells" due to Rh-LfB4-9 under the same conditions as in (A). (E) Rh-LfB4-9 concentration dependence on P_{entry}.

Next, I investigated the interaction of various concentrations of Rh-LfB4-9 into single cells of *E. coli* for 9.0 μM peptide and found the entry of Rh-LfB4-9 into its cytoplasm in all examined cells (i.e., 12 *E. coli* cells; 8 non-septating and 4 septating cells), (i.e., P_{entry} (600 sec) = 1.0). In this case, the FI of *E. coli* cell due to calcein decreased greatly in some cells, indicating that the leakage of calcein occurred (Fig. 3.4). This result indicates that a high concentration of Rh-LfB4-9 (9.0 μM) induced pore formation in the cell membrane. Before the starting the leakage, the FI of the *E. coli* cell due to Rh-LfB4-9 increased, indicating that Rh-LfB4-9 entered the cell before pore formation. However, after the leakage, the FI due to the peptide greatly increased. This result suggests that the peptides enter the cytoplasm through the pores. In contrast, for 1.0 μM peptide, examined 12 *E. coli* cells (9 non-septating cells and 3 septating cells) and observed in 9 cells the FI of the cytoplasm of *E. coli* cells was lower than that of the rim of the cells (8 non-septating and 1 septating cells). These results indicate that Rh-LfB4-9 could not enter into their cytoplasm in most cells. Figure 3.3 E shows the peptide concentration dependence of P_{entry} (600 sec), indicating that the cell-penetrating activity of Rh-LfB4-9 against *E. coli* increased with increasing its concentration. Figure 3E also shows the peptide concentration dependence of the fraction of leaked *E. coli* cells among all examined *E. coli* cells at 600 sec, P_{leak} (600 sec). At and less than 5.0 μM peptide, no leakage occurred in all GUVs (i.e., P_{leak} (600 sec) = 0), but at 9.0 μM peptide, P_{leak} (600 sec) = 0.38.

Next, I investigated the effect of a proton-ionophore, CCCP on the entry of Rh-LfB4-9 into single *E. coli* cells. As described in Chap. 2, it is recognized that CCCP suppresses the membrane potential. The effect of 100 μM CCCP (final concentration) on the interaction of 5.0 μM Rh-LfB4-9 with single *E. coli* cells in the EZ medium was examined at 25 °C. The FI of the cell due to calcein decreased a little during 600 sec interaction due to the photobleaching of calcein (Figure 3.5A (1) and a green line in Figure 3.5B), indicating that Rh-LfB4-9 did not induce pore formation in the membrane and calcein did not leaked. In contrast, the increase in the FI due to Rh-LfB4-9 was small. This result suggests that Rh-LfB4-9 binds to the cell membrane but cannot enter the cytoplasm (Figure 3.5A (2) and a red line in Figure 3.5B). This experiment was repeated using 12 cells (i.e., 10 non-septating and 2 septating cells), and the same results were observed performed two experiments independently using 10-12 *E. coli* cells ($N = 2$), producing the same results.
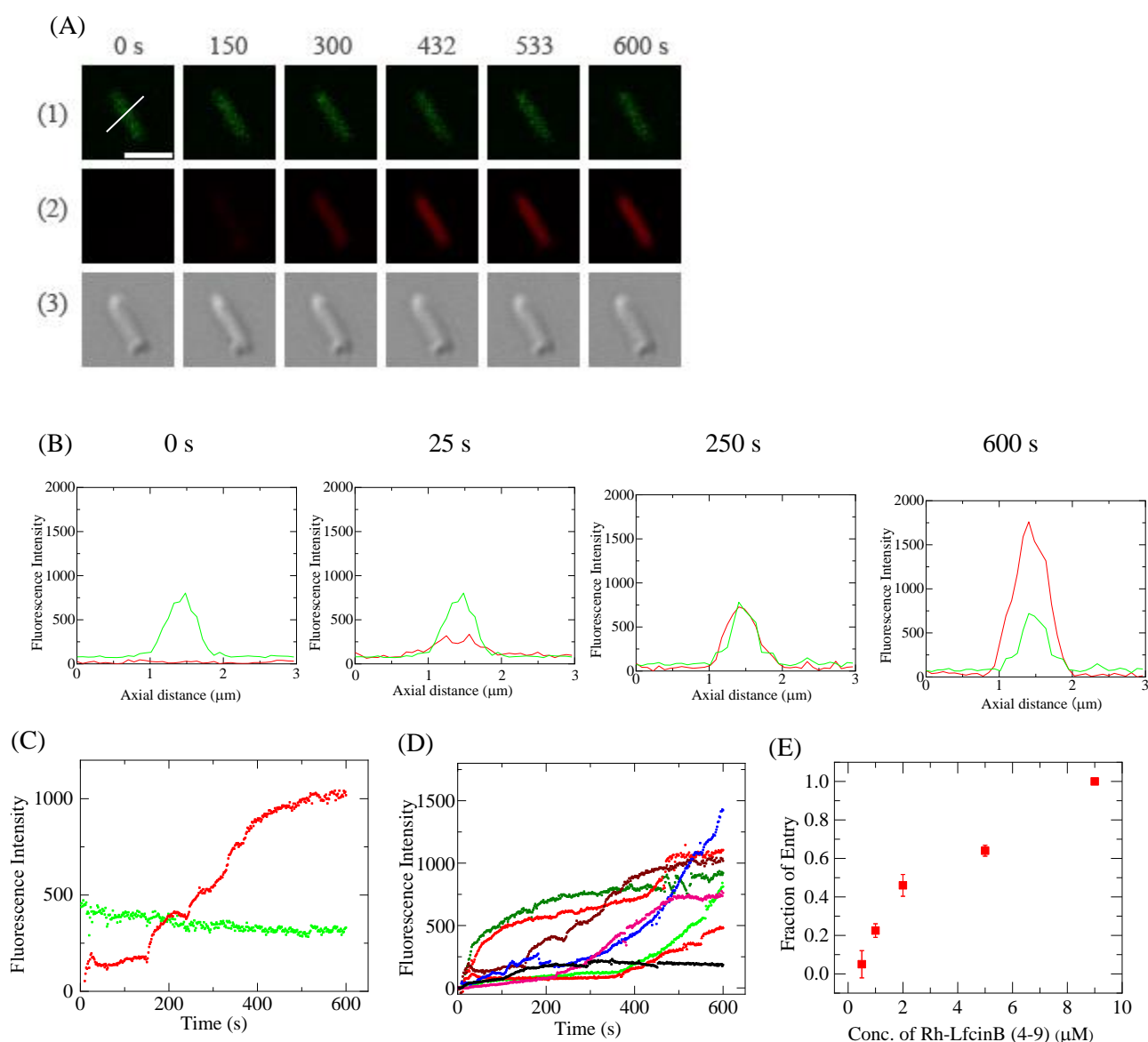
Figure 3.4

(A)

(B)
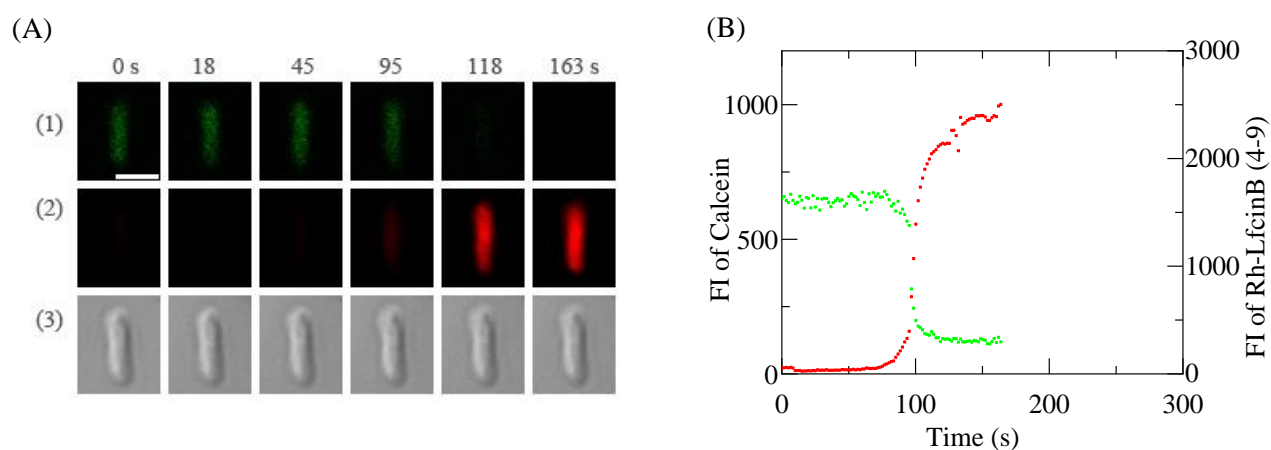
Figure 3.4: Interaction of Rh-LfB4-9 with single *E. coli* cells comprising calcein. (A) showing images from CLSM of (1) calcein, (2) Rh-LfB4-9 and (3) DIC image on the interaction of an *E. coli* cell with 9.0 µM Rh-LfB4-9. The numbers top on each image showing the time in sec during the interaction. The following CLSM conditions were used; Laser (473 nm): 0.1%, HV: 660v, Gain: 4.125x, offset: 6%; laser (559 nm): 0.5%, HV: 440v, Gain: 4.875x, offset: 7%). The bar is 2 µm. (B) Time course of FI change of the cell due to calcein (green line) and Rh-LfB4-9 (red line).

Figure 3.5

(A)

(B)

(C)
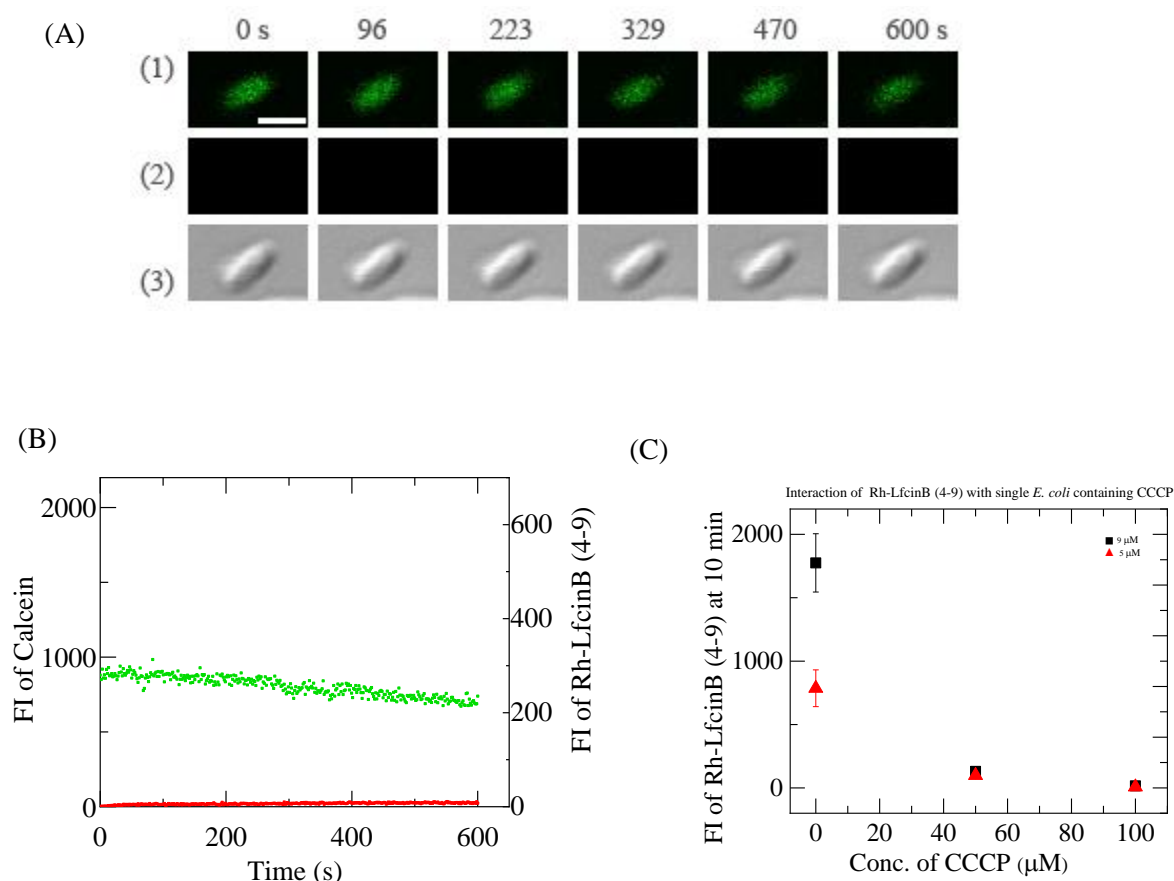
Figure 3.5: Interaction of Rh-LfB4-9 with single *E. coli* cells comprising of calcein in presence of CCCP. (A) showing images from CLSM of (1) calcein, (2) Rh-LfB4-9 and (3) DIC image on the interaction of *E. coli* with 5.0 μM Rh-LfB4-9. The numbers top on each image showing the time in sec during the interaction of Rh-LfB4-9 with *E. coli*. The following CLSM conditions were used; Laser (473 nm): 0.1%, HV: 660v, Gain: 4.125x, offset: 6%; laser (559 nm): 0.5%, HV: 440v, Gain: 4.875x, offset: 7%). The bar is 2 μm. (B) Time course of FI change of the *E. coli* due to calcein (green line) and Rh-LfB4-9 (red line). (C) CCCP concentration during the interaction between Rh-LfB4-9 and single *E. coli* cells. (red ■) 5.0 μM, and (■) 9.0 μM Rh-LfB4-9.

I also examined the CCCP concentration dependence on the interaction of Rh-LfB4-9 with single $E.$ $coli$ cells (Figure 3.5C). With an increase in CCCP concentration FI due to Rh-LfB4-9 of total cells at 600 sec decreased. In the presence of 50 μM CCCP, P_{entry} (600 sec) = 0 and P_{leak} (600 sec) = 0 (N = 2 using each 10-15 spheroplasts). The FI due to Rh-LfB4-9 of the total cells at 600 sec in the presence of 50 μM CCCP was larger than that in the presence of 100 μM CCCP. This result suggests that the higher concentration of CCCP suppressed the binding of Rh-LfB4-9 with the cell membrane.

To detect the membrane potential in the $E.$ $coli$, I examined the interaction of 100 nM membrane potential-sensitive dye DiOC6(3) with $E.$ $coli$ cells using CLSM. I investigated the effect of CCCP on membrane potential of $E.$ $coli$. I observed that there is significant FI of total $E.$ $coli$ cells due to $DiOC_6(3)$ in the absence of CCCP but in the presence of 100 μm CCCP found very low FI of total $E.$ $coli$ cells (Figure 3.6A). Two independent experiments were conducted and the same results were obtained. I also examined the CCCP concentration dependence on its interaction and found that FI due to $DiOC_6(3)$ of total $E.$ $coli$ cells decreased with increase of CCCP concentration (Figure 3.6B).

Therefore, all these results indicate that the membrane potential in the $E.$ $coli$ cells plays an important role in the entry of Rh-LfB4-9 into the cytoplasm of $E.$ $coli$.

3.3.4 Interaction of Rh-LfB4-9 with single $E.$ $coli$ spheroplasts

To examine the interaction of Rh-LfB4-9 with $E.$ $coli$ cell membrane in more detail, I investigated the interaction of the peptide with single $E.$ $coli$ spheroplasts using CLSM. Calcein was loaded in the spheroplast lumen by interacting calcein-AM with spheroplasts (Hossain et al. 2019). First, I investigated the interaction of 2.0 μM Rh-LfB4-9 with single spheroplasts in the same buffer described in chapter 2, section 2.3.2. During 600 sec observation of a single spheroplasts containing calcein, the FI of the inside of spheroplast greatly decreased (Fig. 3.7), which is due to photobleaching of calcein. The average normalized FI decrement after 600 sec was 30 ± 6 % (n = 2). To decrease the photobleaching, the FI of a spheroplast was observed for 10 s at every 200 s, and the other time the shutter of incident laser was closed. Under this condition, the FI due to calcein did not decrease significantly (Fig. 3.8A (1) and green circles in Fig. 3.8B). An Rh-LfB4-9 solution in the same buffer was continuously added to the vicinity of a spheroplast through a

Figure 3.6

(A)

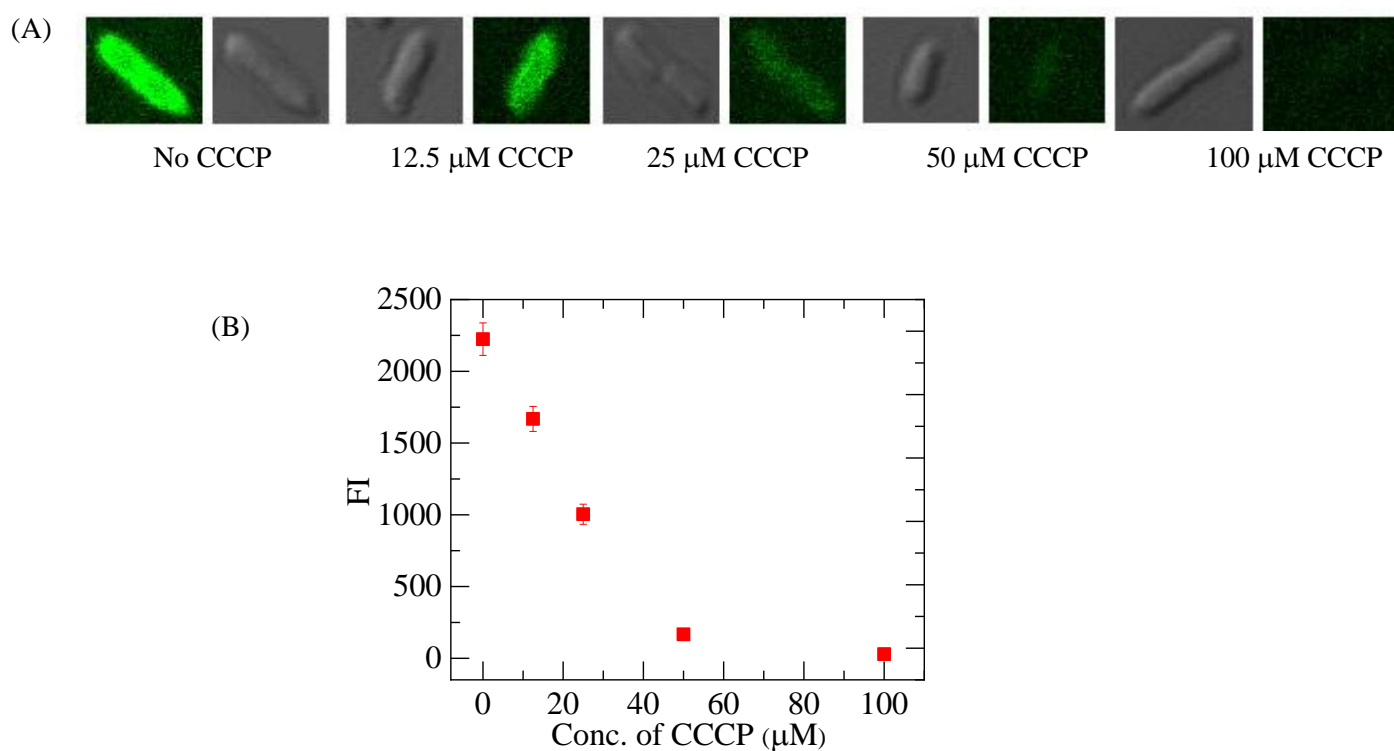| No CCCP | 12.5 μM CCCP | 25 μM CCCP | 50 μM CCCP | 100 μM CCCP |

(B)

Figure 3.6: Effect of CCCP on membrane potential of *E. coli* due to DiOC6(3) dye. (A) Showing images from CLSM of *E. coli* gained by the fluorescence emission of DiOC6(3). The following CLSM conditions were used; Laser (473 nm): 0.5%, HV: 600v, Gain: 4 x, offset: 7%. (B) Dependence of total FI of *E. coli* on CCCP concentration. Data showed along with average values and SDs.

micropipette. The FI of the spheroplast membrane (i.e., the rim intensity) due to Rh-LfB4-9 initially increased to reach a small, steady value (800) at 100 s, which was kept constant for 500 s. Figure 3.8C shows the FI profile along a white line in the image of Fig. 3.8A (0 s of calcein image). The FI of the rim of spheroplast is greater than the FI of its central region, indicating that this FI is due to the binding of the peptide to the cell membrane of the spheroplast. The FI of the rim of spheroplast remained constant from 145 s to 528 s, indicating that the peptide concentration in the membrane is constant. During this time the FI of its central region increased with time (Fig. 3.8C and red line in Fig. 3.8B). The diameter of the spheroplasts is small (4−6 μm), and thus, the FI of the membrane (i.e., rim intensity) may affect the FI at the central region even if the CLSM was used (Wei et al., 2016). However, in the above result, the FI of its central region increased with time when the rim intensity was constant, indicating that the increase in the FI of the central region is not due to the increase in the binding of Rh-LfB(4-9) in the membrane. Therefore, these results indicate Rh-LfB4-9 entered the cytoplasm of the spheroplast. The experiment shown in Fig. 3.8A was repeated using 10 single spheroplasts ($N = 2$), and the similar results were obtained. Rh-LfB4-9 entered the cytoplasm of 5 spheroplasts.

Next, I examined the interaction of 3.0 μM Rh-LfB4-9 with single spheroplasts under the same conditions (Fig. 3.9). In 11 spheroplasts among all examined spheroplasts ($n = 12$), the FI of the central region of spheroplast increased with time, indicating that Rh-LfB4-9 entered the cytoplasm.

At present, the rate of entry of Rh-LfB4-9 into the spheroplast cytoplasm, V_{entry} cannot be determined quantitatively. However, this rate can be determined by averages of the fraction of spheroplasts into which Rh-LfB4-9 entered before a specific time t, with respect to the whole investigated spheroplasts (hereafter, fraction of entry), $P_{entry}(t)$. For 3.0 μM Rh-LfB4-9, P_{entry} (600 sec) = 0.86±0.09. P_{entry} (600 sec) decreased with a decrease in Rh-LfB4-9 concentration (Fig. 3.8D). On the other hand, Fig. 3.9D shows the peptide concentration dependence of the fraction of leaked spheroplasts among all examined spheroplasts at 600 sec, P_{leak} (600 sec). At 2.0 μM peptide, no leakage occurred in all spheroplasts (i.e., P_{leak} (600 sec) = 0), but at 3.0 μM peptide, P_{leak} (600 sec) = 0.65±0.07.

Figure 3.7
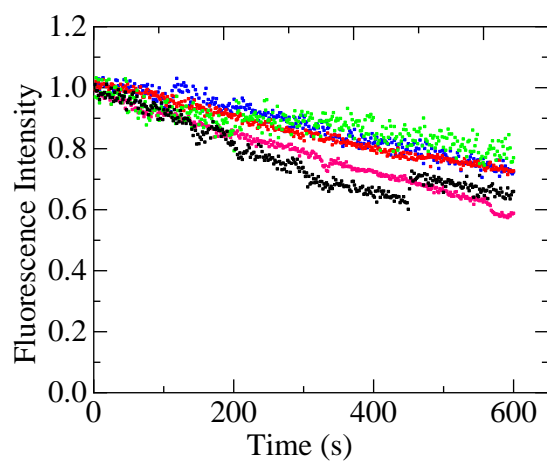
Figure 3.7: Time course of normalized FI of several spheroplasts in the absence of Rh-LfB4-9.

Figure 3.8

Figure 3.8: Interaction of Rh-LfB4-9 with single *E. coli*-spheroplasts comprising of calcein. (A) showing images from CLSM of (1) calcein, (2) Rh-LfB4-9 and (3) DIC image on the interaction of spheroplast with 2.0 μM Rh-LfB4-9. The numbers top on each image showing the time in sec during the interaction. The following CLSM conditions were used; Laser (473 nm): 0.1%, HV: 580v, Gain: 4.5x, offset: 7%; laser (559 nm): 0.5%, HV: 400v, Gain: 4.25x, offset: 7%). The bar is 5 μm. (B) Time course of FI change of total spheroplast due to calcein (green line) and Rh-LfB4-9 (red line), spheroplast rim due to Rh-LfB4-9 (brown square) and central region of spheroplast due to Rh-LfB4-9 (blue triangles) (C) FI profile along white line in the Rh-LfB4-9 images at 0 s in the panel A (2). (D) Rh-LfB4-9 concentration dependence on P_{entry}.

76

Figure 3.9

(A)

(C)

(B)

(D)
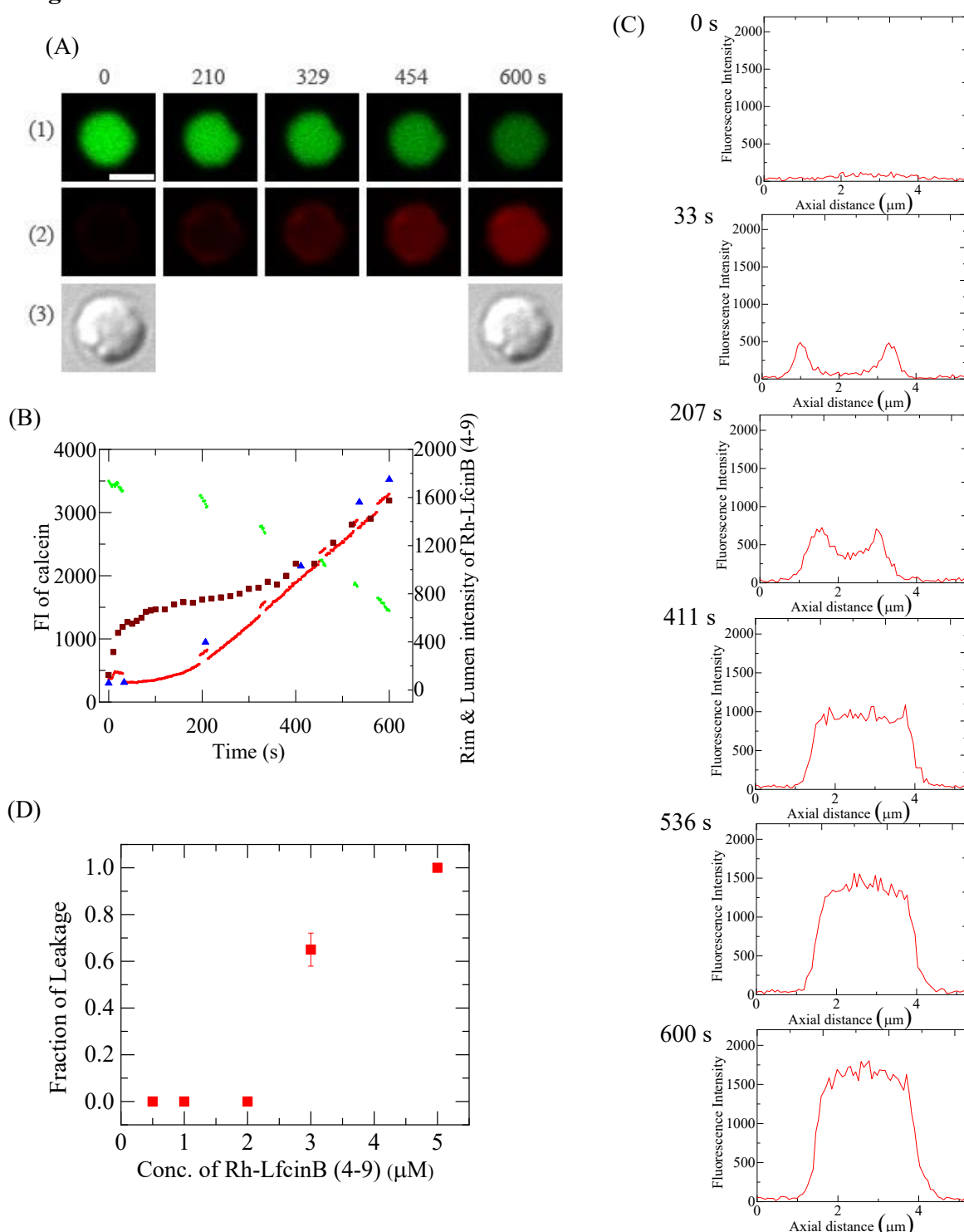
Figure 3.9: Interaction of Rh-LfB4-9 with single *E. coli*-spheroplasts comprising of calcein. (A) showing images from CLSM of (1) calcein, (2) Rh-LfB4-9 and (3) DIC image on the interaction o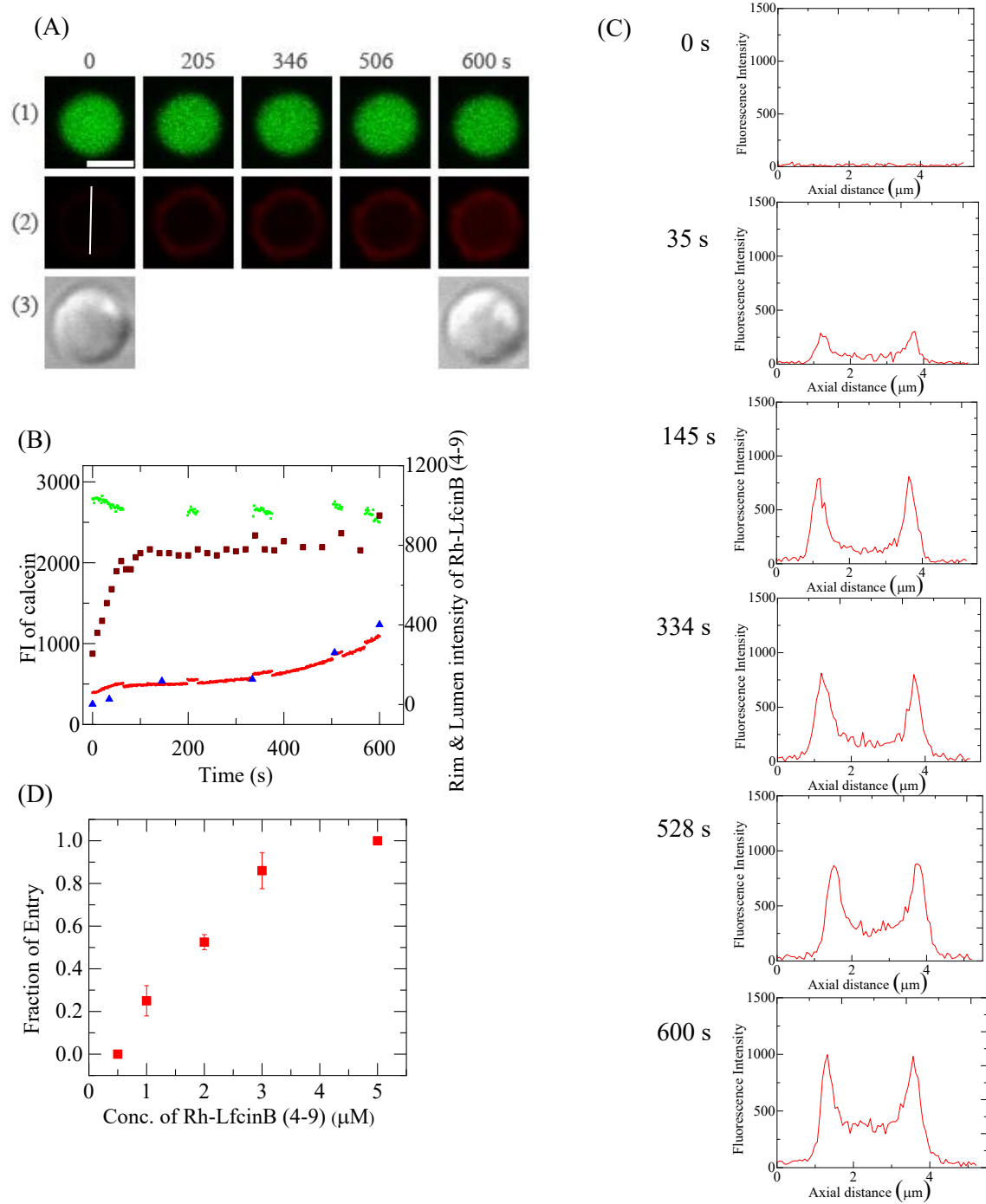f spheroplast with 3.0 µM Rh-LfB4-9. The numbers top on each image showing the time in sec during the interaction. The following CLSM conditions were used; Laser (473 nm): 0.1%, HV: 580v, Gain: 4.5x, offset: 7%; laser (559 nm): 0.5%, HV: 400v, Gain: 4.25x, offset: 7%). The bar is 5 µm. (B) Time course of FI change of total spheroplast due to calcein (green line) and Rh-LfB4-9 (red line), spheroplast rim due to Rh-LfB4-9 (brown square) and central region of spheroplast due to Rh-LfB4-9 (blue triangles) (C) FI profile along white line in the Rh-LfB4-9 images at 0 s in the panel A (2).

The effect of 100 μM CCCP (final concentration) on the interaction of 5.0 μM Rh-LfB4-9 with single spheroplast was examined at 25 °C. The FI of the spheroplast due to calcein decreased a little during 600 sec interaction due to the photobleaching of calcein (Figure 3.10A (1) and a green line in Figure 3.10B), indicating that Rh-LfB4-9 did not induce pore formation in the membrane. In contrast, the increase in the FI due to Rh-LfB4-9 was small (Figure 3.10A (2) and a red line in Figure 3.10B). This result suggests that Rh-LfB4-9 binds to the cell membrane but cannot enter the cytoplasm. The same experiments were performed using 12 spheroplasts, and the same results were observed (i.e., $P_{leak} = 0$ and no entry). Conducted two independent experiments using 10-12 spheroplasts ($N = 2$), producing the same results.

Here also I examined the interaction of 1 nM membrane potential-sensitive dye DiOC6(3) with spheroplast using CLSM. I investigated the effect of CCCP on membrane potential of spheroplast. Here I observed similar type of result and found that there is significant FI of total spheroplast due to $DiOC_6(3)$ in the absence of CCCP but in the presence of 100 μm CCCP found very low FI of total spheroplast (Figure 3.11A). Two independent experiments were conducted and the same results were obtained. I also examined the CCCP concentration dependence on its interaction and found that FI due to $DiOC_6(3)$ of total spheroplast decreased with increase of CCCP concentration (Figure 3.11B).

Therefore, all these results indicate that the membrane potential in the spheroplasts plays an important role in the entry of Rh-LfB4-9 into the cytoplasm of spheroplasts.

Figure 3.10

(A)

(B)
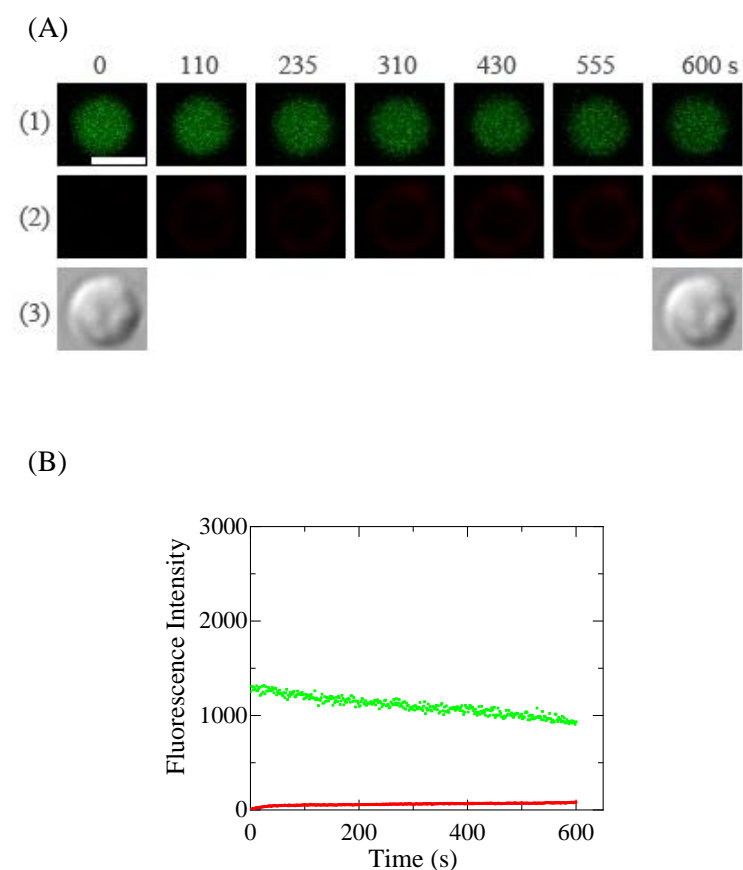
Figure 3.10: Interaction of Rh-LfB4-9 with single *E. coli*-spheroplasts comprising of calcein along with the presence of CCCP. (A) showing images from CLSM of (1) calcein, (2) Rh-LfB4-9 and (3) DIC image on the interaction of spheroplast with 5.0 µM Rh-LfB4-9. The numbers top on each image showing the time in sec during the interaction. The following CLSM conditions were used; Laser (473 nm): 0.1%, HV: 580v, Gain: 4.5x, offset: 7%; laser (559 nm): 0.5%, HV: 400v, Gain: 4.25x, offset: 7%). The bar is 5 µm. (B) Time course of FI change of the spheroplast due to calcein (green line) and Rh-LfB4-9 (red line).

Figure 3.11

(A) 1 nM DiOC6(3) + No CCCP   1 nM DiOC6(3) + 50 µm CCCP   1 nM DiOC6(3) + 75 µm CCCP   1 nM DiOC6(3) + 100 µm CCCP

(B)

Figure 3.11: Effect of CCCP on membrane potential of *E. coli* spheroplasts due to DiOC6(3) dye. (A) Showing images from CLSM of spheroplast gained by the fluorescence emission of DiOC6(3). The following CLSM conditions were used; Laser (473 nm): 0.5%, HV: 650v, Gain: 6 x, offset: 7%. (B) Dependence of total FI of spheroplast on CCCP concentration. Data showed along with average values and SDs.

3.4 GENERAL DISCUSSION

In this study, we demonstrated the effect of $\Delta\varphi$ on the entry of Rh-LfB4-9 into the lumen of *E. coli* lipid-GUVs, into the cytosol of *E. coli* cells and their spheroplasts. First, lower concentrations (0.2–0.5 µM) of Rh-LfB4-9 significantly enter single GUV lumen without pore formation in t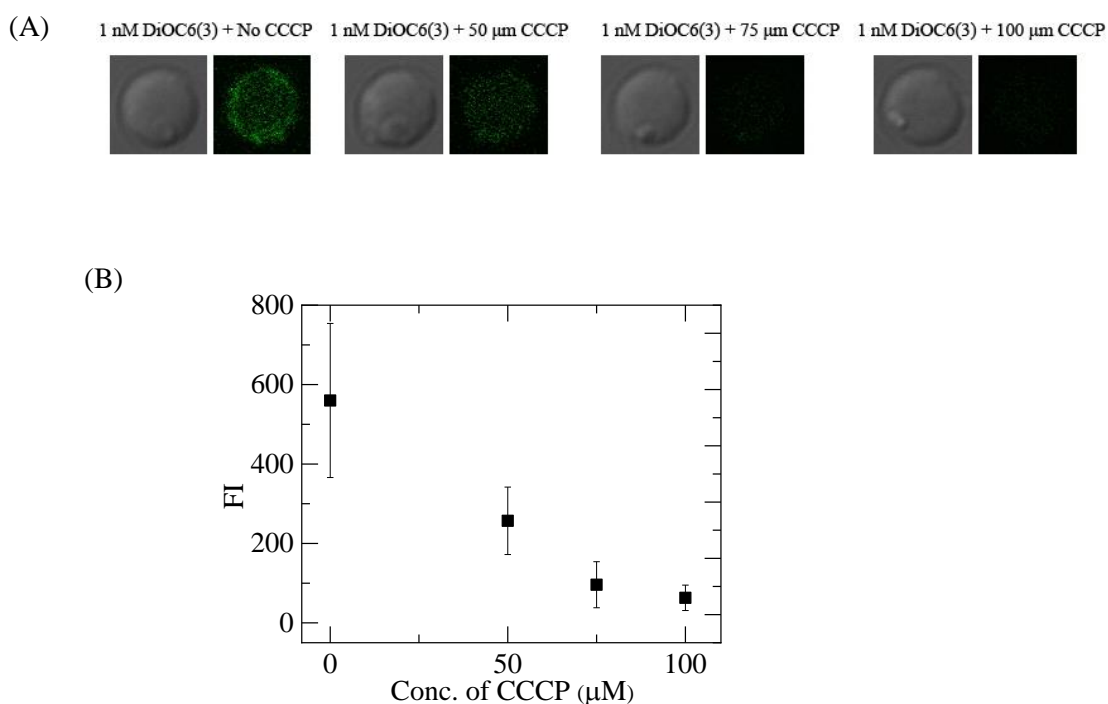he presence of membrane potential. The fraction of entry of Rh-LfB4-9 increased with increasing negative membrane potential, indicating that the rate of entry of peptides into single GUV lumen increased with increasing negative membrane potential. Second, at low concentrations (≤ 5.0 µM) Rh-LfB4-9 enters the cytosol of single E. coli cells without damage of their cell membrane, but the proton-ionophore CCCP suppressed this entry of Rh-LfB4-9 into E. coli cells. Third, at low concentrations (≤ 2.0 µM) Rh-LfB4-9 enters the cytosol of single E. coli spheroplasts without damage of their cell membrane, but the CCCP suppressed this entry of Rh-LfB4-9 into the spheroplasts. These results indicate that the negative $\Delta\varphi$ enhances the entry of Rh-LfB4-9 into single GUVs and E. coli cells.

In this chapter, I applied different negative membrane potentials to the *E. coli* lipid-GUVs using various K_+ diffrence across the GUV membrane. Here, I observed that in the presence of membrane potential, the interaction of lower concentration of Rh-LfB4-9 caused its entry inside GUV without pore formation, which indicates membrane potential increased the rate of entry of Rh-LfB4-9. I also found that, fraction of entry (P_{entry}) inside GUV elevated greatly with an increase in negative membrane potential. As I mentioned earlier, membrane potential exists in eukaryotic cells in their cell membranes. Membrane potential affects greatly cell membranes structure and function e.g., hamper the function of membrane proteins (Hille, 1992; Sakmann and Neher, 1995), organization of lipids such as phosphatidylserine and phosphatidylinositol 4,5-bisphosphate and binding of proteins such as K-Ras (Zhou et al., 2015), cell cycle and cell proliferation (Blackiston et al., 2009; Suderacruz et al., 2009). However, the results obtained in this chapter clearly shows that the negative $\Delta\varphi$ increases the rate of translocation of Rh-LfB4-9 greatly across the lipid bilayer using the single GUV method and also greatly elevated the rate of entry inside a GUV without pore formation. Therefore, one can reasonably infer that the $\Delta\varphi$ plays a vital role on the entry of Rh-LfB4-9 into the lipid vesicles.

Here, we demonstrated that lower concentrations (0.2 - 0.5 μM) of Rh-LfB4-9 significantly enter single GUV lumen without pore formation in the presence of membrane potential, Δφ. The fraction of entry of Rh-LfB4-9 increased with increasing Δφ, indicating that the rate of entry of peptides into single GUV lumen increased with increasing Δφ. The fraction of entry of Rh-LfB4-9 to E. coli-lipid-GUVs at 600 sec interaction, P_{entry} (600 sec), which is a measure of the rate of entry of Rh-LfB4-9, greatly increased with negative membrane potential. For example, 0.50 μM Rh-LfB4-9 P_{entry} (600 sec) increased from 0.05 at Δφ = 0 mV to 0.39 at $\Delta\varphi = -59$ mV, then to 0.90 at $\Delta\varphi = -102$ mV. This membrane potential dependence is a little smaller than that of the fraction of entry of CF-TP10 into DOPG/DOPC(2/8)-GUVs (for example, for 0.5 μM CF-TP10 Pentry (600 sec) increased from 0 at $\Delta\varphi = 0$ mV to 1.0 at $\Delta\varphi = -59$ mV).

In the interaction of Rh-LfB4-9 with single live *E. coli* cells, first these peptides interact with outer membrane of *E. coli* cell, then enter the periplasm containing peptidoglycan which is connected of the cell membrane and the outer membrane, and finally they interact with the cell membrane. In outer membrane, several types of porins exist, and among them OmpG has a large size pore, whose diameter was estimated as 2.0 nm. (Fajardo et al., 1998). Therefore, I consider that Rh-LfB4-9 can pass through the pore of OmpG to enter the periplasm. In this study I found that, Rh-LfB4-9 translocated through the cell membrane of *E. coli* cells and entered inside the cytoplasm without leaking calcein during 600 sec interaction, indicating no pore formation occur in its cell membrane through which calcein leaked. But at very high concentration (above MIC) after entry Rh-LfB4-9 might induce damage or pore formation in the membrane of some *E. coli* through which calcein leaked. I also observed that fraction of entry of Rh-LfB4-9 into *E. coli* increases with increase of Rh-LfB4-9 concentration.

In the interaction of Rh-LfB4-9 with single *E. coli* spheroplast, I observed that Rh-LfB4-9 translocated through the cell membrane of spheroplast and entered into the spheroplast lumen before pore formation during 600 sec interaction. But at high concentration after entry, a decrease in calcein FI found during 600 sec observation when laser (473) is shut off, indicating that leakage of calcein occur during interaction of Rh-LfB4-9 with spheroplast, which is not photobleaching. I also observed that fraction of entry of Rh-LfB4-9 into spheroplast increases with increase of Rh-LfB4-9 concentration.

At low concentrations of Rh-LfB4-9, the peptides enter the cytosol of *E-coli* spheroplasts without pore formation. However, its concentration in the spheroplast cytosol was lower than that in *E-coli* cytosol judging from the FI due to Rh-LfB4-9. At higher concentration of Rh-LfB4-9 greater that 3.0 μM, first the entry of the peptide into the cytosol occurred and subsequently the leakage of calcein occurred in some spheroplasts (P_{leak} = 0.65±0.07), indicating that Rh-LfB4-9 induced pore formation in the cell membrane. After that, the peptide concentration in the cytosol greatly increased, which may be due to the entry of the peptides through the pores. In contrast, in the interaction of Rh-LfB4-9 with *E. coli*-lipid-GUVs, the leakage of AF647 did not occur after 10 min reaction for all peptide concentrations ≤ 9.0 μM. This result indicates that the interaction of only Rh-LfB4-9 with the lipid bilayer regions of the cell membrane of spheroplasts does not induce formation of pores through which calcein leaks. Therefore, the comparison of the results of spheroplasts and GUVs suggests that in the case of the spheroplasts after Rh-LfB4-9 enter the cytosol and binds with proteins or DNAs, which may induce pore formation in the cell membrane. In contrast, in the interaction of Rh-LfB4-9 with *E. coli* cells, the leakage of calcein did not occur after 10 min reaction for all peptide concentrations ≤ 5.0 μM, but 9 μM peptide induced the leakage. The difference of the results between *E. coli* cells and spheroplasts suggests that Rh-LfB4-9 binds the outer membrane and/or peptide glycans and thus the effective Rh-LfB4-9 concentration near the cell membrane in the cells decreases.

In this study I also observed that in the interaction of Rh-LfB4-9 with single *E. coli* cells and single spheroplast in the presence of CCCP, no entry of Rh-LfB4-9 occur into the cytoplasm of *E. coli* cells and spheroplast, and also no leakage of calcein occur during 600 sec interaction, but at low concentration of CCCP, some entry observed in case of spheroplasts. So, the proton-ionophore CCCP suppressed the entry of Rh-LfB4-9 into single *E. coli* cells and single *E. coli* spheroplasts.

In the interaction of Rh-LfB4-9 with *E. coli* cells and their spheroplasts, we have to consider many factors such as membrane proteins, proteins, and DNA. Suppression of membrane potential due to CCCP also induces many changes such as location of membrane proteins. Therefore, it is not easy to elucidate the effect of $\Delta\varphi$ on the interaction of the peptide with lipid bilayer region of the cell membranes, In contrast, in the interaction of Rh-LfB4-9 to *E. coli*-lipid-GUVs, we can consider only the interaction of the peptide with pure lipid bilayer and the effect of $\Delta\varphi$ on this interaction.

Here we consider the mechanism of the effect of $\Delta\varphi$ on the entry of Rh-LfB4-9. The results of the rim intensity of single GUVs due to Rh-LfB4-9 indicate that the steady, maximum concentration of peptides in the GUV membrane and also the rate of increase in peptide concentration in the GUV membrane increase with increasing membrane potential (Fig. 3.2E). However, the quenching of Rh fluorescence at higher membrane potential prevents accurate estimation of the $\Delta\varphi$ dependence of Rh-LfB4-9 concentration in the GUV membrane. In our previous report, we investigated the effect of membrane potential on the entry of CPP, transportan 10 (TP10) into single GUV lumen (Moghal et al., 2019). The rate of entry of CF-TP10 and the rim intensity due to CF-TP10 (which is proportional to CF-TP10 concentration in the GUV membrane) increased with negative membrane potential. It is known that CF-TP10 translocates across lipid bilayer from the outer leaflet to the inner leaflet. Based on these results, we inferred that the increase in CF-TP10 concentration in the inner leaflet is the main cause of the increase in the rate of entry of CF-TP10 into GUV lumen with negative $\Delta\varphi$ (Moghol et al., 2019). Based on the results in the study of CF-TP10, one can infer that the increase in the rate of entry of Rh-LfB4-9 with negative $\Delta\varphi$ is induced by the increase in peptide concentration in the GUV membrane especially in the inner leaflet with increasing negative $\Delta\varphi$.

Several mechanisms for the translocation of peptides such as CPPs across the lipid bilayer have been proposed (Islam et al., 2018; Mishra et al., 2008; Ciobanasu et al., 2010; Mishra et al., 2011; Berlose et al., 1996; Kawamoto et al., 2011; Swiecicki et al., 2014; Sharmin et al., 2016; Islam et al., 2017; Levadny et al., 2013). One is the pore model: first peptides induce a pore in a lipid bilayer, through which peptides permeate to translocate across the lipid bilayer (Mishra et al., 2008; Ciobanasu et al., 2010; Mishra et al., 2011). The pore is defined as a water channel which opens for all time and through which small water-soluble fluorescent dyes such as calcein and AF647 can permeate. In the case of the interaction of Rh-LfB4-9 with *E. coli*-lipid-GUVs and DOPG/DOPC-GUVs (Moniruzzaman et al., 2017), such pores are not produced, and thus, this pore model cannot explain the translocation of Rh-LfB4-9. Another model is the inverted micelle model: positively charged peptides form a complex with a specific amount of negatively-charged lipids and the structure of the complex is similar to the inverted micelle (Mishra et al., 2011; Berlose et al., 1996; Kawamoto et al., 2011). Recently Yamazaki and his collegue proposed a new model, the prepore model (Moghal et al., 2020; Islam et al., 2018; Sharmin et al., 2016; Islam et al., 2017). In a lipid bilayer in the liquid-disordered

phase, various thermal motions of lipid molecules are observed. For example, lateral diffusion of a lipid, extensive conformational changes of hydrocarbon chains and hydrophilic segments, protrusion, and undulation motion of the membrane. Thermal fluctuation of lipid density in a lipid bilayer observed, which induces tentatively a nanodomain with smaller lipid density (i.e., a prepore) (Islam et al., 2017). The structure of the prepore is unstable because at the wall of the prepore the outer and the inner monolayer bend to connect each other, producing an extra free energy, called the line tension. Thus, if such a pre-pore is formed, it immediately closes. However, if peptides are bound to the outer monolayer, a peptide can bind to the wall of a prepore immediately after it forms, which may greatly decrease the free energy of the prepore. As a result, the prepore becomes stabilized, increasing its life time. During this brief life time, the peptide can diffuse laterally along the combined monolayer at the prepore, and then reach the inner monolayer (Islam et al., 2018). This lateral diffusion of the peptide at the wall of the prepore is enhances by the electric field due to the membrane potential (Moghal et al., 2019). This prepore model can explain the translocation of Rh-LfB4-9 across the lipid bilayer and the increase in the rate of translocation with increasing negative membrane potential.

Here we compare the results of the interaction of Rh-LfB4-9 with single *E. coli* cells in EZ rich medium (obtained in this study) with those with single *E. coli* cells in a buffer (10 mM PIPES buffer, pH 7.0. 150 mM NaCl, 1 mM EGTA) (Moniruzzaman et al., 2017). The large difference between EZ rich medium and buffer is that amounts of nutrients, and the buffer does not contain nutrients and thus *E. coli* cells in the buffer is in starvation condition (Groat et al., 1986; Wei et al., 1998; Mandel et al., 2005; Biselli et al., 2020). The most important response in the cells against starvation is a decrease in growth or no growth. We observed in increase in cell length of a cell fixed on a poly-lysine coated cover slip in EZ rich medium, but we did not observe any increase in cell length of a cell on a cover slip in the buffer (Moniruzzaman et al., 2017). Another large difference is that *E. coli* cells in the buffer can be adsorbed on a coverslip (without poly-lysine coating) strongly but *E. coli* cells in EX rich medium cannot be adsorbed on a coverslip without poly-lysine coating (thus, to fix the cells on a coverslip the poly lysine coating is indispensable). This is due to the starvation-induced changes in motility of the cells (Wei et al., 1998). The rate of entry of Rh-LfB4-9 in EZ rich medium is similar to that in the buffer. There is some difference in the Rh-LfB4-9-induced leakage of calcein: at low

concentrations of ≤ 5 μM no leakage occurs in both cases, but a high concentration (9 μM) of Rh-LfB4-9 induced leakage of calcein from some *E. coli* cells in EZ rich medium whereas no leakage occurred from the cells in the buffer. MIC of Rh-LfB4-9 is 5 μM (Moniruzzaman et al., 2017) and the effective concentration of peptide for single cell experiments is higher than that for cell suspension method used in the MIC assay. Therefore, a very high concentration of peptide may induce leakage of calcein. Currently, I do not know the mechanism for the high concentration of Rh-LfB4-9-inudced damage of cell membrane of *E. coli* cells in EZ rich medium (but no damage in cell membrane in cells in the buffer). On the other hand, the photobleaching of calcein did not occur from *E. coli* cells in the buffer but it occurred from *E. coli* cells in EZ rich medium. This difference may be explained by the oxygen concentration in the cytosol of *E. coli* cells. The oxygen concentration in the cytosol of *E. coli* cells in EZ rich medium is high because these cells are active to produce oxygen, whereas *E. coli* cells in the buffer does not produce oxygen gas and hence the oxygen concentration in the cytosol is low.

These results indicate that the negative $\Delta\varphi$ enhances the entry of Rh-LfB4-9 into single GUVs and *E. coli* cells. Therefore, all these results discussed above indicate that $\Delta\varphi$ has a vital role on the entry of Rh-LfB4-9 across lipid vesicles and into the cytoplasm of *E. coli* cells and spheroplast.

3.5 CONCLUSION

In this report, I found that Rh-LfB4-9 translocated across the membrane and entered cytoplasm of *E. coli* cells, spheroplast and GUV lumen without damage of membranes, indicating that its bactericidal property is not the cause of damage of *E. coli* cell membrane. But at high concentration after entry, induced some damage or pore formation in the membrane of the *E. coli* and spheroplast. Hence the presence of CCCP (decrease of negative $\Delta\varphi$) suppressed the rate of entry in *E. coli* and spheroplast. On the other hand, the rate of entry of Rh-LfB4-9 inside GUV lumen elevated greatly with an increase in negative $\Delta\varphi$ without pore formation. These results indicate that the $\Delta\varphi$ plays an important role on the entry of Rh-LfB4-9 into the lipid bilayer region of the cell membrane of *E. coli* cells.

Chapter 4

General Conclusion

Chapter-4

General Conclusion

In this thesis, I investigated the bactericidal activity of one of AMPs LfB and a six residue fragments of it LfB4-9. Here, I choose these two AMPs due its different mechanistic activity, LfB induces membrane damage whereas LfB4-9 can enter the lipid bilayer without damaging the membrane. In this study, I revealed the role of membrane potential on the antimicrobial activities of these two AMPs with lipid vesicles and also with cell membranes of (*E. coli*) cells.

The results obtained in chapter 2, showed that LfB induced rapid, complete leakage of calcein from the cytosol of *E. coli* cells and spheroplasts, indicating that LfB causes rapid permeabilization due to local damage or pore formation in the cell membrane. Therefore, it can be concluded that permeabilization or damage of cell membrane is the main cause of bactericidal acivity of LfB which is induced by the direct interaction of it with the cell membrane of *E. coli* cells. LfB induced rapid leakage of AF647 stochastically during interaction with single *E. coli* lipid-GUVs. But here I found that higher LfB concentrations (almost 10 times) were required to induce a significant rate of damage compared with that observed in *E. coli* cells and spheroplasts. This result indicates other factors are necessary to induce rapid local rupture in *E. coli* lipid-GUVs caused by LfB. I considered membrane potential as one of these factors. I found that the rate of LfB-induced local rupture in GUVs increased greatly with an increase in negative membrane potential. I also observed that during interaction of LfB with single spheroplasts and *E. coli* cells in the presence of CCCP, the CCCP-induced dissipation of membrane potential greatly decreased the rate of permeabilization in the cell membrane. To the best of our knowledge, this is the first report that indicates the significant role of membrane potential in the permeabilization activity of AMPs in GUVs of lipid bilayers and spheroplasts. Therefore, the results obtained in this study revealed that membrane potential plays an important role in LfB-induced local rupture of lipid bilayers and with lipid bilayer regions of the cell membrane of bacterial cells to induce rapid permeabilization, resulting in their bactericidal activity.

In chapter 3, I found that Rh-LfB4-9 translocated across the membrane and entered the GUV lumen and cytoplasm of *E. coli* cells and spheroplast without damage of membranes, indicating that its bactericidal activity is not due to the damage of cell membrane. Hence, the rate of entry of Rh-LfB4-9 into GUV lumen increased greatly with an increase in negative membrane potential without pore formation. On the other hand, the presence of CCCP (decrease of membrane potential) suppressed the rate of entry in *E. coli* and spheroplast greatly. Therefore, all these results found here indicate that the membrane potential has a vital role on the interaction and translocation mechanism of Rh-LfB4-9 into the lipid bilayer region of GUVs and into the cytoplasm of *E. coli* cells.

Therefore, the results obtained in this study are indispensable in revealing the mechanism of action of these two peptides and also other AMPs against cell membrane of bacterial cells, including the membrane potential effects. To design new peptides which have an antimicrobial activity, it is necessary to consider the effect of membrane potential on the interaction mode of the peptides with lipid bilayers.

REFERENCES

Abdul Kadir, L., Stacey, M., and Barrett-Jolley, R. (2018) Emerging roles of the membrane potential: action beyond the action potential. *Frontiers in physiology* **9**, 1661

Aguilera, O., Ostolaza, H., Quiros, L., and Fierro, J. (1999) Permeabilizing action of an antimicrobial lactoferricin-derived peptide on bacterial and artificial membranes. *FEBS letters* **462**, 273-277

Alam, J. M., Kobayashi, T., and Yamazaki, M. (2012) The single-giant unilamellar vesicle method reveals lysenin-induced pore formation in lipid membranes containing sphingomyelin. *Biochemistry* **51**, 5160-5172

Amsterdam, D. (1996) Susceptibility testing of antimicrobials in liquid media. *Antibiotics in laboratory medicine*

Andersen, J. H., Jenssen, H., and Gutteberg, T. J. (2003) Lactoferrin and lactoferricin inhibit Herpes simplex 1 and 2 infection and exhibit synergy when combined with acyclovir. *Antiviral research* **58**, 209-215

Andersen, J. H., Osbakk, S. A., Vorland, L. H., Traavik, T., and Gutteberg, T. J. (2001) Lactoferrin and cyclic lactoferricin inhibit the entry of human cytomegalovirus into human fibroblasts. *Antiviral Research* **51**, 141-149

Andersen, O. S. (1983) Ion movement through gramicidin A channels: Interfacial polarization effects on single-channel current measurements. *Biophys. J.* **41**, 135-146.

Andreu, D., and Rivas, L. (1998) Animal antimicrobial peptides: an overview. *Peptide Science* **47**, 415-433

Arnold, R., Brewer, M., and Gauthier, J. (1980) Bactericidal activity of human lactoferrin: sensitivity of a variety of microorganisms. *Infection and immunity* **28**, 893-898

Arseneault, M., Bédard, S., Boulet-Audet, M., and Pézolet, M. (2010) Study of the interaction of lactoferricin B with phospholipid monolayers and bilayers. *Langmuir* **26**, 3468-3478

Avitabile, C., D'andrea, L. D., and Romanelli, A. (2014) Circular dichroism studies on the interactions of antimicrobial peptides with bacterial cells. *Scientific reports* **4**, 4293

Barns, K. J., and Weisshaar, J. C. (2013) Real-time attack of LL-37 on single Bacillus subtilis cells. *Biochimica et Biophysica Acta (BBA)-Biomembranes* **1828**, 1511-1520

Bechinger, B. (1999) The structure, dynamics and orientation of antimicrobial peptides in membranes by multidimensional solid-state NMR spectroscopy. *Biochimica et Biophysica Acta (BBA)-Biomembranes* **1462**, 157-183

Bellamy, W., Takase, M., Wakabayashi, H., Kawase, K., and Tomita, M. (1992) Antibacterial spectrum of lactoferricin B, a potent bactericidal peptide derived from the N-terminal region of bovine lactoferrin. *Journal of Applied Bacteriology* **73**, 472-479

Berlose, J. P., Convert, O., Derossi, D., Brunissen, A., and Chassaing, G. (1996) Conformational and associative behaviours of the third helix of antennapedia homeodomain in membrane-mimetic environments. *European journal of biochemistry* **242**, 372-386

Berneche, S., Nina, M., and Roux, B. (1998) Molecular dynamics simulation of melittin in a dimyristoylphosphatidylcholine bilayer membrane. *Biophysical journal* **75**, 1603-1618

Bierbaum, G., and Sahl, H. (1987) Autolytic system of Staphylococcus simulans 22: influence of cationic peptides on activity of N-acetylmuramoyl-L-alanine amidase. *Journal of Bacteriology* **169**, 5452-5458

Biselli, E., Schink, S. J., and Gerland, U. (2020) Slower growth of *Escherichia coli* leads to longer survival in carbon starvation due to a decrease in the maintenance rate. *Mol. Syst. Biol.* **16**, e9478.

Blackiston, D. J., McLaughlin, K. A., and Levin, M. (2009) Bioelectric controls of cell proliferation: ion channels, membrane voltage and the cell cycle. *Cell cycle* **8**, 3527-3536

Boman, H. G., Agerberth, B., and Boman, A. (1993) Mechanisms of action on Escherichia coli of cecropin P1 and PR-39, two antibacterial peptides from pig intestine. *Infection and immunity* **61**, 2978-2984

Boman, H. G., and Hultmark, D. (1987) Cell-free immunity in insects. *Annual Reviews in Microbiology* **41**, 103-126

Boman, H., Marsh, J., and Goode, J. (1994) Ciba Foundation Symposium 186: Antimicrobial Peptides. Chichester, England: John Wiley & Sons

Bot, C. T., and Prodan, C. (2010) Quantifying the membrane potential during E. coli growth stages. *Biophysical chemistry* **146**, 133-137

Brogden, K. A. (2005) Antimicrobial peptides: pore formers or metabolic inhibitors in bacteria? *Nature reviews microbiology* **3**, 238-250

Brouwer, C. P., Rahman, M., and Welling, M. M. (2011) Discovery and development of a synthetic peptide derived from lactoferrin for clinical use. *Peptides* **32**, 1953-1963

Campos, M. A., Vargas, M. A., Regueiro, V., Llompart, C. M., Albertí, S., and Bengoechea, J. A. (2004) Capsule polysaccharide mediates bacterial resistance to antimicrobial peptides. *Infection and immunity* **72**, 7107-7114

Castle, M., Nazarian, A., and Tempst, P. (1999) Lethal effects of apidaecin on Escherichia coliinvolve sequential molecular interactions with diverse targets. *Journal of Biological Chemistry* **274**, 32555-32564

Centeno, J. M., Burguete, M. C., Castelló-Ruiz, M., Enrique, M., Vallés, S., Salom, J. B., Torregrosa, G., Marcos, J. F., Alborch, E., and Manzanares, P. (2006) Lactoferricin-related peptides with inhibitory effects on ACE-dependent vasoconstriction. *Journal of agricultural and food chemistry* **54**, 5323-5329

Chan, D. I., Prenner, E. J., and Vogel, H. J. (2006) Tryptophan-and arginine-rich antimicrobial peptides: structures and mechanisms of action. *Biochimica et Biophysica Acta (BBA)-Biomembranes* **1758**, 1184-1202

Christensen, B., Fink, J., Merrifield, R., and Mauzerall, D. (1988) Channel-forming properties of cecropins and related model compounds incorporated into planar lipid membranes. *Proceedings of the National Academy of Sciences* **85**, 5072-5076

Ciobanasu, C., Siebrasse, J. P., and Kubitscheck, U. (2010) Cell-penetrating HIV1 TAT peptides can generate pores in model membranes. *Biophys. J.* **99**, 153-162.

Couto, M. A., Harwig, S., and Lehrer, R. I. (1993) Selective inhibition of microbial serine proteases by eNAP-2, an antimicrobial peptide from equine neutrophils. *Infection and immunity* **61**, 2991-2994

Daniels, C. J., Bole, D. G., Quay, S. C., and Oxender, D. L. (1981) Role for membrane potential in the secretion of protein into the periplasm of *Escherichia coli*. *Proc. Natl. Acad. Sci. U.S.A.* 78, 5396-5400.

Dubey, G. P. and Ben-Yehuda, S. (2011) Intercellular nanotubes mediate bacterial communication. *Cell*, 144, 590-600.

Duclohier, H., Molle, G., and Spach, G. (1989) Antimicrobial peptide magainin I from Xenopus skin forms anion-permeable channels in planar lipid bilayers. *Biophysical journal* **56**, 1017-1021

Duong, F., Eichler, J., Price, A., Leonard, M. R., and Wickner, W. (1997) Biogenesis of the gram-negative bacterial envelope. *Cell* **91**, 567-573

Elsbach, P., and Weiss, J. (1993) Bactericidal/permeability increasing protein and host defense against gram-negative bacteria and endotoxin. *Current opinion in immunology* **5**, 103-107

Fantner, G. E., Barbero, R. J., Gray, D. S., and Belcher, A. M. (2010) Kinetics of antimicrobial peptide activity measured on individual bacterial cells using high-speed atomic force microscopy. *Nature nanotechnology* **5**, 280

Farnaud, S., and Evans, R. W. (2003) Lactoferrin—a multifunctional protein with antimicrobial properties. *Molecular immunology* **40**, 395-405

Felle, H., Porter, J., Slayman, C., and Kaback, H. (1980) Quantitative measurements of membrane potential in Escherichia coli. *Biochemistry* **19**, 3585-3590

Fernández-Musoles, R., López-Díez, J. J., Torregrosa, G., Vallés, S., Alborch, E., Manzanares, P., and Salom, J. B. (2010) Lactoferricin B-derived peptides with inhibitory effects on ECE-dependent vasoconstriction. *Peptides* **31**, 1926-1933

Finkelstein, A., and Andersen, O. S. (1981) The gramicidin A channel: A review of its permeability characteristics with special reference to the single-file aspect of transport. *J. Memb. Biol*. **59**, 155-171.

Fulda. S., Scaffidi, C., Susin, S. A., Krammer, P. H., Kroemer, G., Peter, M. E., and Debatin, K.-M. (1998) Activation of mitochondria and release of mitochondrial apoptogenic factors by betulinic acid. *J. Biol. Chem*. *273*, 33942-33948.

Gazit, E., Boman, A., Boman, H. G., and Shai, Y. (1995) Interaction of the mammalian antibacterial peptide cecropin P1 with phospholipid vesicles. *Biochemistry* **34**, 11479-11488

Gerondakis, S., and Siebenlist, U. (2010) Roles of the NF-κB pathway in lymphocyte development and function. *Cold Spring Harbor perspectives in biology* **2**, a000182

Giansanti, F., Panella, G., Leboffe, L., and Antonini, G. (2016) Lactoferrin from milk: nutraceutical and pharmacological properties. *Pharmaceuticals* **9**, 61

Gifford, J. L., Hunter, H. N., and Vogel, H. (2005) Lactoferricin. *Cellular and molecular life sciences* **62**, 2588

Gifford, J. L., Hunter, H. N., and Vogel, H. J. (2005) Lactoferricin: a lactoferrin-derived peptide with antimicrobial, antiviral, antitumor, and immunological properties. *Cell. Mol. Life. Sci*. **62**, 2588-2598.

Groat, E. G., Schultz, J. E., Zychlinsky, E., Bockman, A., and Matin, A. (1986) Starvation proteins in *Escherichia coli*: Kinetics of synthesis and role in starvation survival. *J. Bacteriol.*, **168**, 486-493.

Hancock, R. E. (1997) Peptide antibiotics. *The Lancet* **349**, 418-422

Hancock, R. E. W., and Hans-Georg, S. (2006) Antimicrobial and host-defense peptides as new anti-infective therapeutic strategies. *Nat. Biotech*. 24, 1551-1557.

Hancock, R. E., and Chapple, D. S. (1999) Peptide antibiotics. *Antimicrobial agents and chemotherapy* **43**, 1317-1323

Hancock, R. E., and Diamond, G. (2000) The role of cationic antimicrobial peptides in innate host defences. *Trends in microbiology* **8**, 402-410

Hancock, R. E., and Rozek, A. (2002) Role of membranes in the activities of antimicrobial cationic peptides. *FEMS microbiology letters* **206**, 143-149

Hartmann, M., Berditsch, M., Hawecker, J., Ardakani, M. F., Gerthsen, D., and Ulrich, A. S. (2010) Damage of the bacterial cell envelope by antimicrobial peptides gramicidin S and PGLa as revealed by transmission and scanning electron microscopy. *Antimicrobial agents and chemotherapy* **54**, 3132-3142

Hasan, M., Karal, M. A. S., Levadnyy, V., and Yamazaki, M. (2018) Mechanism of initial stage of pore formation induced by antimicrobial peptide magainin 2. *Langmuir*, 34, 3349-3362.

Hasan, M., and Yamazaki, M. (2019) Elementary processes and mechanisms of interactions of antimicrobial peptides with membranes −single giant unilamellar vesicle studies−, in: "Antimicrobial Peptides: Basic for Clinical Application", Matsuzaki, K. Ed., Springer Nature, pp. 17-32.

Haukland, H., Ulvatne, H., Sandvik, K., and Vorland, L. (2001) The antimicrobial peptides lactoferricin B and magainin 2 cross over the bacterial cytoplasmic membrane and reside in the cytoplasm. *Febs Letters* **508**, 389-393

Heller, W. T., Waring, A. J., Lehrer, R. I., Harroun, T. A., Weiss, T. M., Yang, L., and Huang, H. W. (2000) Membrane thinning effect of the β-sheet antimicrobial protegrin. *Biochemistry* **39**, 139-145

Henriques, S. T., Costa, J., and Castanho, M. A. (2005) Translocation of β-galactosidase mediated by the cell-penetrating peptide pep-1 into lipid vesicles and human HeLa cells is driven by membrane electrostatic potential. *Biochemistry* **44**, 10189-10198

Hille, B. (1992) Ionic channels in excitable membranes, 2nd edn Sinauer. *Sunderland, Mass*, 127-130

Hossain, F., Moghal, M. M. R., Islam, M. Z., Moniruzzaman, M., and Yamazaki, M. (2019) Membrane potential is vital for rapid permeabilization of cell membranes and lipid bilayers by the antimicrobial peptide lactoferricin B. *Journal of Biological Chemistry* **294**, 10449-10462

Huang, H. W. (2000) Action of antimicrobial peptides: two-state model. *Biochemistry* **39**, 8347-8352

Huang, H. W. (2009) Free energies of molecular bound states in lipid bilayers: lethal concentrations of antimicrobial peptides. *Biophysical journal* **96**, 3263-3272

Huang, H.-C., Lin, H., and Huang, M.-C. (2017) The lactoferricin B-derived peptide, LfB17-34, induces melanogenesis in B16F10 cells. *International journal of molecular medicine* **39**, 595-602

Hwang, P. M., Zhou, N., Shan, X., Arrosmith, C. H., and Vogel, H. J. (1998) Three-dimensional solution structure of lactoferricin B, an antimicrobial peptide derived from bovine lactoferrin, *Biochemistry* 37, 4288-4298.

Hwang, P. M., and Vogel, H. J. (1998) Structure-function relationships of antimicrobial peptides, *Biochem. Cell Biol.* 76, 235-246.

Ihssen, J., Grasselli, E., Bassin, C., François, P., Piffaretti, J.-C., Köster, W., Schrenzel, J., and Egli, T. (2007) Comparative genomic hybridization and physiological characterization of environmental isolates indicate that significant (eco-) physiological properties are highly conserved in the species Escherichia coli. *Microbiology* **153**, 2052-2066

Ishihara, Y., and Shimamoto, N. (2006) Involvement of endonuclease G in nucleosomal DNA fragmentation under sustained endogenous oxidative stress. *J. Biol. Chem. 281*, 6726-6733.

Islam, M. Z., Alam, J. M., Tamba, Y., Karal, M. A. S., and Yamazaki, M. (2014b) The single GUV method for revealing the functions of antimicrobial, pore-forming toxin, and cell-penetrating peptides or proteins. *Physical Chemistry Chemical Physics* **16**, 15752-15767

Islam, M. Z., Ariyama, H., Alam, J. M., and Yamazaki, M. (2014a) Entry of cell-penetrating peptide transportan 10 into a single vesicle by translocating across lipid membrane and its induced pores. *Biochemistry* **53**, 386-396

Islam, M. Z., Sharmin, S., Levadnyy, V., Alam Shibly, S. U., and Yamazaki, M. (2017) Effects of mechanical properties of lipid bilayers on the entry of cell-penetrating peptides into single vesicles. *Langmuir* **33**, 2433-2443

Islam, M. Z., Sharmin, S., Moniruzzaman, M., and Yamazaki, M. (2018) Elementary processes for the entry of cell-penetrating peptides into lipid bilayer vesicles and bacterial cells. *Applied microbiology and biotechnology* **102**, 3879-3892

Kagan, B. L., Selsted, M. E., Ganz, T., and Lehrer, R. I. (1990) Antimicrobial defensin peptides form voltage-dependent ion-permeable channels in planar lipid bilayer membranes. *Proceedings of the National Academy of Sciences* **87**, 210-214

Kang, J. H., Lee, M. K., Kim, K. L., and Hahm, K. –S. (1996) Structure-biological activity relationships of 11-residue highly basic peptide segment of bovine lactoferrin, *Int. J. Pept. Protein Res.*, 48, 357-363.

Karal, M. A. S., Alam, J. M., Takahashi, T., Levadny, V., and Yamazaki, M. (2015) Stretch-activated pore of the antimicrobial peptide, magainin 2. *Langmuir* **31**, 3391-3401

Kawamoto, S., Takasu, M., Miyakawa, T., Morikawa, R., Oda, T., Futaki, S., and Nagao, H. (2011) Inverted micelles formation of cell-penetrating peptide studied by coarse-grained simulation: Importance of attractive force between cell-penetrating peptides and lipid head group. *J. Chem. Phys.* **134**, 095103.

Kiviet, D. J., Nghe, P., Walker, N., Boulineau, S., Sunderlikova, V., and Tans, S. J. (2014) Stochasticity of metabolism and growth at the single-cell level. *Nature* 514, 376-379.

Kragol, G., Lovas, S., Varadi, G., Condie, B. A., Hoffmann, R., and Otvos, L. (2001) The antibacterial peptide pyrrhocoricin inhibits the ATPase actions of DnaK and prevents chaperone-assisted protein folding. *Biochemistry* **40**, 3016-3026

Kuwata, H., Yip, T. T., Tomita, M., and Hutchens, T. W. (1998) Direct evidence of the generation in human stomach of an antimicrobial peptide domain (lactoferricin) from ingested lactoferrin, *Biochim. Biophys. Acta*, 1429, 129-141.

Last, N. B., and Miranker, A. D. (2013) Common mechanism unites membrane poration by amyloid and antimicrobial peptides. *Proceedings of the National Academy of Sciences* **110**, 6382-6387

Lee, C.-C., Sun, Y., Qian, S., and Huang, H. W. (2011) Transmembrane pores formed by human antimicrobial peptide LL-37. *Biophysical journal* **100**, 1688-1696

Lee, M.-T., Sun, T.-L., Hung, W.-C., and Huang, H. W. (2013) Process of inducing pores in membranes by melittin. *Proceedings of the National Academy of Sciences* **110**, 14243-14248

Lehrer, R., Barton, A., Daher, K. A., Harwig, S., Ganz, T., and Selsted, M. E. (1989) Interaction of human defensins with Escherichia coli. Mechanism of bactericidal activity. *The Journal of clinical investigation* **84**, 553-561

Levadny, V., Tsuboi, T., Belaya, M., and Yamazaki, M. (2013) Rate Constant of Tension-Induced Pore Formation in Lipid Membranes. *Langmuir* **29**, 3848-3852.

Li, A., Lee, P., Ho, B., Ding, J., and Lim, C. (2007) Atomic force microscopy study of the antimicrobial action of Sushi peptides on Gram negative bacteria. *Biochimica et Biophysica Acta (BBA)-Biomembranes* **1768**, 411-418

Liu, Y., Han, F., Xie, Y., and Wang, Y. (2011) Comparative antimicrobial activity and mechanism of action of bovine lactoferricin-derived synthetic peptides. *Biometals* **24**, 1069-1078

Lohner, K., and Prossnigg, F. (2009) Biological activity and structural aspects of PGLa interaction with membrane mimetic systems. *Biochimica et Biophysica Acta (BBA)-Biomembranes* **1788**, 1656-1666

Ludtke, S. J., He, K., Heller, W. T., Harroun, T. A., Yang, L., and Huang, H. W. (1996) Membrane pores induced by magainin. *Biochemistry* **35**, 13723-13728

Ludtke, S., He, K., and Huang, H. (1995) Membrane thinning caused by magainin 2. *Biochemistry* **34**, 16764-16769

Maki, N., Gestwicki, J. E., Lake, E. M., Kiessling, L. L., and Adler, J. (2000) Motility and chemotaxis of filamentous cells of *Escherichia coli*. *J. Bacteriol*. 182, 4337-4342.

Mandel, M. J., and Silhavy, T. J. (2005) Starvation for different nutrients in *Escherichia coli* results in differential modulation of RpoS levels and stability. *J. Bacteriol.*, **187**, 434-442.

Mangoni, M. L., and Shai, Y. (2011) Short native antimicrobial peptides and engineered ultrashort lipopeptides: similarities and differences in cell specificities and modes of action. *Cellular and Molecular Life Sciences* **68**, 2267

Martinac, B., Buechner, M., Delcour, A. H., Adler, J., and Kung, C. (1987) Pressure-sensitive ion channel in *Escherichia coli*. *Proc. Natl. Acad. Sci. U. S. A*. 84, 2297-2301.

Matsuzaki, K. (1998) Magainins as paradigm for the mode of action of pore forming polypeptides. *Biochimica et Biophysica Acta (BBA)-Reviews on Biomembranes* **1376**, 391-400

Matsuzaki, K. (1999) Why and how are peptide–lipid interactions utilized for self-defense? Magainins and tachyplesins as archetypes. *Biochimica et Biophysica Acta (BBA)-Biomembranes* **1462**, 1-10

Matsuzaki, K., Murase, O., Fujii, N., and Miyajima, K. (1996) An antimicrobial peptide, magainin 2, induced rapid flip-flop of phospholipids coupled with pore formation and peptide translocation. *Biochemistry* **35**, 11361-11368

Melo, M. N., Ferre, R., and Castanho, A. R. B. (2009) Antimicrobial peptides: linking partition, activity and high membrane-bound concentrations, *Nat. Rev. Microbiol.* 8, 1-5.

Mishra, A., Gordon, V. D., Yang, L., Coridan, R., and Wong, G. C. (2008) HIV TAT forms pores in membranes by inducing saddle-splay curvature: potential role of bidentate hydrogen bonding. *Angewandte Chemie International Edition* **47**, 2986-2989

Mishra, A., Lai, G. H., Schmidt, N. W., Sun, V. Z., Rodriguez, A. R., Tong, R., Tang, L., Cheng, J., Deming, T. J., and Kamei, D. T. (2011) Translocation of HIV TAT peptide and analogues induced by multiplexed membrane and cytoskeletal interactions. *Proceedings of the National Academy of Sciences* **108**, 16883-16888

Moghal, MMR, Hossain, F, Yamazaki, M (2020) Action of antimicrobial peptides and cell-penetrating peptides on membrane potential revealed by the single GUV method. Biophys Rev. 12:339-348

Moghal, MMR, Islam, M, Hossain, F, Saha, S. K., Yamazaki, M (2019) Role of Membrane potential on Entry of Cell- Penetrating Peptide Transportan 10 into Single Vesicles. Biophys J 118:57-69

Moniruzzaman, M., Alam, J. M., Dohra, H., and Yamazaki, M. (2015) Antimicrobial peptide lactoferricin B-induced rapid leakage of internal contents from single giant unilamellar vesicles. *Biochemistry* **54**, 5802-5814

Moniruzzaman, M., Islam, M.Z., Sharmin, S., Dohra, H., and Yamazaki, M. (2017) Entry of a Six-Residue Antimicrobial Peptide Derived from Lactoferricin B into Single Vesicles and *Escherichia coli* Cells without Damaging their Membranes. *Biochemistry* 56, 4419-4431.

Müller, S., Ullrich, S., Lösche, A., Loffhagen, N., and Babel, W. (2000) Flow cytometric techniques to characterise physiological states of Acinetobacter calcoaceticus. *Journal of microbiological methods* **40**, 67-77

Neidhardt, F. C., Bloch, P. L., Smith, D. F. (1974) Culture medium for enterobacteria. *J. Bacteriol*. 119, 736-747.

Nguyen, L. T., Haney, E. F., and Vogel, H. J. (2011) The expanding scope of antimicrobial peptide structures and their modes of action. *Trends in biotechnology* **29**, 464-472

Nguyen, L. T., Schibli, D., and Vogel, H. J. (2005) Structural studies and model membrane interactions of two peptides derived from lactoferricin, *J. Peptide Sci.*, 11, 379-389.

Nishikata, M., Kanehira, T., Oh, H., Tani, H., Tazaki, M., and Kuboki, Y. (1991) Salivary histatin as an inhibitor of a protease produced by the oral bacterium Bacteroides gingivalis. *Biochemical and biophysical research communications* **174**, 625-630

Novo, D., Perlmutter, N. G., Hunt, R. H., and Shapiro, H. M. (1999) Accurate flow cytometric membrane potential measurement in bacteria using diethyloxacarbocyanine and a ratiometric technique. *Cytometry: The Journal of the International Society for Analytical Cytology* **35**, 55-63

Oren, Z., and Shai, Y. (1998) Mode of action of linear amphipathic α-helical antimicrobial peptides. *Peptide Science* **47**, 451-463

Osella, M., Tans, S. J., Lagomarsino, M. C. (2017) Step by step, cell by cell: quantification of the bacterial cell cycle. *Trend. Microbiol*. 25, 250-256.

Otvos, L., O, I., Rogers, M. E., Consolvo, P. J., Condie, B. A., Lovas, S., Bulet, P., and Blaszczyk-Thurin, M. (2000) Interaction between heat shock proteins and antimicrobial peptides. *Biochemistry* **39**, 14150-14159

Pag, U., Oedenkoven, M., Sass, V., Shai, Y., Shamova, O., Antcheva, N., Tossi, A., and Sahl, H.-G. (2008) Analysis of in vitro activities and modes of action of synthetic antimicrobial peptides derived from an α-helical 'sequence template'. *Journal of Antimicrobial Chemotherapy* **61**, 341-352

Park, C. B., Kim, H. S., and Kim, S. C. (1998) Mechanism of action of the antimicrobial peptide buforin II: buforin II kills microorganisms by penetrating the cell membrane and inhibiting cellular functions. *Biochemical and biophysical research communications* **244**, 253-257

Patrzykat, A., Friedrich, C. L., Zhang, L., Mendoza, V., and Hancock, R. E. (2002) Sublethal concentrations of pleurocidin-derived antimicrobial peptides inhibit macromolecular synthesis in Escherichia coli. *Antimicrobial agents and chemotherapy* **46**, 605-614

Pouny, Y., Rapaport, D., Mor, A., Nicolas, P., and Shai, Y. (1992) Interaction of antimicrobial dermaseptin and its fluorescently labeled analogs with phospholipid membranes. *Biochemistry* **31**, 12416-12423

Ramos, J. L., Gallegos, M. a.-T., Marqués, S., Ramos-González, M.-I., Espinosa-Urgel, M., and Segura, A. (2001) Responses of Gram-negative bacteria to certain environmental stressors. *Current opinion in microbiology* **4**, 166-171

Rangarajan, N., Bakshi, S., and Weisshaar, J. C. (2013) Localized permeabilization of E. coli membranes by the antimicrobial peptide Cecropin A. *Biochemistry* **52**, 6584-6594

Rekdal, Ø., Andersen, J., Vorland, L. H., and Svendsen, J. S. (1999) Construction and synthesis of lactoferricin derivatives with enhanced antibacterial activity. *Journal of Peptide Science: An Official Publication of the European Peptide Society* **5**, 32-45

Renner, L. D., and Weibel, D. B. (2011) Cardiolipin microdomains localize to negatively curved regions of *Escherichia coli*. *Proc. Natl. Acad. Sci. U.S.A.*108, 6264-6269.

Rolinson, G. N. (1980) Effect of β-lactam antibiotics on bacterial cell growth rate. *J. Gen. Microbiol.* 120, 317-323.

Rothbard, J. B., Jessop, T. C., Lewis, R. S., Murray, B. A., and Wender, P. A. (2004) Role of membrane potential and hydrogen bonding in the mechanism of translocation of guanidinium-rich peptides into cells. *Journal of the American Chemical Society* **126**, 9506-9507

Rothbard, J. B., Jessop, T. C., and Wender, P. A. (2005) Adaptive translocation: the role of hydrogen bonding and membrane potential in the uptake of guanidinium-rich transporters into cells. *Advanced drug delivery reviews* **57**, 495-504

Ruiz-Gimenez, P., Ibanez, A., Salom, J. B., Marcos, J. F., López-Díez, J. J., Valles, S., Torregrosa, G., Alborch, E., and Manzanares, P. (2010) Antihypertensive properties of lactoferricin B-derived peptides. *Journal of agricultural and food chemistry* **58**, 6721-6727

Ruthe, H.-J., and Adler, J. (1985) Fusion of bacterial spheroplasts by electric fields. *BBA-Biomembranes* 819, 105-113.

Sakmann, B. (2013) *Single-channel recording*, Springer Science & Business Media

Schibli, D. J., Epand, R. F., Vogel, H. J., and Epand, R. M. (2002) Tryptophan-rich antimicrobial peptides: comparative properties and membrane interactions, *Biochem. Cell Biol*. 80, 667-677.

Shai, Y. (1995) Molecular recognition between membrane-spanning polypeptides. *Trends in biochemical sciences* **20**, 460-464

Shai, Y. (1999) Mechanism of the binding, insertion and destabilization of phospholipid bilayer membranes by α-helical antimicrobial and cell non-selective membrane-lytic peptides. *Biochimica et Biophysica Acta (BBA)-Biomembranes* **1462**, 55-70

Shapiro, H. M. (1994) Cell membrane potential analysis. *Methods Cell Biol*. *41*, 121-133.

Sharmin, S., Islam, M. Z., Karal, M. A. S., Alam Shibly, S. U., Dohra, H., and Yamazaki, M. (2016) Effects of lipid composition on the entry of cell-penetrating peptide oligoarginine into single vesicles. *Biochemistry* **55**, 4154-4165

Silvestro, L., Gupta, K., Weiser, J. N., and Axelsen, P. H. (1997) The concentration-dependent membrane activity of cecropin A. *Biochemistry* **36**, 11452-11460

Soblosky, L., Ramamoorthy, A., and Chen, Z. (2015) Membrane interaction of antimicrobial peptides using E. coli lipid extract as model bacterial cell membranes and SFG spectroscopy. *Chemistry and physics of lipids* **187**, 20-33

Sochacki, K. A., Barns, K. J., Bucki, R., and Weisshaar, J. C. (2011) Real-time attack on single Escherichia coli cells by the human antimicrobial peptide LL-37. *Proceedings of the National Academy of Sciences* **108**, E77-E81

Sperelakis, N. (2012) *Cell physiology source book: essentials of membrane biophysics*, Elsevier

Steiner, H., Andreu, D., and Merrifield, R. B. (1988) Binding and action of cecropin and cecropin analogues: antibacterial peptides from insects. *Biochimica et Biophysica Acta (BBA)-Biomembranes* **939**, 260-266

Strahl, H., and Hamoen, L. W. (2010) Membrane potential is important for bacterial cell division. *Proc. Natl. Acad. Sci. U.S.A.* 107, 12281-12286.

Strøm, M. B., Haug, B. E., Skar, M. L., Stensen, W., Stiberg, T., and Svendsen, J. S. (2003) The pharmacophore of short cationic antibacterial peptides. *Journal of medicinal chemistry* **46**, 1567-1570

Strøm, M. B., Haug, B. E., Rekdal, Ǿ., Skar, M. L., Strensen, W., and Svendsen, J. S. (2002) Important structural features of 15-residue lactoferricin derivatives and methods for improvement of antimicrobial activity, *Biochem. Cell Biol.* 80, 65-74.

Subbalakshmi, C., and Sitaram, N. (1998) Mechanism of antimicrobial action of indolicidin. *FEMS microbiology letters* **160**, 91-96

Sun, Y., Sun, T.-L., and Huang, H. W. (2014) Physical properties of Escherichia coli spheroplast membranes. *Biophysical journal* **107**, 2082-2090

Sun, Y., Sun, T.-L., and Huang, H. W. (2016) Mode of action of antimicrobial peptides on E. coli spheroplasts. *Biophysical journal* **111**, 132-139

Swiecicki, J.-M., Bartsch, A., Tailhades, J., Di Pisa, M., Heller, B., Chassaing, G., Mansuy, C., Burlina, F., and Lavielle, S. (2014) The efficacies of cell-penetrating peptides in accumulating in large unilamellar vesicles depend on their ability to form inverted micelles. *ChemBioChem.* **15**, 884-891.

Tamba, Y., Ariyama, H., Levadny, V., and Yamazaki, M. (2010) Kinetic pathway of antimicrobial peptide magainin 2-induced pore formation in lipid membranes. *The journal of physical chemistry B* **114**, 12018-12026

Tamba, Y., Terashima, H., and Yamazaki, M. (2011) A membrane filtering method for the purification of giant unilamellar vesicles. *Chem. Phys. Lipids* 164, 351-358.

Tamba, Y., and Yamazaki, M. (2005) Single giant unilamellar vesicle method reveals effect of antimicrobial peptide magainin 2 on membrane permeability. *Biochemistry* **44**, 15823-15833

Tamba, Y., and Yamazaki, M. (2005) Single giant unilamellar vesicle method reveals effect of antimicrobial peptide Magainin 2 on membrane permeability. *Biochemistry* 44, 15823-15833.

Tamba, Y., and Yamazaki, M. (2009) Magainin 2-induced pore formation in the lipid membranes depends on its concentration in the membrane interface. *The Journal of Physical Chemistry B* **113**, 4846-4852

Terrone, D., Sang, S. L. W., Roudaia, L., and Silvius, J. R. (2003) Penetratin and related cell-penetrating cationic peptides can translocate across lipid bilayers in the presence of a transbilayer potential. *Biochemistry* **42**, 13787-13799

Tomita, M., Takase, M., Bellamy, W., and Shimamura, S. (1994) A review: The active peptide of lactoferrin, *Acta Paediatr. J.* 36, 585-591.

Tu, Y.-H., Ho, Y.-H., Chuang, Y.-C., Chen, P.-C., and Chen, C.-S. (2011) Identification of lactoferricin B intracellular targets using an Escherichia coli proteome chip. *PloS one* **6**

Ulvatne, H., Haukland, H., Olsvik, Ø., and Vorland, L. (2001) Lactoferricin B causes depolarization of the cytoplasmic membrane of Escherichia coli ATCC 25922 and fusion of negatively charged liposomes. *FEBS letters* **492**, 62-65

Ulvatne, H., Samuelsen, Ø., Haukland, H. H., Krämer, M., and Vorland, L. H. (2004) Lactoferricin B inhibits bacterial macromolecular synthesis in Escherichia coli and Bacillus subtilis. *FEMS microbiology letters* **237**, 377-384

Van Elsas, J. D., Semenov, A. V., Costa, R., and Trevors, J. T. (2011) Survival of Escherichia coli in the environment: fundamental and public health aspects. *The ISME journal* **5**, 173-183

Van der Strate, B., Beljaars, L., Molema, G., Harmsen, M., and Meijer, D. (2001) Antiviral activities of lactoferrin. *Antiviral research* **52**, 225-239

Vorland, L. H., Ulvatne, H., Andersen, J., Haukland, H. H., Rekdal, Ø., Svendsen, J. S., and Gutteberg, T. J. (1998) Lactoferricin of bovine origin is more active than lactoferricins of human, murine and caprine origin. *Scandinavian journal of infectious diseases* **30**, 513-517

Vorland, L., Ulvatne, H., Andersen, J., Haukland, H., Rekdal, Ø., Svendsen, J., and Gutteberg, T. (1999) Antibacterial effects of lactoferricin B. *Scandinavian journal of infectious diseases* **31**, 179-184

Waggoner, A. S. (1979) Dye indicators of membrane potential. *Ann. Rev. Biophys. Bioeng.* 8, 47-68.

Wakabayashi, H., Matsumoto, H., Hashimoto, K., Teraguchi, S., Takase, M., and Hayasawa, H. (1999) N-acylated and D enantiomer derivatives of a nonamer core peptide of lactoferricin B showing improved antimicrobial activity, *Antimicrob. Agents Chemothera.* 43, 1267-1269.

Wakabayashi, H., Takase, M., and Tomita, M. (2003) Lactoferricin derived from milk protein lactoferrin, *Curr. Pharm. Des*. 9, 1277-1287.

Wei, L., LaBouyer, M. A., Darling, L. E., and Elmore, D. E. (2016) Bacterial spheroplasts as a model for visualizing membrane translocation of antimicrobial peptides. *Antimicrobial agents and chemotherapy* **60**, 6350-6352

Wei, X., and Bauer, W. D. (1998) Starvation-induced changes in motility, chemotaxis, and flagellation of *Rhizobium meliloti*. *Appl. Environ. Microbiol.* **64**, 1708-1714.

Wu, M., Maier, E., Benz, R., and Hancock, R. E. (1999) Mechanism of interaction of different classes of cationic antimicrobial peptides with planar bilayers and with the cytoplasmic membrane of Escherichia coli. *Biochemistry* **38**, 7235-7242

Yamauchi, K., Tomita, M., Giehl, T. J., and Ellison III, R. T. (1993) Antibacterial activity of lactoferrin and a pepsin-derived lactoferrin peptide fragment. *Inf. Immu.* 61, 719-728.

Yamazaki, M. (2008) The single GUV method to reveal elementary processes of leakage of internal contents from liposomes induced by antimicrobial substances. *Adv. Planar Lipid Bilayers Liposomes.* 7, 121-142.

Yan, D., Chen, D., Shen, J., Xiao, G., Van Wijnen, A. J., and Im, H. J. (2013) Bovine lactoferricin is anti-inflammatory and anti-catabolic in human articular cartilage and synovium. *Journal of cellular physiology* **228**, 447-456

Yang, L., Harroun, T. A., Weiss, T. M., Ding, L., and Huang, H. W. (2001) Barrel-stave model or toroidal model? A case study on melittin pores. *Biophysical journal* **81**, 1475-1485

Yang, M., and Brackenbury, W. J. (2013) Membrane potential and cancer progression. *Frontiers in physiology* **4**, 185

Yeaman, M. R., Bayer, A. S., Koo, S.-P., Foss, W., and Sullam, P. M. (1998) Platelet microbicidal proteins and neutrophil defensin disrupt the Staphylococcus aureus cytoplasmic membrane by distinct mechanisms of action. *The Journal of clinical investigation* **101**, 178-187

Yeaman, M. R., and Yount, N. Y. (2003) Mechanisms of antimicrobial peptide action and resistance. *Pharmacological reviews* **55**, 27-55

Zasloff, M. (2002) Antimicrobial peptides of multicellular organisms. *nature* **415**, 389-395

Zhang, X., Jin, Y., Plummer, M. R., Pooyan, S., Gunaseelan, S., and Sinko, P. J. (2009) Endocytosis and membrane potential are required for HeLa cell uptake of RI-CKTat9, a retro-inverso Tat cell penetrating peptide. *Molecular pharmaceutics* **6**, 836-848

Zhou, Y., Wong, C.-O., Cho, K.-j., Van Der Hoeven, D., Liang, H., Thakur, D. P., Luo, J., Babic, M., Zinsmaier, K. E., and Zhu, M. X. (2015) Membrane potential modulates cell membrane phospholipid dynamics and K-Ras signaling. *Science* **349**, 873-876